ISTANBUL TECHNICAL UNIVERSITY ★ GRADUATE SCHOOL

ANALYTICAL BASED MODELING OF DAMAGE INDUCED BY ELECTROMAGNETIC PRESSURE IMPACT OF LIGHTNING ON AERODYNAMIC SURFACES: AIRCRAFT WING AND WIND TURBINE BLADE

Ph.D THESIS

Aysun SOYSAL

Department of Mathematical Engineering

Mathematical Engineering Programme

MAY 2024

ISTANBUL TECHNICAL UNIVERSITY ★ GRADUATE SCHOOL

ANALYTICAL BASED MODELING OF DAMAGE INDUCED BY ELECTROMAGNETIC PRESSURE IMPACT OF LIGHTNING ON AERODYNAMIC SURFACES: AIRCRAFT WING AND WIND TURBINE BLADE

Ph.D THESIS

Aysun SOYSAL
(509162290)

Department of Mathematical Engineering

Mathematical Engineering Programme

Thesis Advisor: Prof. Dr. Ibrahim OZKOL
Thesis Co-Advisor: Prof. Dr. Erol UZAL

MAY 2024

ISTANBUL TEKNİK ÜNİVERSİTESİ ★ LİSANSÜSTÜ EĞİTİM ENSTİTÜSÜ

UÇAK KANADI VE RÜZGAR TÜRBİNİ PALİ AERODİNAMİK YÜZEYLERİNDE YILDIRIMIN ELEKTROMANYETİK BASINÇ ETKİSİNDEN KAYNAKLANAN HASARIN ANALİTİK TABANLI MODELLEMESİ

DOKTORA TEZİ

Aysun SOYSAL
(509162290)

Matematik Mühendisliği Anabilim Dalı

Matematik Mühendisliği Programı

Tez Danışmanı: Prof. Dr. İbrahim ÖZKOL
Eş Danışman: Prof. Dr. Erol UZAL

MAYIS 2024

Aysun SOYSAL, a Ph.D. student of ITU Graduate School student ID 509162290 successfully defended the dissertation entitled "ANALYTICAL BASED MODELING OF DAMAGE INDUCED BY ELECTROMAGNETIC PRESSURE IMPACT OF LIGHTNING ON AERODYNAMIC SURFACES: AIRCRAFT WING AND WIND TURBINE BLADE", which she prepared after fulfilling the requirements specified in the associated legislations, before the jury whose signatures are below.

Thesis Advisor :	**Prof. Dr. Ibrahim OZKOL** Istanbul Technical University	.....
Co-advisor :	**Prof. Dr. Erol UZAL** Istanbul University-Cerrahpasa	.....
Jury Members :	**Prof. Dr. Kamil ORUCOGLU** Istanbul Technical University	.....
	Prof. Dr. Aytac ARIKOGLU Istanbul Technical University	.....
	Prof. Dr. Hale GONCE KOCKEN Yildiz Technical University	.....
	Prof. Dr. Osman Erguven VATANDAS Istanbul Gelisim University	.....
	Asst. Prof. Dr. Hayri ACAR Istanbul Technical University	.....

Date of Submission : 22 February 2024
Date of Defense : 8 May 2024

This work is dedicated to my parents
Pamuk and Ahmet Soysal,

FOREWORD

I would like to express my gratitude to my supervisors Professor Ibrahim OZKOL and Professor Erol UZAL for their guidance, advice, and pretty patience over the past seven years. I also would like to thanks my committee members Professor Aytac ARIKOGLU, Professor Kamil ORUCOGLU, and Associate Professore Hale GONCE KOCKEN for their valuable advice and supports during all stages of this phd thesis.

My most sincere gratitude is for my family due to their love, encouragement, and endless support throughout my life.

May 2024

Aysun SOYSAL
(Mathematical Engineer)

TABLE OF CONTENTS

Page

ABBREVIATIONS

ARP	**:** Aerospace Recommended Practice
C-C	**:** Clamped-Clamped Boundary Condition
C-F	**:** Clamped-Free Boundary Condition
DTM	**:** Differential Transform Method
EPI	**:** Electromagnetic Pressure Impact
IEC	**:** International Electrotechnical Commission
IEPIM	**:** Improved Electromagnetic Pressure Impact Model
SAE	**:** Society of Aerospace Engineers
SDICOM	**:** SuperDICOM lightning current generator
S-S	**:** Simply Supported-Simply Supported Boundary Condition

SYMBOLS

μ_0 : Magnetic permeability
$I(t)$: Lightning current
r_c : Time-invariant radius of the arc channel of lightning
r : Radial distance to the lightning strike attachment point
P_1, P_2 : Coefficient
τ_1, τ_2 : Time constant
μ_r : Relatively permeability of the non-magnetic lightning protection
$R_r(t)$: Radius of arc root
t : Time
α, β : Parameter
A, B, C, D : Lightning current components
$r_c(t)$: Time-dependent radius of the arc channel of lightning
α_0 : Constant
ρ_0 : Air density at atmosphere pressure
L : Length of the structure
r_c^m : Maximum point reached by radius of the arc channel of lightning
$u(x,t)$: Bending translation
$\psi(x,t)$: Torsional rotation
$\theta(x,t)$: Rotation of the cross-section due to bending alone
x : Distance from the origin
x_α : Geometric coupling term
EI : Bending rigidity
GJ : Torsional rigidity
kAG : Shear rigidity
I : Second moment of area
m : Mass
A : Cross-sectional area
ρ : Density
I_α : Polar mass moment of inertia per unit length

c_1, c_2, c_3 : Linear viscous damping term for bending, torsional, rotatory deformation due to bending

P : Axial load

$U_n(x)$: Vibration model shape for bending motion

$\Psi_n(x)$: Vibration model shape for torsinal motion

$\theta_n(x)$: Vibration model shape for rotational motion due to bending alone

ω_n : Vibration frequency

ϕ_1, ϕ_2, ϕ_3 : Phase angles

$f(x)$: An analytical function

η_0 : Center of a power series

$F_D[k]$: Differential transform of $f(x)$

$f[x]$: Inverse differential transform of $f(x)$

$U_D[k]$: Differential transfrom of $U_n(x)$

$\Psi_D[k]$: Differential transfrom of $\Psi_n(x)$

$T_D[k]$: Differential transfrom of $\Theta_n(x)$

$M_D[k]$: Differential transform of bending moment

$S_D[k]$: Differential transform of shear force

$Q_D[k]$: Differential transform of torque

N : Number of terms included in differential transfrom method

μ_n : Generalized mass in the nth mode

δ_{mn} : Kronecker delta function

$q_n(t)$: Time-dependent generalized coordinate for the n^{th} mode

$D(x)$: Spatial distribution

$f(t)$: Time-dependent function factor of the external flexural load

ξ_n : Non-dimensional damping coefficient in the nth mode

x_o : Lightning strike point

A_n, B_n : Coefficients related to the initial conditions

LIST OF TABLES

Page

LIST OF FIGURES

Page

ANALYTICAL BASED MODELING OF DAMAGE INDUCED BY ELECTROMAGNETIC PRESSURE IMPACT OF LIGHTNING ON AERODYNAMIC SURFACES: AIRCRAFT WING AND WIND TURBINE BLADE

SUMMARY

The survivability of systems (e.g., aircrafts and wind turbine blades) routinely operating in open terrain and weather-independent conditions is generally defined as the ability of the systems to avoid or resist harsh environments, including man-made and non-man-made. One of the non-man-made enemy environments is the lightning strike. Thus, the interaction of lightning strike and the materials of such systems must be considered in the procedures regarding design, production, certification requirements, and hence survivability of the systems.

In the present thesis, the interaction of lightning strike with an aeronautical material is investigated. In this context, firstly, an analytical-based improved electromagnetic pressure impact model (IEPIM) of lightning is established. Subsequently, with the help of the pressure impact model established, two analytical-based damage models are established. The first one is the damage model for an aircraft wing and the latter one is the damage model for a wind turbine blade. For each damage model, two different beam theories are considered: Bernoulli- Euler beam theory and Timoshenko beam theory. Then, some applications of the pressure model and damage models established are performed, and then the results obtained are confirmed with appropriate studies in open the literature whenever the comparison is possible.

According to the findings of the thesis, it was found that the pressure model (IEPIM) established in the thesis study was in good agreement with the experimental studies taken from the open literature for 100 kA and 200 kA lightning current. Moreover, it was observed that the pressure model provided quite correct results during the first 25 μs for 100 kA current and the first 50 μs for 200 kA current.

In the damage model of an aircraft wing, which is one of the models developed in the thesis, the damage caused by the pressure impact of lightning on an aircraft wing was obtained with respect to the Timoshenko type damage model and the Bernoulli-Euler type damage model. Then, the amounts of the damage when lightning struck the root, middle and tip of the aircraft wing were calculated according to both the Timoshenko type damage model and the Bernoulli-Euler type damage model. Considering the results of the Bernoulli-Euler type damage model and the Timoshenko type damage model, it was seen that at the wing root, middle of the wing and wing tip, the largest deflections were respectively the bending deflection, torsional deflection, and bending-induced rotational deflection. In the aircraft wing damage model established, even though there was a flexural forcing function, not only bending deflection but also both torsional deflection and rotational deflection caused by cross-sectional area rotation emerged in the aircraft wing. The reason for this is that the damage model developed is established in a coupled (i.e., interactive) form. This chosen approximation is closer to the physical nature of the aircraft wing system. When the Timoshenko type damage model and the Bernoulli-Euler type damage model are

compared in terms of efficiency, it has been determined that the Timoshenko type model provides less deviation than the Bernoulli-Euler type model in terms of the maximum positive damage amount, based on the lightning strike points considered. In the applications of structural analysis problems, when a Timoshenko type model is compared with a Bernoulli-Euler type model for the same material properties, it is claimed that the Bernoulli-Euler type model is used for more rigid structures and therefore gives less deflection. However, in the damage model we have established, there is a dynamic analysis and the forcing function considered in the damage model has a more complex structure than the known standard forcing functions. For these reasons, it is expected that the results of this study can be different from the known standard results. Moreover, in the free vibration analysis subsection performed before the forced vibration analysis subsection of the thesis study, it was seen that the Timoshenko type model gave lower vibration frequencies than the Bernoulli-Euler type model for the same material properties. Furthermore, it was found that the vibration mode shapes associated with these vibration frequencies had lower amplitudes compared to those obtained from the Bernoulli-Euler type model. Thus, it is an expected result that the amounts of the deflection obtained from the Timoshenko type model are lower than the amounts of the deflection obtained from the Bernoulli-Euler type model. Additionally, regarding the deflected shape of the aircraft wing, it was found that in both models, even if lightning strikes a single point on the wing, the deflections in the wing spread throughout the wing. This is because the physical behavior of the forcing function considered in the damage model corresponds to a distributed load form.

In the case of the damage model of the wind turbine blade, when lightning strikes the middle of a wind turbine blade, the amount of damage to the blade caused by the pressure impact of the lightning is calculated according to both the Timoshenko type damage model and the Bernoulli-Euler type damage model for the clamped-free (C-F), clamped-clamped (C-C), and simply supported-simply supported (S-S) boundary conditions and then the results obtained were compared for both models. Accordingly, firstly, the damage model was solved by free vibration analysis and then by forced vibration analysis. Then, using the solution of the model, results were obtained for both the Timoshenko type damage model and the Bernoulli-Euler type damage model for the same material properties. Compared the both models with each other for different boundary conditions, when lightning strikes the middle of a wind turbine blade with C-C boundary condition, the Bernoulli-Euler type damage model provides better result in terms of the result of an experimental study with similar conditions taken from the literature than the Timoshenko type damage model in calculating the damage caused by the electromagnetic pressure impact of lightning. The reason for this is that wind turbine blades are relatively slender structures (i.e., structures with width ratios of at least 1/10 of the length ratios), which makes them more suitable for Bernoulli-Euler type models. On the other hand, the Timoshenko type model is more suitable for relatively shorter and thicker (stubby) structures. When the effect of the boundary conditions of the blade on the occurrence of lightning-induced damage on the wind turbine blade is investigated, in case of neglect of the axial load caused by the rotation of the blade, lightning-induced damage occurs most in the C-C, C-F and S-S boundary conditions, respectively. Among these boundary conditions, in the case of the absence of axial load, when a comparison is made on the basis of the damage model, the Bernoulli-Euler type damage model gives more damage in terms of bending deflection than the Timoshenko type damage model. In addition, while the Bernoulli-Euler type damage model gives larger results in terms of torsional deflection in the C-

C and C-F boundary conditions, the Timoshenko type damage model gives more torsional deflection in the S-S boundary condition. Additionally, again in the absence of axial load, the largest damage types are bending, bending-induced rotational and torsional damage, respectively. As in the lightning damage model of the aircraft wing, even though there is only a flexural forcing function in the lightning damage model of the wind turbine blade, torsional and bending-induced rotational deflections as well as bending deflection occur due to the coupled form of the model. Furthermore, as in the aircraft wing damage model, the forcing function in the damage model has a distributed load effect. Therefore, even if the lightning strike hits a single point in the middle of the wind turbine blade, a pressure spread occurs on the blade surface due to the impact of the lightning, and this pressure spread acts in a radial direction along the blade. On the other hand, in the presence of axial load for the C-F boundary condition, the Timoshenko type damage model gives more deflection amount in terms of bending and torsional deflection than the Bernoulli-Euler type damage model.

UÇAK KANADI VE RÜZGAR TÜRBİNİ PALİ AERODİNAMİK YÜZEYLERİNDE YILDIRIMIN ELEKTROMANYETİK BASINÇ ETKİSİNDEN KAYNAKLANAN HASARIN ANALİTİK TABANLI MODELLEMESİ

ÖZET

Açık arazide ve hava koşullarından bağımsız koşullarda rutin olarak çalışan sistemlerin (örneğin, uçaklar ve rüzgar türbini kanatları) beka kabiliyeti (hayatta kalma yeteneği), genellikle bu tür sitemlerin, insan yapımı ve insan yapımı olmayanlar da dahil olmak üzere zorlu ortamlardan kaçınma veya bunlara direnme yeteneği olarak tanımlanır. İnsan yapımı olmayan zorlu ortamlarından biri de yıldırım çarpmasıdır. Bu nedenle, bu tür sistemlerin tasarımı, üretimi, sertifikasyon gereklilikleri ve dolayısıyla beka kabiliyeti ile ilgili prosedürlerde yıldırım çarpması ile sistem malzemelerinin etkileşimi dikkate alınmalıdır.

Bu tezde, yıldırım çarpmasının bir havacılık malzemesi ile etkileşimi incelenmiştir. Bu kapsamda, öncelikle yıldırımın analitik tabanlı geliştirilmiş elektromanyetik basınç darbe modeli (IEPIM) kurulmuştur. Ardından, kurulan basınç darbe modeli yardımıyla analitik temelli iki hasar modeli kurulmuştur. Bunlardan ilki uçak kanadı için hasar modeli, ikincisi ise rüzgar türbini kanadı için hasar modelidir. Her hasar modeli için iki farklı kiriş teorisi dikkate alınmaktadır: Bernoulli-Euler kiriş teorisi ve Timoshenko kiriş teorisi. Daha sonra oluşturulan basınç modeli ve hasar modellerinin bazı uygulamaları gerçekleştirilmekte ve elde edilen sonuçlar, karşılaştırmanın mümkün olduğu durumlarda açık literatürdeki uygun çalışmalarla doğrulanmaktadır.

Tezin bulgularına göre, tez çalışmasında oluşturulan basınç modelinin (IEPIM) 100 kA ve 200 kA yıldırım akımı için açık literatürden alınan deneysel çalışmalarla iyi bir uyum içinde olduğu bulunmuştur. Bununla birlikte, 100 kA lik akım için ilk 25 μs ve 200 kA lik akım için ise ilk 50 μs süresince model doğru sonuç verdiği gözlenmiştir.

Tezde geliştirilen modellerden biri olan bir uçak kanadının hasar modelinde, bir uçak kanadında yıldırımın basınç etkisinden kaynaklanan hasar, Timoshenko tipli hasar modeli ve Bernoulli-Euler tipli hasar modeline göre elde edilmiştir. Daha sonra, yıldırımın uçak kanadının köküne, ortasına ve ucuna çarpması durumlarındaki hasar miktarları hem Timoshenko tipli hasar modeline hem de Bernoulli-Euler tipli hasar modeline göre hesaplanmıştır. Bernoulli-Euler tipli hasar modelinin ve Timoshenko tipli hasar modelin sonuçları dikkate alındığında kanat kökü, kanat ortası ve kanat ucunda en büyük sapmanın sırasıyla eğilme sapması, burulma sapması ve eğilme kaynaklı dönme sapması olduğu görülmüştür. Oluşturulan uçak kanadı hasar modelinde, yalnızca eğilmeye neden olan bir zorlama fonksiyonu olsa bile uçak kanadında yalnızca eğilme sapması değil hem burulma sapması hem de kesit alan dönmesinin neden olduğu dönme sapması ortaya çıkmıştır. Bunun nedeni, oluşturulan hasar modelinin etkileşimli (coupled) biçimde kurulmasıdır. Seçilen bu yaklaşım, uçak kanat sisteminin fiziksel yapısına daha yakındır. Timoshenko tipi hasar modeli ile Bernoulli-Euler tipi hasar modeli verimlilik açısından karşılaştırıldığında, dikkate alınan yıldırım çarpma noktaları bazında, maksimum pozitif hasar miktarı açısından Timoshenko tipi modelin Bernoulli-Euler tipi modele göre daha az sapma sağladığı

tespit edilmiştir. Yapısal analiz problemlerinin uygulamalarında, aynı malzeme özellikleri için Timoshenko tipi bir model Bernoulli-Euler tipi bir modelle karşılaştırıldığında, Bernoulli-Euler tipi modelin daha rijit yapılar için kullanıldığı ve bu nedenle daha az sehim verdiği iddia edilmektedir. Ancak, kurduğumuz hasar modelinde hem bir dinamik analiz söz konusu hem de hasar modelinde ele alınan zorlama fonksiyonu, bilinen standart zorlama fonksiyonlarından öte daha kompleks bir yapıya sahiptir. Bu nedenlerden dolayı bu çalışmanın sonuçlarının bilinen standart sonuçlardan farklı olabileceği beklenmektedir. Ayrıca tez çalışmasının zorlanmış titreşim analizi alt bölümünden önce gerçekleştirilen serbest titreşim analizi alt bölümünde, aynı malzeme özellikleri için Timoshenko tipi modelin Bernoulli-Euler tipi modele göre daha düşük titreşim frekansları verdiği görülmüştür. Ayrıca bu titreşim frekanslarıyla ilişkili titreşim modu şekillerinin Bernoulli-Euler tipi modelden elde edilenlere göre daha düşük genliklere sahip olduğu bulunmuştur. Dolayısıyla, Timoshenko tipli modelden elde edilen çökmemiktarının, Bernoulli-Euler tipli modelden elde edilen çökme miktarından düşük olması beklenen bir sonuçtur. Ek olarak, uçak kanadının sapmış şekliyle ilgili, her iki modelde de yıldırım, kanatta tek bir noktaya düşse bile kanattaki sapmaların kanat boyunca yayıldığı tespit edilmiştir. Bunun sebebi, hasar modelinde ele alınan zorlama fonksiyonunun fiziksel davranışının, dağılmış bir yük formuna karşılık gelmesidir.

Rüzgar türbini palinin hasar modeli durumunda, bir rüzgar türbini palinin ortasına yıldırım çarptığında, yıldırımın basınç etkisinden kaynaklanan hasarın paldeki miktarı hem Timoshenko tipli hasar modeline göre hem de Bernoulli-Euler tipli hasar modeline göre ankastre-ankastre (clamped-clamped) (C-C), ankastre-serbest (clamped-free) (C-F) ve basit mesnetli-basit mesnetli (simply supported-simply supported) (S-S) sınır şartları için elde edilmiş ve sonuçlar her iki model için de kıyaslanmıştır. Buna göre, öncelikle hasar modelini çözümü serbest titreşim ve ardından zorlanmış titreşim analizleri yapılarak çözülmüştür. Daha sonra, modelin çözümü kullanılarak aynı malzeme özellikleri için hem Timoshenko tipli hasar modeli hem de Bernoulli-Euler tipli hasar modeli için sonuçlar elde edilmiştir. Farklı sınır şartları için her iki model karşılaştırıldığında, C-C sınır şartına sahip bir rüzgar türbini palinin ortasına yıldırım çarptığında, yıldırımın elektromanyetik basınç etkisinden kaynaklanan hasarın hesaplanmasında Bernoulli-Euler tipli hasar modeli, Timoshenkotipli hasar modeline kıyasla literatürden alınan benzer şartlara sahip bir deneysel çalışmanın sonucuna daha yakın sonuç vermiştir. Bunun nedeni, rüzgar türbinleri pallerinin nispeten narin yapılı (en oranları boy oranlarının yaklaşık olarak en az 1/10 kadar olan yapılar) olmasından, ki böylece de Bernoulli-Euler tipli modellere daha uygun olmasındadır. Diğer taraftan, Timoshenko tipli model ise nispeten daha kısa ve kalın (stubby) yapılar için daha uygundur. Rüzgar türbini palindeki yıldırım kaynaklı hasarın oluşmasında, palin sınır şartlarının etkisi incelendiğinde, palin dönmesinden kaynaklanan eksenel yükün ihmali durumunda, yıldırım kaynaklı hasar sırasıyla en fazla C-C, C-F ve S-S sınır şartlarında ortaya çıkmaktadır. Bu sınır şartları arasında, eksenel yükün yokluğu durumunda, hasar modeli bazında bir kıyaslama yapıldığında, Bernoulli-Euler tipli hasar modeli Timoshenko tipli hasar modelinden eğilme bakımından daha fazla hasar miktarı vermektedir. Rüzgar türbini palinin hasar modeli durumunda, bir rüzgar türbini palinin ortasına yıldırım çarptığında, yıldırımın basınç etkisinden kaynaklanan hasarın paldeki miktarı hem Timoshenko tipli hasar modeline göre hem de Bernoulli-Euler tipli hasar modeline göre ankastre-ankastre(clamped-clamped) (C-C), ankastre-serbest (clamped-free) (C-F) ve basit mesnetli-basit mesnetli (simply supported-simply supported) (S-S) sınır şartları için elde edilmiş ve sonuçlar her iki model için de kıyas-

lanmıştır. Buna göre, öncelikle hasar modelini çözümü serbest titreşim ve ardından zorlanmış titreşim analizleri yapılarak çözülmüştür. Daha sonra, modelin çözümü kullanılarak aynı malzeme özellikleri için hem Timoshenko tipli hasar modeli hem de Bernoulli-Euler tipli hasar modeli için sonuçlar elde edilmiştir. Farklı sınır şartları için her iki model karşılaştırıldığında, C-C sınır şartına sahip bir rüzgar türbini palinin ortasına yıldırım çarptığında, yıldırımın elektromanyetik basınç etkisinden kaynaklanan hasarın hesaplanmasında Bernoulli-Euler tipli hasar modeli, Timoshenkotipli hasar modeline kıyasla literatürden alınan benzer şartlara sahip bir deneysel çalışmanın sonucuna daha yakın sonuç vermiştir. Bunun nedeni, rüzgar türbinleri pallerinin nispeten narin yapılı (en oranları boy oranlarının yaklaşık olarak en az 1/10 kadar olan yapılar) olmasından, ki böylece de Bernoulli-Euler tipli modellere daha uygun olmasındadır. Diğer taraftan, Timoshenko tipli model ise nispeten daha kısa ve kalın (stubby) yapılar için daha uygundur. Rüzgar türbini palindeki yıldırım kaynaklı hasarın oluşmasında, palin sınır şartlarının etkisi incelendiğinde, palin dönmesinden kaynaklanan eksenel yükün ihmali durumunda, yıldırım kaynaklı hasar sırasıyla en fazla C-C, C-F ve S-S sınır şartlarında ortaya çıkmaktadır. Bu sınır şartları arasında, eksenel yükün yokluğu durumunda, hasar modeli bazında bir kıyaslama yapıldığında, Bernoulli-Euler tipli hasar modeli Timoshenko tipli hasar modelinden eğilme bakımından daha fazla hasar miktarı vermektedir. Ayrıca, Bernoulli-Euler tipli hasar modeli C-C ve C-F sınır şartlarında burulma hasarı bakımından daha büyük sonuçlar verirken Timoshenko tipli hasar modeli S-S sınır şartı durumunda daha fazla burulma hasarı vermektedir. Ek olarak, yine eksenel yükün yokluğu durumunda, en büyük hasar tipleri sırasıyla eğilme, eğilme-kaynaklı dönme ve burulma hasar miktarıdır. Uçak kanadındaki yıldırım kaynaklı hasar modelinde olduğu gibi, rüzgar türbini palindeki yıldırım kaynaklı hasar modelinde de yalnızca eğilme davranışına neden olan bir zorlama fonksiyonu olsa bile, modelin etkileşimli formu nedeniyle eğilme sapmasının yanı sıra burulma ve eğilme-kaynaklı dönme hasarları da ortaya çıkmaktadır. Ayrıca yine uçak kanadı hasar modelindeki gibi, hasar modelindeki zorlama fonksiyonu dağılmış yük etkisine sahiptir. Bundan kaynaklı, yıldırım çarpması rüzgar türbini palinin ortasında tek bir noktaya çarpsa bile, çarpmanın etkisi nedeniyle pal yüzeyinde bir basınç yayılması meydana gelir ve bu basınç yayılması pal boyunca radyal yönde etki eder. Diğer taraftan, C-F sınır şartı için eksenel yükün varlığı durumunda ise, Timoshenko tipli hasar modeli, Bernoulli-Euler tipli hasar modelinden eğilme ve burulma sapması anlamında daha fazla çökme miktarı vermektedir.

1. INTRODUCTION

In recent years, two of major sectors making rapid progress in the technological advancements are air transportation and wind turbine industry. Air transportation has played a key role in both global economic growth and traveling long distances by aircrafts in a shorter time while wind turbines have an indispensable place in obtaining wind energy, which is an important renewable energy source in terms of improving climate-and-environmental friendliness and increasing economic competitiveness. However, one of the common occurrences that any aircraft and wind turbine encounter during operation is lightning strikes. In the case of aircrafts flying at low altitude and weather independent conditions, the threat can reach critical levels. For example, past lightning events and aircraft accidents revealed that the impact of lightning can result in structural damage [1], operational disruptions [2], and loss of life and property [3]. Furthermore, in last years, it has been stated that the flying ring cost of lightning-caused disruptions (e.g., delays and cancellations) can be nearly five times the cost of replacing an existing facility [4]. In the case of wind turbine blades, according to the Dutch Center for Energy Research, wind turbine blades are the most sensitive components to lightning strikes [5], and high-frequency damage in blade caused by direct impacts of lightning often results in structural failure inducing high repair costs. Furthermore, failure in wind turbine blade can damage other blades, the wind turbine itself, and other wind turbines located in neighbor. For this reason, investigation of the interaction of aeronautical materials used in the construction of both aircrafts and wind turbine blades with lightning is of undeniable importance. Thus, improvements in this field of research can contribute to the identification and minimization of damage caused by lightning, the reduction of costs caused by lightning, and the procedures for design, production and certification standards [6] for civil-and-commercial aircrafts and wind turbine blades.

The frequency of lightning strikes that a structure experiences is affected by several factors. In terms of aircrafts, the geographic area where the aircraft operates [7], how often the aircraft passes through takeoff and landing altitudes which is where lightning

activity is most prevalent [8], and geometry of the aircraft [9] are some of the factors. For commercial airliners, the statistical in-flight analysis indicates that an aircraft is subject to a lightning strike in the range of 1,000 – 10,000 flight hours, which can be approximated to one lightning annually [10]. On the other hand, in terms of wind turbine blades, the lightning striking distance, the height and blade angle of wind turbines, and the return lightning stroke current are some of major factors affecting the frequency of lightning strike for wind turbine blades [11].

Lightning event arises once a supercooled liquid and ice particles above freezing encounter. As a result of this event, large-and-distinct positive and negative electric charges in the clouds arise. Then, the lightning current discharge starts and an intense current of around 30,000 amps' flows through the arc channel of lightning [12]. If a structure is exposed to the intense current, a large amount of energy is transmitted to one of the front extremities of the structure and then exits from another extremity. The air around the structure exposed to lightning begins to ionize and then the electromagnetic field intensity increases in this part, which generates a pressure impact. Thereafter, the wave of the pressure coming from the arc channel of the lightning propagates by acting as axial, lateral, and radial pressure on nearby structures [13].

1.1 Literature Review

Some authors [13-18] in the literature studied with the lateral pressure loading of lightning as a transverse force applied to a structure in the thickness direction of the structure by using different approaches. While some of them pointed that the lateral pressure loading is electromagnetic (or magnetic) pressure [13-15], the others suggested that the lateral pressure loading is a resultant pressure that consists of electromagnetic and acoustic pressure [16-18]. The modeling approaches proposed by the authors were given in Table 1.1. The findings of the studies of the authors indicated that when the arc channel of lightning attaches to the surface of a structure, the radius of the arc channel expands over time, which supports that the radius of the arc channel is time-varying. Moreover, once any structural part of the structure is subjected to lightning strike, while the arc channel of lightning stands in its initial position, the structure travels forward a significant distance during flash lifetime [19]. Therefore, although lightning hits to a single point of on the structure, the lightning currents [20]

and pressure effect [13] of lightning are distributed over the structure. As seen in Table 1.1, in the modeling approches of the lateral pressure loading of lightning, some of the authors considered the distributed pressure effect of lightning but neglected the time-varying radius of the arc channel in the model. On the other hand, some took into account the time-varying radius of the arc channel but ignored the distributed pressure effect of lightning. Although these modeling approaches gave relatively acceptable and reasonable results, new modeling approaches are always possible to represent the natural behavior of lightning, for instance a model that includes both the distributed pressure effect and the time-varying radius of the arc channel, because lightning is a multi-physical phenomenon [21-22] and it is almost impossible to fully understand its nature.

Table 1.1: Pressure loading of lightning in existing literature.

Author	Model
Kawakami (2011) [13]	$P(r,t) = \frac{\mu_0 I^2(t)}{8\pi^2 r_c^2}$
Chemartin et al. (2012) [18]	$P(r,t) = \frac{\mu_0 I^2(t)}{4\pi^2 r^2}$
Munoz et al. (2014) [16]	$P(r,t) = \begin{cases} \frac{\mu_0 I^2(t)}{4\pi^2 r_c^2}, & r < r_c \\ \frac{\mu_0 I^2(t)}{4\pi^2 r^2}, & r > r_c \end{cases}$
Sousa Martins (2016) [14]	$P(0,t) = P_1 e^{-t/\tau_1} + P_2 e^{-t/\tau_2}$
Karch et al. (2018) [15]	$P(r,t) = \frac{\mu_r \mu_0 I^2(t)}{4\pi}\left[\frac{1}{4} + ln\left(\frac{r_c}{R_r(t)}\right)\right]$
Lee et at. (2021) [17]	$P(r,t) = -\frac{\mu_0 I^2(t)}{8\pi^2 r_c^2}$

In Table 1.1, μ_0 is the magnetic permeability, $\mu_0 = 4\pi \times 10^{-7}\ N/A$; $I(t)$ is the lightning current; r_c is the time-invariant radius of the arc channel of lightning; r is the radial distance to the lightning strike attachment point; P_1 and P_2 are coefficients and τ_1 and τ_2 are time constants; μ_r is the relatively permeability of the non-magnetic lightning protection, $\mu_r = 1$; $R_r(t)$ is the value of the radius of arc root, and t is time.

Since lightning strike is a threat to all aircraft and wind turbine blade structures made of metallic or composite material, numerous experimental and numerical studies were covered in the literature to investigate the damage behavior of structural materials exposed to pressure loading of lightning. Among the experimental studies, Damghani et al. [23] examined the effects of transverse impact loading of lightning on two laminate configurations to determine the shear-buckling behavior of the laminate. Boushab et al. [24] studied the lightning damage resistance of a carbon-epoxy panel by considering lightning arc channel expansion to find out the cause of the widespread surface damage. Guerrero et al. [25] analyzed a carbon-aluminum wing box subjected to loading of lightning to improve the structural behavior of the wing box. Although experimentation is the safest way to solve an engineering problem, providing reasonably good experimental solutions to the lightning problems for aeronautical materials in the appropriate physical environment and under ideal conditions can be quite burdensome, both financially and temporally. To overcome such difficulties, some numerical models of lightning-induced damages in aeronautical materials were proposed in the literature. In the case of aircrafts, Lee et al. [26] predicted the mechanical damage caused by impact of lightning by considering the shock wave overpressure and lightning arc channel expansion via the finite element method (FEM). Foster et al. [27] investigated the potential contribution of lightning pressure loading to composite sample damage in terms of the form and scale of damage. Bigand et al. [28] proposed a numerical model of the damage caused by overpressure of lightning strike on composite structure protected with a metallic mesh and painted. Qian et al. [29] realized the simulation of a turbofan engine of an aircraft encountering a lightning strike to investigate the electromagnetic effect of lightning strike on motor control cables by using CST software based on the transmission line matrix method in the simulation. In the case of wind turbine blades, Zhou et al. [5] proposed a numerical method based on finite element methodology to investigate lightning attachment characteristic of wind turbine blades. The authors analyzed the development mechanism of the line lightning leader by establishing the lightning initial attachment zones. Harrell et al. [30] determined the lightning-induced damage in a composite wind blade by developing a numerical model called a multi-scale model based on finite element method. Then, the results of the numerical model were validated by an experimental study in terms of the effect of a lightning strike on the load response and failure behavior of the blade material. Mitchard et al. [31] developed a static numerical

model by using the COMSOL Multiphysics Software package, which uses finite element analysis, to predict the amount of the deflection caused by the electromagnetic force of lightning strike at a wind turbine blade for a range of lightning currents; and then, they verified the static model with an experimental study. In spite of progress in the experimantal studies to model the lightning-induced damages on aeronautical materials, a complete analysis is almost unable under current technological conditions because of the multi-physical nature of lightning [32]. Furthermore, despite the tremendous development of computers and numerical algorithms, it is also impossible to solve the lightning problem numerically today [33]. However, by simplifying engineering structures under some assumptions, utilizing the power of analytical modeling can be guiding in solving engineering problems. Moreover, even if it may seem unfeasible to understand the relationships between different parameters of a structure and forces that influence a particular outcome, analytical modeling is an effective and reliable technique for turning many different variables and conditions into information one can use. Radicevic et al. [34] are some of the rare authors in the literature who examined the lightning-induced damage behavior of wind turbines from analytical perspective. They put forward a theoretical and an experimental study by developing a model, called reduced-size wind turbine model, to determine the influence of blade rotation on the lightning behavior.

1.2 Purpose of Thesis (Second Level Title: First Letters Capital)

The purpose of this thesis is to model the lightning-induced damage on aredynamic surfaces with an analytical perspective. For this purpose,

1. An analytical-based improved pressure impact model of lightning is established. Then, the model established is validated by using two experimental studies borrowed from the open literature.
2. With the help of the impact model established, two analytical-based damage models are established. The first one is for an aircraft wing and the latter is for a wind turbine blade. Firstly, the damage models are solved by carrying out free vibration and forced vibration analysis. Then, the results of the damage models are compared with the results of the similar experimental studies borrowed from the open literature to verify the damage models.

3. Some parameter studies are performed to measure the effects of the parameters making up the model on the damage models established.

A diagram summarizing the stages of the present study is given in Figure 1.1.

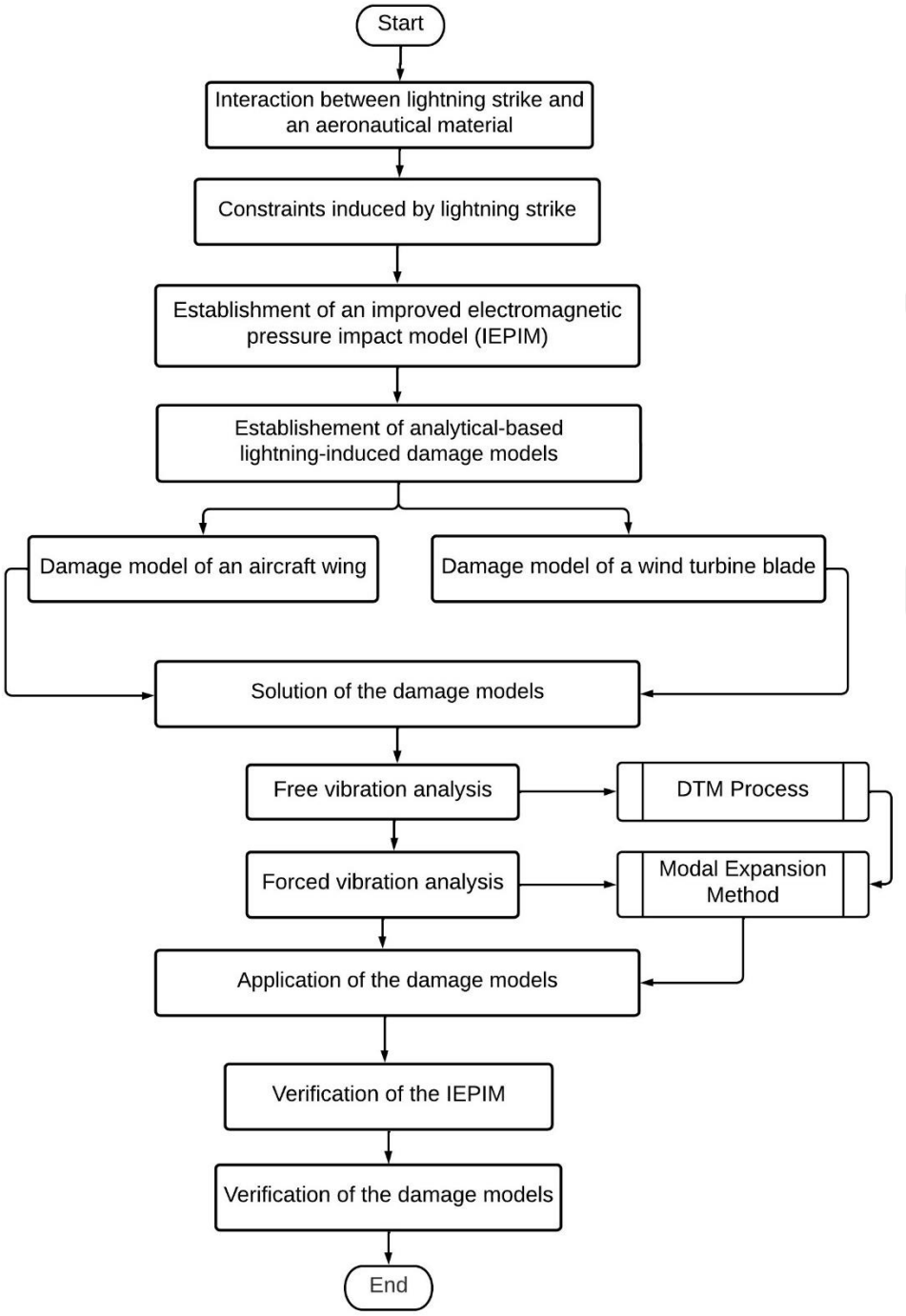

Figure 1.1: A diagram that summarizes the stages of the thesis.

1.3 Structure of Thesis

The thesis is structured into five chapters.

The first chapter includes importance of research question, literature review, and purposes of the thesis.

The second chapter is regarding with the interaction between lightning and a structure exposed to lightning. In this context, firstly, lightning strike zones, lightning current components, and lightning-induced-mechanical constraints in the structure are investigated. Then, an analytical-based improved pressure impact model (IEPIM) of lightning is established.

The third chapter includes the establishment of two lightning-induced damage models for an aircraft and a wind turbine blade, respectively. The models are evaluated in terms of two different beam theories: Bernoulli-Euler beam theory and Timoshenko beam theory. Then, the models are solved by performing free vibration and forced vibration analysis.

The fourth chapter presents the applications for the IEPIM and damage models established. Firstly, the results of the IEPIM are compared with the results of two different experimental studies for verification. Secondly, applications of the damage models are carried out. In this context, for the damage model of an aircraft wing, the bending, torsional, and rotational deflection at the wing root, mid-wing, and wind tip are calculated based on the type of the model when lightning hits to the wing root, mid-wing, and wing tip, respectively. Subsequently, for the damage model of a wind turbine blade, depending on the boundary conditions of the blade, the lightning-induced-deflection at the blade are computed in terms of bending, torsional, and rotational deflection based on the type of the model. Then, the results of the applications are compared with the results of some experimental studies taken form the open literature whenever the comparison is possible. In addition, parameter analysis is carried out for the lightning-induced damage model of a wind tubine blade. Accordingly, the results of the damage models are evaluated for the different values of the axial load and boundary conditions of the blade.

The fifth chapter includes the conclusions of the thesis, some suggestions related the findings of the thesis, and recommendations for the future studies.

2. INTERACTION BETWEEN LIGHTNING STRIKE AND A STRUCTURE EXPOSED TO LIGHTNING

2.1 Lightning Strike Zones

According to some international certification standards, the structures that may be exposed to lightning must be met some security conditions as a precaution against unexpected hazards and serious accidents that may occur as a result of lightning strikes. In the case of aircrafts, aviation regulatory bodies around the world have established some regulations to ensure that aircrafts can withstand lightning strikes and land safely at a suitable airport at the end of the flight. Considering the regulations, modern aircraft manufacturers have used various lightning protection systems to prevent and/or reduce potential direct and indirect hazards caused by lightning strikes. The main purpose of protecting an aircraft's fuselage and structures is to identify areas on the aircraft that are most vulnerable to lightning strikes (i.e., lightning strike zones). Thus, the surface of the aircraft can be classified as a function of the lightning threat, which results in the information about the intensity of lightning and the extent of damage in the aircraft. In the case of wind turbine blades, according to the principles related with lightning protection followed by the international electrotechnical commission (IEC) [35], all subcomponents of wind turbines, including the blade, be protected against severe lightning events. For this reason, a wind turbine blade is divided into lightning protection zones where the possible lightning electromagnetic environment is [5].

Dividing a structure into lightning strike zones or lightning protection zones depends on many parameters; however, the main standards are increasingly similar for most structures in terms of type of the structures. In the open literature, the lightning strike zones for aircrafts were determined according to the Aerospace Recommended Practice (ARP) 5414 standards of the Society of Aerospace Engineers (SAE) [16]. The lightning strike zones for an aircraft wing are given in Figure 2.1 [36] and the descriptions of these zones are presented in Table 2.1 [37]. In the case of a wind turbine blade, the blade is divided into lightning strike protection zones based on the principles

of the IEC; these zones are given in a study carried out by Madsen et al. [38]. The authors described the lightning strike protection zones of a wind turbine blade as in Table 2.2 and depicted these zones on a blade approximately as in Figure 2.2.

Figure 2.1: Lightning strike zones of an aircraft wing.

Table 2.1: Descriptions of lightning strike zones on an aircraft wing.

Zone	Descriptions of lightning strike zones
Zone 1A	Initial attachment point with low possibility of lightning channel hang-on.
Zone 1B	Initial attachment point with high possibility of lightning channel hang-on
Zone 2A	Swept stroke zone with low possibility of lightning channel hang-on.
Zone 2B	Swept stroke zone with high possibility of lightning channel hang-on.
Zone 3	Areas not in Zone 1A, 1B, 2A, or 2B, where damage least probable

Table 2.2: Descriptions of lightning strike protection zones on a wind turbine blade.

Zone	Containing amout of lightning current
Zone 0A1	It contains 200 kA lightning current
Zone 0A2	It contains 100 kA lightning current
Zone 0A3	It contains 50 kA lightning current
Zone 0B	It is not exposed to direct attachments of the lightning strike, but a substantial amount of magnetic energy is conducted in this zone

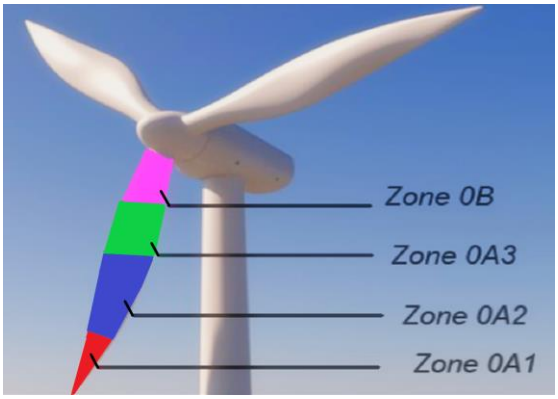

Figure 2.2: Lightning protection zones of a wind turbine blade.

Based on experimental studies, a lightning current was formulated as the following expression [14,15]

$$I(t) = I_0\left(exp(-\alpha t) - exp(-\beta t)\right) \tag{2.1}$$

where α and β are parameters and their values change depending on the lightning current components that are A, B, C, and D, as shown in Table 2.3 [39]. The durations and amplitudes of the components are shown in Figure 2.3 [13]. In addition, the relationships between lightning current components and lightning strike zones are given in Table 2.4. [1,13].

Table 2.3: Values of the lightning current parameters.

Lightning current components	$I_0(Amper)$	$\alpha(s^{-1})$	$\beta(s^{-1})$
A	218810	11354	647265
B	11300	700	2000
C	400	Not applicable	Not applicable
D	109405	22708	1294530

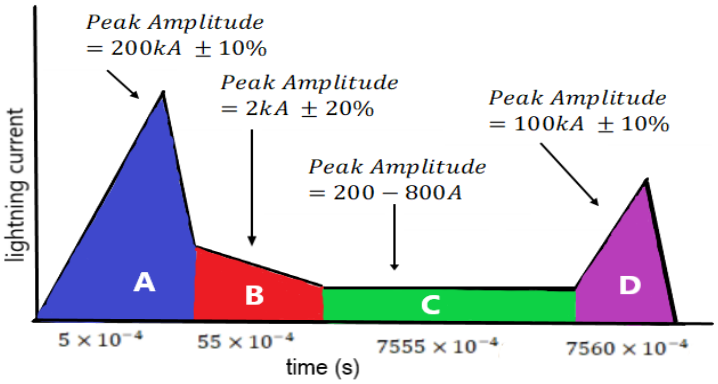

Figure 2.3: Duration and amplitude of the lightning current components.

Table 2.4: Relations between lightning strike zones and lightning current components.

Lightning strike zone	**Ligtning current components**
Zone 1A	A + B
Zone 1B	A + B + C + D
Zone 2A	B + D
Zone 2B	B + C +D
Zone 3	A + D

2.2 Constraints Induced by Lightning

Structures operating in lightning-prone areas can trigger lightning. Once the trigger starts, the lightning process begins. One of the main stages of this process is the leading stage [36]. The leading stage is the onset and development of a conductive arc channel of lightning. After the arc channel is developed, lightning discharges begin to flow through the arc channel. The lightning discharges are generally grouped depending on beginning and ending of the discharges, which are intra-cloud, cloud-to-ground, and cloud-to-cloud discharges [35]. The most common type of lightning discharge is cloud-to-ground, which accounts for 90 percent of all lightning strikes [8]. The percentage of the form of lightning discharge varies depending on the storm in the current geography [7]. However, according to the findings of a study [7], it was revealed that single-lightning flashes are much more common among lightning flashes recorded by lightning detection systems. Even a single lightning hits to a structure, the structure is exposed to the effects of lightning strike including thermal [15], electrical [17], and mechanical [14] effects. These effects of lightning can be broadly divided into two categories: thermal-mechanical constraints and electromagnetic constraints. The thermal-mechanical constraints relate to the damage to the frame materials and can lead to destructive effects such as vibrations that resonate the structure [40], rupture of the extremities of the structure [41], pitting [42], deflection [31], etc. Coversely, the electromagnetic constraints relate to the damage to any electronic system, causing interference to the electronic equipment on board and thus leading to computer control systems to malfunction [43].

Figure 2.4 shows the life cycle of damage caused by a single-lightning strike on an aerodynamic surface made of a metallic material. If the material of the structure has high thermal and electrical conductivity, the electrical and thermal energy generated by the lightning strike are swept from the structure and given back to the air [36], as shown in Figure 2.4; and therefore, if negligible local thermal effects coming from the energy conversion are not considered, only mechanical constraints caused by the pressure impact of lightning occur in the area struck by lightning. At this stage, the arc channel of lightning interacts with the surface of the structure, and then the radius of the arc channel expands over time [6,14-18]. During this time, the magnetic interaction occurs between the current flow in the arc channel and the current flow in the surface of the structure. Then, this interaction exerts an impulsive force on the surface [16],

which generates the pressure waves propagating from the arc channel by acting on nearby structures [13]. The lateral pressure waves arising in the expanding arc channel contributes significantly to the mechanical constraints [16] including elastic displacements, deflection, etc.

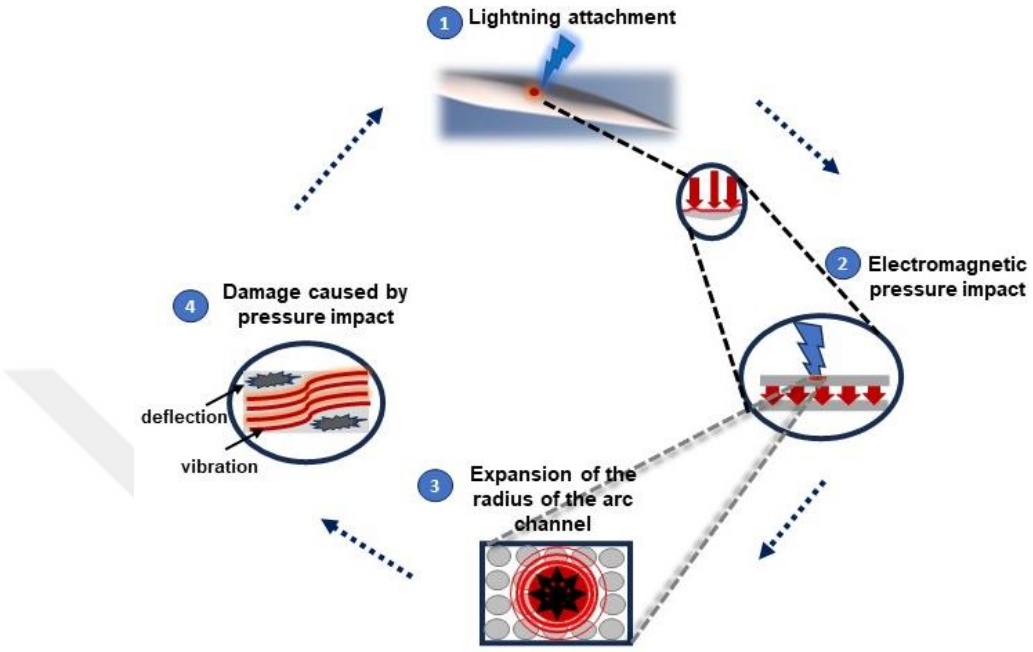

Figure 2.4: Life cycle of damage in an aerodynamic surface struck by lightning.

One of the factors affecting the lightning-induced damage in a structure exposed to lightning is the slenderness ratio of the structure. For thinner structures with high slenderness ratio such as cables, the effect of the pressure enhances by the slenderness ratio, so that even low-pressure states far from the buckling stage may have a significant impact on dynamics of the structure [44]. For instance, when an overhead ground wire that has high slenderness ratio (almost all one dimensional structure) and is generally made of an aluminum clad steel strand [45] is struck by lightning, termal ablation damage [46] or rupture accident [47] can occur in the structure. However, due to mission requirements, aircrafts present high-aspect-ratio wings that result in relatively flexible structures [48]. Therefore, the high flexibility and large aspect ratios can cause large deflections of up to approximately 25% of the wing half-span [49] rather than rupture hazards or thermal ablation.

During lightning strikes, another source of mechanical constraints is acoustic overpressure [16]. Lightning releases substantial amounts of energy into a quite narrow volume of air and in a very short period [50]. Thereby, the air in the ionized lightning arc channel is heated to extremely high temperatures almost instantly [51], and hence

arising high pressures of the expanding plasma in the arc channel [13]. This pressure generates radial pressure and resulting shock waves in the heated channel [52]. Then, the shock waves expand and propagate radially outwards from the center of the discharge channel, leading to mechanical constraints in the structures, especially in the structures that are more sensitive to breakage (e.g., composite skin) [16]. In this thesis, the acoustic pressure propagating in radial directions of the ionization channel is neglected and only the lateral pressure effect (i.e., electromagnetic pressure impact) is considered due to subject of the thesis.

2.3 Establishement of an Improved Electromagnetic Pressure Impact Model

According to some studies [53], the radius of the arc channel of lightning can be modelled as a function of response time as follows:

$$r_c(t) = \alpha_0 \rho_0^{-1/6} [I(t)]^{1/3} t^{1/2} \tag{2.2}$$

where $r_c(t)$ is radius of the arc channel (in meters) expanding in time, α_0 is constant, $\alpha_0 = 0.102$, ρ_0 is the air density at atmosphere pressure, and $\rho_0 = 1.29\ kg/m^3$, $I(t)$ is lightning current.

The author in [16] considered the distributed pressure effect of lightning with a time-invariant radius of the arc channel in the pressure model. To propose an improved electromagnetic pressure impact model involving not only the distributed pressure effect of lightning but also the time-dependent radius of the arc channel, the time-dependent radius of the arc channel given in equation (2.2) is combined with the pressure model of lightning, which is also given in Table 1.1, in [16]. The radial distance relative to the lightning strike point, r, can be expressed as $L - x$ in the formulation of the pressure in terms of the strike point on the structure. Therefore, an improved electromagnetic pressure impact model (IEPIM) of lightning can be obtained as follows:

$$P_G(x,t) = \begin{cases} \dfrac{\mu_0 I^{\frac{4}{3}}(t)}{4\pi^2 \alpha_0^2 \rho_0^{-1/3} t}, & x \le L - 2r_c^m \\ \dfrac{\mu_0 I^2(t)}{4\pi^2 (L-x)^2}, & x > L - 2r_c^m \end{cases} \tag{2.3}$$

where x denotes any point of a structure subjected to the electromagnetic pressure impact, L is the length of the structure, and r_c^m is the maximum point reached by radius of the arc channel of lightning.

In the next chapter, by using the IEPIM expressed in equation (2.3), two analytical-based lightning induced damage models are established to investigate the lightning-induced damage behavior of an aeronautical structural material. The first one is for an aircraft wing while the latter is for a wind turbine blade. In the damage models to be established, a single cloud-to-ground type lightning strike is considered because it is more common and more observable in nature [7-8].

3. ANALYTICAL BASED LIGHTNING-INDUCED DAMAGE MODELS

3.1 Establishment of a Damage Model for an Aircraft Wing

One of the most vulnerable locations to lightning strikes is the wing for most aircrafts [54]. In the construction of an aircraft wing and examination of its resistance deviation against static and dynamic loads, beam structures can be used [18,21,55]. Especially, beams, which are clamped at the origin of the body axes and have coupled bending and torsional behavior, are good approaches to the aircraft wing structures [20]. For this reason, in the establishment of an analytical model of the lightning-induced damage in an aircraft wing, an average uniform aircraft wing structure made of a material with high thermal and electrical conductivity is considered as a bending-torsion coupled beam while the pressure impact of lightning is modelled as a flexural loading applied to the beam.

It should be noted that when lightning hits to an aircraft wing material, the constraints caused by the lightning strike in the material occur in a time interval of the order of microseconds [56]; for this reason, the effects of the aerodynamic forces, which are the forces acting on the body moving through the air such as lift, drag, and downforce in the air, can be negligible in this process. Moreover, the local heat effects caused by the energy conversion are not included in the model since these effects are quite small when compared with the mechanical effects in an aircraft wing. Furthermore, due to the subject of the thesis, the other parts (such as rips, spars, engines, or avionics systems) of the wing structure are not included in the damage model.

Figure 3.1 shows an aircraft wing profile with length L. Here, $u(x,t)$ denotes bending translation, $\psi(x,t)$ denotes torsional rotation, and $\theta(x,t)$ denotes the rotation of the cross-section due to bending alone, where x denotes distance from the origin and t denotes time; x_α is geometric coupling term.

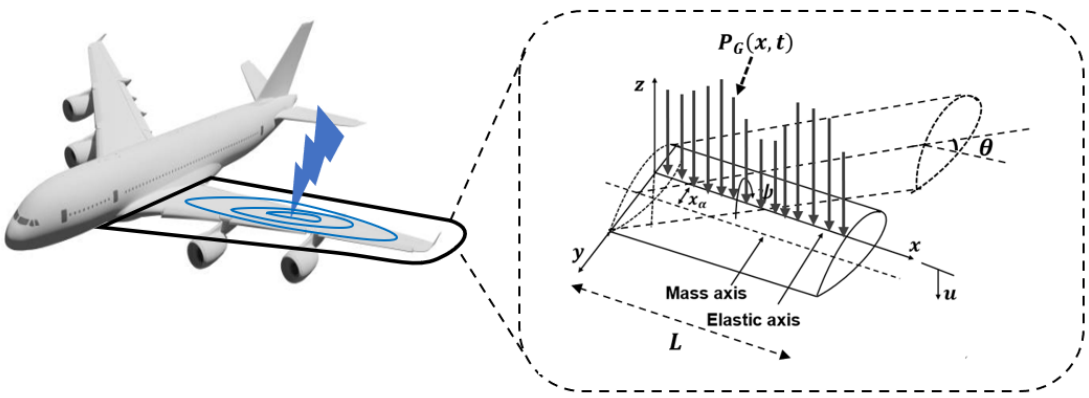

Figure 3.1: Profile of an aircraft wing exposed the pressure loading of lightning.

Two types of lightning-induced-damage model have been proposed for an aircraft wing: Bernoulli-Euler type damage model and Timoshenko type damage model. The partial differential equations and boundary conditions of the damage models are given as follows:

a) Bernoulli-Euler type model:

$$EIu'''' - c_1(\dot{u} - x_\alpha\dot{\psi}) - m(\ddot{u} - x_\alpha\ddot{\psi}) = P_G(x,t) \tag{3.1}$$

$$GJ\psi'' - c_2\dot{\psi} + c_1x_\alpha\dot{u} - I_\alpha\ddot{\psi} + mx_\alpha\ddot{u} = 0 \tag{3.2}$$

$$u = u' = \psi = 0 \qquad at\ x = 0, \tag{3.3}$$

$$u'' = u''' = \psi' = 0 \qquad at\ x = L \tag{3.4}$$

b) Timoshenko type model:

$$EI\theta'' + kAG(u' - \theta) - c_3\dot{\theta} - \rho I\ddot{\theta} = P_G(x,t) \tag{3.5}$$

$$GJ\psi'' - c_2\dot{\psi} + c_1x_\alpha\dot{u} - I_\alpha\ddot{\psi} + mx_\alpha\ddot{u} = 0 \tag{3.6}$$

$$kAG(u'' - \theta') - c_1(\dot{u} - x_\alpha\dot{\psi}) - m(\ddot{u} - x_\alpha\ddot{\psi}) = 0 \tag{3.7}$$

$$u = \theta = \psi = 0 \qquad at\ x = 0 \tag{3.8}$$

$$S = M = T = 0 \qquad at\ x = L \tag{3.9}$$

with

$$P_G(x,t) = \begin{cases} \dfrac{\mu_0 I^{\frac{4}{3}}(t)}{4\pi^2 \alpha_0^2 \rho_0^{-1/3} t}, & x \le L - 2r_c^m \\ \dfrac{\mu_0 I^2(t)}{4\pi^2 (L-x)^2}, & x > L - 2r_c^m \end{cases} \tag{3.10}$$

$$M = -EI\theta' \quad \text{(Bending moment)} \tag{3.11}$$

$$S = -kAG(u' - \theta) \qquad \text{(Shear force)} \tag{3.12}$$

$$T = GJ\psi' \qquad \text{(Torque)} \tag{3.13}$$

where $EI, GJ,$ and kAG are, consecutively, the bending, torsional, and shear rigidities of the wing; I is the second moment of area of the wing cross section; m (i.e., ρA, where A is the cross-sectional area and ρ is density) is mass of the wing per unit length; I_α is polar mass moment of inertia per unit length of the wing; c_1, c_2, and c_3 are linear viscous damping terms of per unit length of the wing in bending deformation, torsional deformation, and rotatory deformation due to bending respectively.

3.2 Establishment of a Damage Model for a Wind Turbine Blade

Wind turbine blades are manufactured in a thin-walled shape to overcome deformations caused by twisting and bending of the wind turbine blade during operation [57]. Since the pressure loading on the blade induces both torsional deformation and bending deformation in the edge and flap directions of the blade [57], a coupled bending-torsion beam can be considered to model a wind turbine blade [58]. Therefore, in establishing the analytical-based lightning-induced damage model of a wind turbine blade, an average uniform bending-torsion coupled beam is considered as a wind turbine blade structure made of high thermal and electrical conductivity. On the other hand, the pressure impact of lightning is considered as a flexural loading applied to the coupled bending-torsion beam in the thickness direction of the blade.

During the rotating process, the rotating wind turbine blades generate a periodic axial load increasing the stiffness of the blades [59]. The axial load generated can be considered the summation of the centrifugal force and the gravity component along the blade [59]. Since the

damage caused by lightning to the structure occurs in a very short time period, the effects of the rotation of the blade can be negligible in this process. But, the effects of the summation of the centrifugal force and the gravity component along the blade, that is an axial load P, is considered in the model. In addition, the local heat effects are ignored in the model.

The profile of a wind turbine blade exposed to pressure loading of lightning is given in Figure 3.2. Here, $u(x,t)$, $\psi(x,t)$, and $\theta(x,t)$ denote bending translation, torsional rotation, and rotation of the cross-section due to bending alone; P is a constant tensile axial load; x_α is geometric coupling term.

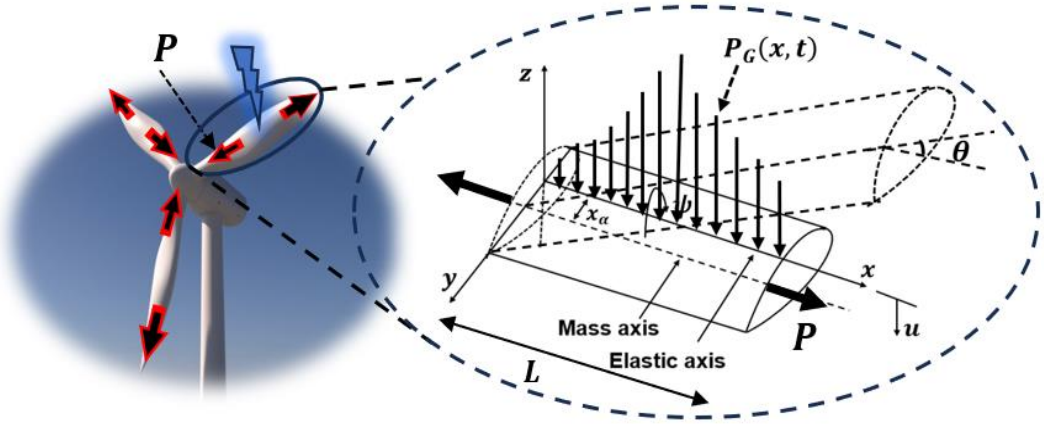

Figure 3.2: The profile of a wind turbine blade exposed to lightning strike.

The governing equations and boundary conditions of the model as follows:

a) Bernoulli-Euler type model:

$$EIu'''' + P(u'' - x_\alpha\psi'') + c_1(\dot{u} - x_\alpha\dot{\psi}) + m(\ddot{u} - x_\alpha\ddot{\psi}) = P_G(x,t) \tag{3.14}$$

$$GJ\psi'' - P\left(\left\{\frac{I_\alpha}{m}\right\}\psi'' - x_\alpha u''\right) - c_2\dot{\psi} + c_1 x_\alpha\dot{u} + mx_\alpha\ddot{u} - I_\alpha\ddot{\psi} = 0 \tag{3.15}$$

with

$$M = -EIu'' \qquad \text{(Bending moment)} \tag{3.16}$$

$$S = EIu''' + P(u' - x_\alpha\psi') \qquad \text{(Shear force)} \tag{3.17}$$

$$T = GJ\psi' - \{PI_\alpha/m\}\psi' + Px_\alpha u' \quad \text{(Torque)} \tag{3.18}$$

b) Timoshenko type model:

$$EI\theta'' + kAG(u' - \theta) - \rho I\ddot{\theta} = P_G(x,t) \tag{3.19}$$

$$kAG(u'' - \theta') + P(u'' - x_\alpha\psi'') - m\left(\ddot{u} - x_\alpha\ddot{\psi}\right) = 0 \tag{3.20}$$

$$GJ\psi'' + P(\{I_\alpha/m\}\psi'' - x_\alpha u'') - I_\alpha\ddot{\psi} + mx_\alpha\ddot{u} = 0 \tag{3.21}$$

with

$$M = -EI\theta' \quad \text{(Bending moment)} \tag{3.22}$$

$$S = -kAG(u' - \theta) - P(u' - x_\alpha\psi') \quad \text{(Shear force)} \tag{3.23}$$

$$T = GJ\psi' - \left\{\frac{PI_\alpha}{m}\right\}\psi' - Px_\alpha u' \quad \text{(Torque)} \tag{3.24}$$

For the following boundary conditions:

Clamped-Free (C-F):

$$u = \theta = \psi = 0\ , \qquad S = M = T = 0 \qquad (\ x = 0, L) \tag{3.25}$$

Clamped-Clamped (C-C):

$$u = \theta = \psi = 0\ , \quad u = \theta = \psi = 0 \qquad (\ x = 0, L) \tag{3.26}$$

Simply Supported-Simply Supported (S-S):

$$u = \psi = M = 0\ , \quad u = \psi = M = 0 \qquad (\ x = 0, L) \tag{3.27}$$

where $EI, GJ,$ and kAG are, consecutively, the bending, torsional, and shear rigidities of the blade; I is the second moment of area of the blade cross section; m (i.e., ρA, where A is the

cross-sectional area and ρ is density) is mass of the blade per unit length; and I_α is polar mass moment of inertia per unit length of the blade.

3.3 Solution of Damage Models

3.3.1 Free vibration analysis

For undamped free vibration analysis, the solutions are assumed in the following form:

$$u(x,t) = U_n(x)sin(\omega_n t + \phi_n) \tag{3.28}$$

$$\psi(x,t) = \Psi_n(x)sin(\omega_n t + \phi_n) \tag{3.29}$$

$$\theta(x,t) = \Theta_n(x)sin(\omega_n t + \phi_n) \tag{3.30}$$

where $U_n(x)$, $\Psi_n(x)$, and $\theta_n(x)$ are vibration modes, ω_n is the vibration frequency, ϕ_n are phase angles, and $n = 1,2,3 \ldots$.

Substituting equation (3.28) – (3.30) into equation (3.1) – (3.13) for the damage model of an aircraft wing and equation (3.14) – (3.27) for the damage model of a wind turbine reduces the partial differential equations to ordinary differential equations as follows:

(i) For the damage model of an aircraft wing

a. Bernoulli-Euler type model:

$$EIU_n'''' - m\omega_n^2 U_n + mx_\alpha \omega_n^2 \Psi_n = 0 \tag{3.31}$$

$$GJ\Psi_n'' + I_\alpha \omega_n^2 \Psi_n - mx_\alpha \omega_n^2 U_n = 0 \tag{3.32}$$

b. Timoshenko type model:

$$EI\Theta_n'' + kAG(U_n' - \Theta_n) + \rho I\omega_n^2 \Theta_n = 0 \tag{3.33}$$

$$kAG(U_n'' - \Theta_n') + m\omega_n^2(U_n - x_\alpha \Psi_n) = 0 \tag{3.34}$$

$$GJ\Psi_n'' - \omega_n^2(mx_\alpha U_n - I_\alpha \Psi_n) = 0 \tag{3.35}$$

with the boundary conditions when $u = U_n$, $\psi = \Psi_n$, and $\theta = \Theta_n$.

(ii) For the damage model of a wind turbine blade

a. Bernoulli-Euler type model:

$$EIU_n{}'''' + P(U_n{}'' - x_\alpha \Psi_n{}'') - m\omega_n^2(U_n - x_\alpha \Psi_n) = 0 \tag{3.36}$$

$$GJ\Psi_n{}'' + \{P/m\}(mx_\alpha U_n{}'' - I_\alpha \Psi_n{}'') - \omega_n^2(mx_\alpha U_n - I_\alpha \Psi_n) = 0 \tag{3.37}$$

b. Timoshenko type model:

$$EI\Theta_n'' + kAG(U_n' - \Theta_n) + \rho I\omega_n^2 \Theta_n = 0 \tag{3.38}$$

$$kAG(U_n'' - \Theta_n') + P(U_n{}'' - x_\alpha \Psi_n{}'') + m\omega_n^2(U_n - x_\alpha \Psi_n) = 0 \tag{3.39}$$

$$GJ\Psi_n{}'' + P\{(I_\alpha/m)\Psi_n{}'' - x_\alpha U_n{}''\} - \omega_n^2(mx_\alpha U_n - I_\alpha \Psi_n) = 0 \tag{3.40}$$

with the boundary conditions when $u = U_n$, $\psi = \Psi_n$ and $\theta = \Theta_n$.

In the solution of the ordinary differential equations, Differential Transform Method (DTM) is applied. According to the theory of DTM [60], an analytical function $f(x)$ is expanded to a power series with the center η_0 in domain of $f(x)$. Then, the differential transform and inverse transform of $f(x)$ are respectively stated by $F_D[k]$ and $f[x]$ as follows:

$$F_D[k] = \frac{1}{k!}\left(\frac{d^k f(x)}{dx^k}\right)\Bigg|_{x=\eta_0} \tag{3.41}$$

$$f[x] = \sum_{k=0}^{\infty} (x - \eta_0)^k F_D[k]. \tag{3.42}$$

After applying the differential transformation rules of DTM given in [61], a set of algebraic equations are obtained as follows:

(i) For the damage model of an aircraft wing

a. Bernoulli-Euler type model:

$$U_D[k+4] = \frac{m{\omega_n}^2 U_D[k] - m x_\alpha {\omega_n}^2 \Psi_D[k]}{EI(k+1)(k+2)(k+3)(k+4)} \tag{3.43}$$

$$\Psi_D[k+2] = \frac{m x_\alpha {\omega_n}^2 U_D[k] - I_\alpha {\omega_n}^2 \Psi_D[k]}{GJ(k+1)(k+2)} \tag{3.44}$$

$$U_D[0] = U_D[1] = \Psi_D[0] = 0 \qquad at\ \ x = 0 \tag{3.45}$$

$$\sum_{k=0}^{N} k(k-1) U_D[k] L^{k-2} = 0 \qquad at\ \ x = L \tag{3.46}$$

$$\sum_{k=0}^{N} k(k-1)(k-2) U_D[k] L^{k-3} = 0 \quad at\ \ x = L \tag{3.47}$$

$$\sum_{k=0}^{N} k \Psi_D[k]\, L^{k-1} = 0 \quad at\ \ x = L \tag{3.48}$$

b. Timoshenko type model:

$$U_D[k+2] = \frac{kAG(k+1)T_D[k+1] - m\omega_n^2 (U_D[k] - x_\alpha \Psi_D)}{kAG(k+1)(k+2)} \tag{3.49}$$

$$\Psi_D[k+2] = \frac{m\omega_n^2 U_D[k] - I_\alpha \omega_n^2 \Psi_D[k]}{GJ(k+1)(k+2)} \tag{3.50}$$

$$T_D[k+2] = \frac{-kAG(k+1)U_D[k+1] + (kAG - \rho I \omega_n^2) T_D[k]}{EI(k+1)(k+2)} \tag{3.51}$$

$$M_D[k] = -EI \sum_{k=0}^{N} k T_D[k] L^{k-1} \tag{3.52}$$

$$S_D[k] = EI \sum_{k=0}^{N} k(k-1) T_D[k] L^{k-2} + \rho I \omega_n^2 \sum_{k=0}^{N} T_D[k] \tag{3.53}$$

$$Q_D[k] = GJ\sum_{k=0}^{N} k\Psi_D[k]L^{k-1} \tag{3.54}$$

(ii) For the damage model of a wind turbine blade

a. Bernoulli-Euler type model:

$$U_D[k+4] = \frac{-P(k+1)(k+2)U_D[k+2] + Px_\alpha(k+1)(k+2)\Psi_D[k+2] + m\omega_n^2 U_D[k] - mx_\alpha\omega_n^2\Psi_D[k]}{EI(k+1)(k+2)(k+3)(k+4)} \tag{3.55}$$

$$\Psi_D[k+2] = \frac{-Px_\alpha(k+1)(k+2)U_D[k+2] + \left(\frac{PI_\alpha}{m}\right)(k+1)(k+2)\Psi_D[k+2] + mx_\alpha\omega_n^2 U_D[k] - \omega_n^2 I_\alpha\Psi_D[k]}{GJ(k+1)(k+2)} \tag{3.56}$$

with

$$\Theta_D[k] = \sum_{k=0}^{N} kU_D[k]L^{k-1} \tag{3.57}$$

$$M_D[k] = \sum_{k=0}^{N} k(k-1)U_D[k]L^{k-2} \tag{3.58}$$

$$S_D[k] = \sum_{k=0}^{N} k(k-1)(k-2)U_D[k]L^{k-3} + \frac{P}{EI}\sum_{k=0}^{N} kU_D[k]L^{k-1} - \frac{Px_\alpha}{EI}\sum_{k=0}^{N} k\Psi_D[k]L^{k-1} \tag{3.59}$$

$$T_D[k] = \sum_{k=0}^{N} k\Psi_D[k]L^{k-1} - \frac{PI_\alpha}{mGJ}\sum_{k=0}^{N} k\Psi_D[k]L^{k-1} + \frac{Px_\alpha}{GJ}\sum_{k=0}^{N} kU_D[k]L^{k-1} \tag{3.60}$$

b. Timoshenko type model:

$$T_D[k+2] = \frac{-kAG(k+1)U_D[k+1] + (kAG - \rho I\omega_n^2)T_D[k]}{EI(k+1)(k+2)} \tag{3.61}$$

$$U_D[k+2] = \frac{(k+1)(Px_\alpha(k+2)\Psi_D[k+2] + kAGT_D[k+1]) - m\omega_n^2(U_D[k] - x_\alpha\Psi_D)}{(kAG+P)(k+1)(k+2)} \tag{3.62}$$

$$\Psi_D[k+2] = \frac{(PI_\alpha x_\alpha/m)(k+1)(k+2)U_D[k+2] - I_\alpha\omega_n^2\Psi_D[k] + m\omega_n^2 U_D[k]}{\left(GJ + \frac{PI_\alpha}{m}\right)(k+1)(k+2)} \tag{3.63}$$

with

$$M_D[k] = -EI \sum_{k=0}^{N} kT_D[k]L^{k-1} \tag{3.64}$$

$$S_D[k] = EI \sum_{k=0}^{N} k(k-1)T_D[k]L^{k-2} - P \sum_{k=0}^{N} kL^{k-1}(U_D[k] - x_\alpha \Psi_D[k]) + \rho I \omega_n^2 \sum_{k=0}^{N} T_D[k] \tag{3.65}$$

$$Q_D[k] = (GJ + PI_\alpha/m) \sum_{k=0}^{N} k\Psi_D[k]L^{k-1} - Px_\alpha \sum_{k=0}^{N} kU_D[k]L^{k-1} \tag{3.66}$$

where $U_D[k]$, $\Psi_D[k]$, and $T_D[k]$ are differential transform of $U_n(x)$, $\Psi_n(x)$, and $\Theta_n(x)$, respectively; $M_D[k]$, $S_D[k]$, and $Q_D[k]$ are respectively the differential transform of the bending moment, shear force, and torque. Moreover, N denotes the number of terms included in the application of DTM; and the value of N is determined depending on the convergence of the vibration frequencies.

Subsequently, using the inverse transform formulation given in equation (3.42), the vibration mode shapes of the aircraft wing and wind turbine blade are obtained as follows:

(i) For the damage model of an aircraft wing

a. Bernoulli-Euler type model:

$$U_n(x) = \sum_{k=0}^{N} U_D[k]x^k \tag{3.67}$$

$$\Psi_n(x) = \sum_{k=0}^{N} \Psi_D[k]x^k \tag{3.68}$$

where $U_D[k]$ and $\Psi_D[k]$ are coming from equation (3.43) – (3.48).

b. Timoshenko type model:

$$U_n(x) = \sum_{k=0}^{N} U_D[k]x^k \tag{3.69}$$

$$\Psi_n(x) = \sum_{k=0}^{N} \Psi_D[k] x^k \tag{3.70}$$

$$\Theta_n(x) = \sum_{k=0}^{N} T_D[k] x^k \tag{3.71}$$

where $U_D[k]$, $\Psi_D[k]$, and $T_D[k]$ are coming from equation (3.49) – (3.54).

(ii) For the damage model of a wind turbine blade

a. Bernoulli-Euler type model:

$$U_n(x) = \sum_{k=0}^{N} U_D[k] x^k \tag{3.72}$$

$$\Psi_n(x) = \sum_{k=0}^{N} \Psi_D[k] x^k \tag{3.73}$$

where $U_D[k]$ and $\Psi_D[k]$ are coming from equation (3.55) – (3.60).

b. Timoshenko type model:

$$U_n(x) = \sum_{k=0}^{N} U_D[k] x^k \tag{3.74}$$

$$\Psi_n(x) = \sum_{k=0}^{N} \Psi_D[k] x^k \tag{3.75}$$

$$\Theta_n(x) = \sum_{k=0}^{N} T_D[k] x^k \tag{3.76}$$

where $U_D[k]$, $\Psi_D[k]$, and $T_D[k]$ are coming from equation (3.61) – (3.66).

The equation (3.67) – (3.76) are conjunction with the boundary conditions. Furthermore, the orthogonality condition can be stated for different vibration mode shapes for Bernoulli-Euler type [58] and Timoshenko type model [62], respectively, as follows:

$$\int_0^L [(mU_mU_n + I_\alpha \Psi_m \Psi_n) - mx_\alpha (U_n \Psi_m + U_m \Psi_n)] d\xi = \mu_n \delta_{mn} \tag{3.77}$$

$$\int_0^L (\rho I \Theta_m \Theta_n + mU_mU_n + I_\alpha \Psi_m \Psi_n) d\xi = \mu_n \delta_{mn} \tag{3.78}$$

where μ_n is the generalized mass in the nth mode and δ_{mn} is the Kronecker delta function.

3.3.2 Forced vibration analysis

In the forced vibration analysis, the modal expansion method is implemented. In this method, the solutions are approximated as follows:

$$u(x,t) = \sum_{n=1}^{\infty} q_n(t) U_n(x) \tag{3.79}$$

$$\psi(x,t) = \sum_{n=1}^{\infty} q_n(t) \Psi_n(x) \tag{3.80}$$

$$\theta(x,t) = \sum_{n=1}^{\infty} q_n(t) \Theta_n(x) \tag{3.81}$$

and the external flexural loading is assumed in the following form

$$P_G(x,t) = D(x) f(t) \tag{3.82}$$

where $U_n(x)$, $\Psi_n(x)$, and $\Theta_n(x)$ are the vibration mode functions, $q_n(t)$ is a time-dependent generalized coordinate for the n^{th} mode; $D(x)$ denotes the spatial distribution, and $f(t)$ denotes the time-dependent function factor of the external flexural load.

Assuming equation (3.79) – (3.81) as the solutions of the equations, multiplication the final equations by $U_m(x)$, $\Psi_m(x)$, $\Theta_m(x)$ and addition the last two equations and then integration the last equation from 0 to L, along with the use of the orthogonality property of the mode functions given in equation (3.77) for Bernoulli-Euler type model and equation (3.78) for Timoshenko type model results in the following equation in the modal coordinates:

$$\ddot{q}_n(t) + 2\xi_n\omega_n\dot{q}_n(t) + \omega_n^2 q_n(t) = F_n(t) \tag{3.83}$$

where ξ_n is the non-dimensional damping coefficient in the nth mode and defined by [62]

$$\xi_n = \frac{c_1}{2m\omega_n} = \frac{c_2}{2I_\alpha\omega_n} = \frac{c_3}{2\rho I\omega_n} \quad 0 \le \xi_n < 1, \tag{3.84}$$

and $F_n(t)$ is calculated as follows:

$$F_n(t) = \frac{\mu_0}{\mu_n 4\pi^2}\left[\frac{I^{4/3}(t)}{\alpha_0^2\rho_0^{-1/3}t}\int_0^{x_0} U_n(x)dx + I^2(t)\int_{x_0}^{L}\frac{U_n(x)}{(L-x)^2}dx\right] \tag{3.85}$$

where x_o is the point where lightning attaches to the aircraft wing exposed to lightning.

By the Duhamel's integral, the solution of equation (3.83) is obtained as follows:

$$q_n(t) = exp(-\xi_n\omega_n t)\{A_n cos(\omega_{nd}t) + B_n sin(\omega_{nd}t)\}$$

$$+\left[\frac{\mu_0}{\mu_n 4\pi^2\omega_{dn}}\int_0^t\left\{\int_0^{x_0-r_c}\frac{U_n(x)}{(x_0-x)^2}dx\right\}[I_0(exp(-\alpha_0\tau)-exp(-\beta_0\tau))]^2 exp\big(-\xi_n\omega_n(t-\tau)\big)sin\big(\omega_{nd}(t-\tau)\big)d\tau\right.$$

$$+\frac{\mu_0\rho_0^{1/3}}{\mu_n 4\pi^2\alpha_0^2\omega_{dn}}\int_0^t\left\{\int_{x_0-r_c}^{x_0+r_c}U_n(x)dx\right\}\frac{[I_0(exp(-\alpha_0\tau)-exp(-\beta_0\tau))]^{\frac{4}{3}}}{\tau}exp\big(-\xi_n\omega_n(t-\tau)\big)sin\big(\omega_{nd}(t-\tau)\big)d\tau$$

$$\left.+\frac{\mu_0}{\mu_n 4\pi^2\omega_{dn}}\int_0^t\left\{\int_{x_0+r_c}^{L}\frac{U_n(x)}{(L-x)^2}dx\right\}[I_0(exp(-\alpha_0\tau)-exp(-\beta_0\tau))]^2 exp\big(-\xi_n\omega_n(t-\tau)\big)sin\big(\omega_{nd}(t-\tau)\big)d\tau\right] \tag{3.86}$$

where A_n and B_n are coefficients related to the initial conditions and ω_{nd} is defined as follows

$$\omega_{nd} = \omega_n\sqrt{1-\xi_n^2} \tag{3.87}$$

Subsequently, substitution of equation (3.86) into equation (3.79) – (3.81) gives the general solution for the bending displacement (i.e., bending deflection), torsional displacement (i.e.,

torsion deflection), and rotational displacement (i.e., rotational deflection) in the aircraft wing and wind turbine blade, respectively, with the following forms:

(i) For the damage model of an aircraft wing

a. Bernoulli-Euler type model:

$$u(x,t) = \sum_{n=1}^{N} U_n(x) q_n(t) \tag{3.88}$$

$$\psi(x,t) = \sum_{n=1}^{N} \Psi_n(x) q_n(t) \tag{3.89}$$

where $U_n(x)$ and $\Psi_n(x)$ are coming from equation (3.67) – (3.68).

b. Timoshenko type model:

$$u(x,t) = \sum_{n=1}^{N} U_n(x) q_n(t) \tag{3.90}$$

$$\psi(x,t) = \sum_{n=1}^{N} \Psi_n(x) q_n(t) \tag{3.91}$$

$$\theta(x,t) = \sum_{n=1}^{N} \Theta_n(x) q_n(t) \tag{3.92}$$

where $U_n(x)$, $\Psi_n(x)$, and $\Theta_n(x)$ are coming from equation (3.69) – (3.71).

(ii) For the damage model of a wind turbine blade

a. Bernoulli-Euler type model:

$$u(x,t) = \sum_{n=1}^{N} U_n(x) q_n(t) \tag{3.93}$$

$$\psi(x,t) = \sum_{n=1}^{N} \Psi_n(x) q_n(t) \tag{3.94}$$

where $U_n(x)$ and $\Psi_n(x)$ are coming from equation (3.72) – (3.73).

b. Timoshenko type model:

$$u(x,t) = \sum_{n=1}^{N} U_n(x) q_n(t) \tag{3.95}$$

$$\psi(x,t) = \sum_{n=1}^{N} \Psi_n(x) q_n(t) \tag{3.96}$$

$$\theta(x,t) = \sum_{n=1}^{N} \Theta_n(x) q_n(t) \tag{3.97}$$

where $U_n(x)$, $\Psi_n(x)$, and $\Theta_n(x)$ are coming from equation (3.74) – (3.76).

4. APPLICATIONS OF THE MODELS ESTABLISHED

In the verification of the models established (i.e., the IEPIM and the damage models), the following steps were realized:

i. The results of the IEPIM are evaluated by using the results of two different experimental studies, borrowed from the open literature, in terms of the relative error,

ii. The results of the damage models are compared with the results of relevant experimental studies, taken form the open literature. In this context, firstly, the dynamic characteristics of an aircraft wing and a wind turbine blade are obtained in the free vibration analysis. Then, by using the dynamic characteristics, deflections occurred in the aircraft wing and wind turbine blade are obtained in terms of bending, torsional, and rotational deflections depending on the type of the model in the forced vibration analysis.

The material properties for an aircraft wing, a wind turbine blade, and a thin-walled beam that are used in the applications are given in Table 4.1

Table 4.1: Material properties of structures that are used in the applications.

Material properties	Goland wing [63]	Wind turbine blade [64]	Thin walled beam [65]
Bending rigidity (EI) (Nm^2)	9.75×10^6	2.2101×10^7	6380
Torsional rigidity (GJ) (Nm^2)	9.88×10^5	5.1483×10^6	43.46
Shear rigidity (kAG) (N)	27×10^{71}	6.081×10^{103}	4.081×10^6
Mass per unit length (m) (kg/m)	35.75	112.0	0.835
Mass moment of inertia per unit length (I_α) (kgm)	8.65	21.8	0.501×10^{-3}
Distance between mass center and shear center (x_α) (m)	0.18	0.153	0.0155
Inertia term (ρI) (kgm)	5.65×10^{-32}	0.25×10^{-34}	0.25×10^{-3}
Length (L) (m)	6	12	0.82

The graphics and results of the models established are realized in the Mathematica and MATLAB/Simulink environment with the codes developed by the user.

[1,2,3,4] These values are taken as approximate values by the user.

4.1 Verification of Improved Electromagnetic Pressure Impact Model

Martins in [14] provided an experimental database to understand the direct effects of lightning strike and validate the lightning arc physical model. The author obtained the value of the electromagnetic pressure impact (EPI) of lightning for $100\ kA$ lightning current by using a current generator. The author showed that for $100\ kA$ lightning current, the radius of the arc channel is about 3.5 mm nearly at $t = 2.6\ \mu s$. $100\ kA$ lightning current is regarding with the component D waveform of lightning as shown in Figure 2.3. Thus, by using equation (2.2), the radius of the arc channel of lightning are found to be reached about 3.6 mm at $t = 2.6\ \mu s$, as shown in Table 4.2, in the present thesis. This result proves that the database provided by Martins and the model of the radius of the arc channel of lightning given in equation (2.2) are consistent.

Table 4.2: Radius of the arc channel at some instants.

Time step (μs)	Lightning current (A)	Length of the radius of the arc channel of lightning (m)
0	0	0
0.5	50899	0.00128
1.0	76968	0.00207
1.5	90047	0.00268
2.0	96332	0.00316
2.5	99066	0.00357
2.6	**99354**	**0.00365**
3.0	99948	0.00392

In another experimantal study, Martins et al. [66] obtained the value of the electromagnetic pressure impact for different lightning currents by using EMMA and SuperDICOM (SDICOM) lightning high current generators at four instants, $t = 6, 9, 14,$ and $26\ \mu s$. In this experimental study, the generators were permitted to transmit intense currents by a conduction electrical arc on a test sample connected to a rig made of aluminum plate. The magnitudes of the electromagnetic pressure impact models obtained in the experimental studies and the magnitudes of the IEPIM are evaluated for $100\ kA$ lightning current in Table 4.3 and for $200\ kA$ lightning current in Table 4.4, in terms of relative errors at the instants $t = 6, 9, 14,$ and $26\ \mu s$. As indicated in Table 4.3 and Table 4.4, it is found that while the results of the IEPIM for $100\ kA$ lightning current are more consistent with the results of certain generators at

certain time points, the results of the IEPIM for 200 kA lightning current are more consistent with the results obtained using the generator so-called SDICOM. More precisely, the results of the IEPIM for 100 kA lightning current are closer to the results of SDICOM at $t = 6$ and 9 μs and closer to the results of EMMA at $t = 14$ and 26 μs, as shown in Table 4.3. On the other hand, the results of the IEPIM for 200 kA lightning current are closer to the result of EMMA at $t = 6$ μs and closer to the results of SDICOM at $t = 9, 14,$ and 26 μs, as shown in Table 4.4. Here, it can be notice that the results of the IEPIM are quite consistent with the results of two experimental studies up to the first 26 microseconds for 100 kA lightning current. At the 26th microsecond, the amount of the relative error is found to be relatively higher. Since 100 kA lightning current is associated with a short-duration component D waveform with a rise time of up to 25 μs [13], the relative error at $t = 26$ μs for 100 kA lightning current can be neglected. This proves that component D waveform is valid before 26 μs. In contrast, it is seen that the results of the IEPIM are quite consistent with the results of the experimental study for 200 kA lightning current. 200 kA lightning current is associated with component A waveform, as shown in Figure 2.3, with a rise time of less than 50 μs [13].

Table 4.3: Magnitudes of the pressure models for 100 kA lightning current.

Magnitude of the electromagnetic pressure impact of lightning							
Time (μs)	For 100kA lightning current						
	IEPIM (Pa)	EMMA [66] (Pa)	Relative error (%)	SDICOM [66] (Pa)	Relative error (%)	EPI [14] (Pa)	Relative error (%)
$t = 6$	31.9e + 05	29.6e + 05	7.7	33.1e + 05	3.6	40.1e + 05	20.4
$t = 9$	30.1e + 05	25.1e + 05	19.9	28.1e + 05	7.1	28.1e + 05	7.1
$t = 14$	24.0e + 05	23.7e + 05	1.3	20.5e + 05	17.1	15.2e + 05	57.9
$t = 26$	17.6e + 05	12.4e + 05	41.9	12.0e + 05	46.7	8.3e + 05	112.0

Table 4.4: Magnitudes of the pressure models for 200 kA lightning current.

Magnitude of the electromagnetic pressure impact of lightning					
Time (μs)	For 200kA lightning current				
	IEPIM (Pa)	EMMA [66] (Pa)	Relative error (%)	SDICOM [66] (Pa)	Relative error (%)
$t = 6$	37.6 + 05	36.3e + 05	3.6	40.7e + 05	7.6
$t = 9$	36.5e + 05	32.4e + 05	12.7	36.3e + 05	0.6
$t = 14$	32.8e + 05	27.3e + 05	20.1	30.2e + 05	8.6
$t = 26$	21.9e + 05	20.9e + 05	4.8	22.1e + 05	0.9

4.2 Verification of Damage Models

4.2.1 Free vibration analysis

In the free vibration analysis, the vibration frequencies and vibration mode shapes are determined depending on the boundary conditions.

4.2.1.1 Vibration frequencies

(i) For an aircraft wing

The thin-walled beam example, whose material properties are given in Table 4.1, is a good example for comparing two different types of beam models with the same material properties because the data for this example are available in the literature for both Bernoulli-Euler-type and Timoshenko-type models. For this reason, the thin-walled beam example with C-F boundary condition is solved separately by using DTM for these models in case of coupled ($x_\alpha \neq 0$) case, and then the results are compared with the results in the available literature, as in Table 4.5. As shown in Table 4.5, a very good agreement is found between the results of DTM and the results of the relevant studies in the literature in terms of relative error. Moreover, Table 4.5 shows that the vibration frequencies of Timoshenko type model are lower valued compared to the vibration frequencies of Bernoulli-Euler type model.

Table 4.5: Vibration frequencies of thin-walled beam for C-F boundary condition.

Vibration frequencies of thin-walled beam								
VF (Hz)	Timoshenko type model (TM)			Bernoulli-Euler type model (BEM)			|BEM-TM|	
	DTM[1]	Ref. [65]	ε_{rel} (%)	DTM[2]	Ref. [67]	ε_{rel} (%)	$\lvert DTM^2 - DTM^1 \rvert$	$\lvert$ Ref. [67] $-$ Ref. [65]$\rvert$
ω_1	62.4	62.4	0.00	62.60	62.60	0.00	0.20	0.20
ω_2	129.9	129.9	0.00	130.18	130.18	0.00	0.28	0.28
ω_3	259.2	259.0	0.08	261.15	261.15	0.00	1.95	2.15
ω_4	418.9	418.0	0.22	421.36	421.36	0.00	2.46	3.36
ω_5	605.1	–	–	612.09	612.09	0.00	6.99	–
ω_6	636.2	–	–	655.86	–	–	19.66	–

Then, to obtain the vibration frequencies of an aircraft wing according to both Bernoulli-Euler type model and Timoshenko type model, Goland wing example with C-F boundary condition, whose features are given in Table 4.1, is considered. For Timoshenko type model, the value of the shear rigidity kAG (N) and inertia term ρI (kgm) are taken approximately as 27×10^7 and 5.65×10^{-3}, repectively, and then the vibration frequencies are obtained in the case of coupled case and uncoupled

case ($x_\alpha = 0$) by using DTM. As shown in Table 4.6, when the results of DTM are compared with the results of the reference [63], DTM provides quite satisfactory results with respect to relative error. Moreover, Table 4.6 shows that, as in the thin-walled beam example, for the coupled case, the vibration frequencies of Timoshenko type model are lower than the vibration frequencies of Bernoulli-Euler type model with approximately the same sensitivity. This represents that the results of Timoshenko type model are acceptable for the shear rigidity and inertia term values considered. Moreover, compared the vibration frequencies in the uncoupled case with these of the coupled case, it is seen that there is no smooth increase or decrease between these two cases, which shows that the values of the vibration frequencies in the uncoupled case do not cause a decisive change on the results of the model.

Table 4.6: Vibration frequencies of Goland wing for C-F boundary condition.

Vibration frequencies of Goland wing							
VF (Hz)	Timoshenko type model		Bernoulli-Euler type model				
	DTM		DTM		Ref. [63]	ε_{rel} (%)	|BEM-TM|
	Uncoupled	Coupled	Uncoupled	Coupled	Coupled	Coupled	Coupled
ω_1	8.09	7.87	8.11	7.89	7.89	0.00	0.02
ω_2	14.08	15.44	14.08	15.44	15.44	0.00	0.00
ω_3	42.24	39.42	42.24	39.60	39.60	0.00	0.18
ω_4	50.06	56.07	50.87	56.59	56.59	0.00	0.52
ω_5	70.41	71.55	70.41	71.85	71.85	0.00	0.30
ω_6	98.57	96.97	98.57	97.13	97.11	0.02	0.16

(ii) For a wind turbine blade

As in the aircraft wing application, to compare two different models for the same material properties in the wind turbine blade application, an axially loaded thin-walled beam example whose properties are given in Table 4.1 is used. In this context, the vibration frequencies of Timoshenko type model and Bernoulli-Euler type model are obtained by using DTM for C-F, C-C, and S-S boundary conditions and different axial load values; and then the results are given in Table 4.7 - Table 4.9. These tables show that the results of Timoshenko type model and Bernoulli-Euler type model are quite compatible with the references in terms of relative error. This confirms the reliability of the existing DTM solutions for Timoshenko type model and Bernoulli-Euler type model.

Table 4.7: Vibration frequencies of thin-walled beam for C-F boundary condition.

Vibration frequencies of thin-walled beam						
VF (Hz)	Timoshenko type model ($P = 5370\ N$)			Bernoulli-Euler type model ($P = 1790\ N$)		
	DTM	Ref. [68]	ε_{rel} (%)	DTM	Ref. [67]	ε_{rel} (%)
ω_1	54.17	54.72	1.00	60.23	60.23	0.00
ω_2	126.02	124.46	1.25	128.42	128.42	0.00
ω_3	249.53	249.51	0.01	257.96	257.96	0.00
ω_4	402.07	401.16	0.23	415.54	415.54	0.00
ω_5	584.03	584.11	0.01	604.60	604.60	0.00
ω_6	623.91	-	-	652.64	-	-

Table 4.8: Vibration frequencies of thin-walled beam for C-C boundary condition.

Vibration frequencies of thin-walled beam						
VF (Hz)	Timoshenko type model ($P = 17900\ N$)			Bernoulli-Euler type model ($P = 1790\ N$)		
	DTM	Ref. [68]	ε_{rel} (%)	DTM	Ref. [67]	ε_{rel} (%)
ω_1	150.29	148.56	1.16	171.77	171.77	0.00
ω_2	305.34	303.33	0.66	349.05	349.05	0.00
ω_3	453.59	449.93	0.81	515.85	515.85	0.00
ω_4	579.07	585.79	1.14	628.89	628.89	0.00
ω_5	615.57	613.11	0.40	703.12	703.12	0.00
ω_6	772.82	-	-	882.69	-	-

Table 4.9: Vibration frequencies of thin-walled beam for S-S boundary condition.

Vibration frequencies of thin-walled beam				
VF (Hz)	Timoshenko type model ($P = 14320\ N$)	Bernoulli-Euler type model ($P = 1790\ N$)		
	DTM	DTM	Ref. [67]	ε_{rel} (%)
ω_1	150.29	146.20	146.20	0.00
ω_2	305.34	316.81	316.81	0.00
ω_3	453.59	339.90	339.90	0.00
ω_4	579.07	522.45	522.45	0.00
ω_5	615.57	702.28	702.28	0.00
ω_6	772.82	881.102	-	-

After verification of Timoshenko type model and Bernoulli-Euler type model for an axially loaded beam for different boundary conditions, the wind turbine example whose properties are given in Table 4.1 are taken into account for an application of the wind turbine blade. Considering the material properties of a wind turbine blade given in the reference, the shear rigidity kAG and inertia term ρI are taken as 6.081×10^{10}

and 0.25×10^{-3} respectively for Timoshenko type model, and then the results of both models for C-F Boundary conditions are obtained by using DTM in the case of absence and existence of the axial load, as shown in Table 4.10. Table 4.10 shows that the differences between the vibration frequencies of both models obtained by using DTM are approximately as small as in the thin-walled beam example. This proves that the shear rigidity and inertia term considered for Timoshenko model of the wind turbine blade provide good accuracy.

Table 4.10: Vibration frequencies of wind turbine blade for C-F boundary condition.

Vibration frequencies of wind turbine blade via DTM								
Axial force	VF (Hz)	Timoshenko type model (TM)		Bernoulli-Euler type model (BEM)				
		DTM		DTM		Ref. [64]	ε_{rel} (%)	|BEM-TM|
		Uncoupled	Coupled	Uncoupled	Coupled	Coupled	Coupled	Coupled
$(P = 0\ kN)$	ω_1	1.72	1.72	1.72	1.72	1.72	0.00	0.00
	ω_2	10.12	10.24	10.12	10.24	10.24	0.00	0.00
	ω_3	10.82	11.33	10.82	11.33	11.33	0.00	0.00
	ω_4	30.28	28.56	30.29	28.56	28.56	0.00	0.00
	ω_5	30.37	33.78	30.37	33.78	33.78	0.00	0.00
	ω_6	50.62	51.22	50.63	51.22	51.22	0.00	0.00
$(P = 190\ kN)$	ω_1	1.24	1.24	1.24	1.24	1.24	0.00	0.00
	ω_2	10.09	9.96	10.09	9.93	9.93	0.00	0.03
	ω_3	10.36	11.13	10.36	11.16	11.16	0.00	0.03
	ω_4	29.90	28.23	29.91	28.22	28.22	0.00	0.01
	ω_5	30.26	33.62	30.27	33.65	33.65	0.00	0.03
	ω_6	50.44	50.94	50.44	50.91	50.91	0.00	0.03

Then, the vibration frequencies of the wind turbine blade are obtained for C-C and S-S boundary conditions in both type models. In this context, the vibration frequencies of the wind turbine blade are given in Table 4.11 for different values of the axial load. As seen in Table 4.11, the results of Bernoulli-Euler type model are close to the results of Timoshenko type model with approximately same sensitivity of the results of the axial-loaded thin-walled beam example for C-C and S-S boundary conditions. Additionally, when the changes in the frequencies of the uncoupled case of the models are examined, it is found that the vibration frequencies in the uncoupled cases do not increase or decrease in a certain order, but increase or decrease locally, compared to the coupled cases. This shows that the effect of the uncoupled case has a negligible effect in the case of free vibration analysis.

Table 4.11: Vibration frequencies of a wind turbine blade for C-C and S-S boundary conditions.

Vibration frequencies of wind turbine blade via DTM									
		C-C				S-S			
Axial force	VF (Hz)	Timoshenko type model		Bernoulli-Euler type model		Timoshenko type model		Bernoulli-Euler type model	
		Uncoup.	Coupled	Uncoup.	Coupled	Uncoup.	Coupled	Uncoup.	Coupled
$(P = 0\ kN)$	ω_1	10.98	10.74	10.98	10.74	4.84	4.83	4.84	4.82
	ω_2	20.25	22.03	20.24	22.03	19.38	19.06	19.39	19.07
	ω_3	30.28	28.66	30.29	28.66	20.25	21.67	20.24	21.66
	ω_4	40.50	45.40	40.50	45.39	40.50	41.48	40.50	41.49
	ω_5	59.35	52.07	59.36	52.08	43.61	43.91	43.61	43.91
	ω_6	60.75	73.35	60.75	73.35	60.75	68.08	60.75	68.09
$(P = 190\ kN)$	ω_1	10.82	10.57	10.82	10.57	4.53	4.51	4.54	4.52
	ω_2	20.18	21.95	20.18	21.96	19.08	18.75	19.08	18.75
	ω_3	30.05	28.44	30.05	28.43	20.18	21.59	20.18	21.60
	ω_4	40.35	45.23	40.35	45.26	40.35	41.18	40.35	41.16
	ω_5	59.10	51.83	59.11	51.80	43.30	43.76	43.31	43.77
	ω_6	60.53	73.11	60.53	73.15	60.53	67.86	60.53	67.85

4.2.1.2 Vibration mode shapes

(i) For an aircraft wing

For an aircraft wing application, first of all, the first five consecutive vibration mode shapes for C-F boundary condition of the thin-walled beam are obtained for both Timoshenko type and Bernoulli-Euler type models, as shown in Figure 4.1. Then, compared the vibration mode shapes obtained with the results of the studies in references [67] and [68], a very good agreement is found between the results. Moreover, when the vibration mode shapes of Timoshenko type model are compared with these of Bernoulli-Euler type model, it is seen that the vibration mode shapes are quite similar in terms of form, including amplitudes. However, unlike Bernoulli-Euler type model, Timoshenko type model also includes a rotational vibration mode that is shown in green color.

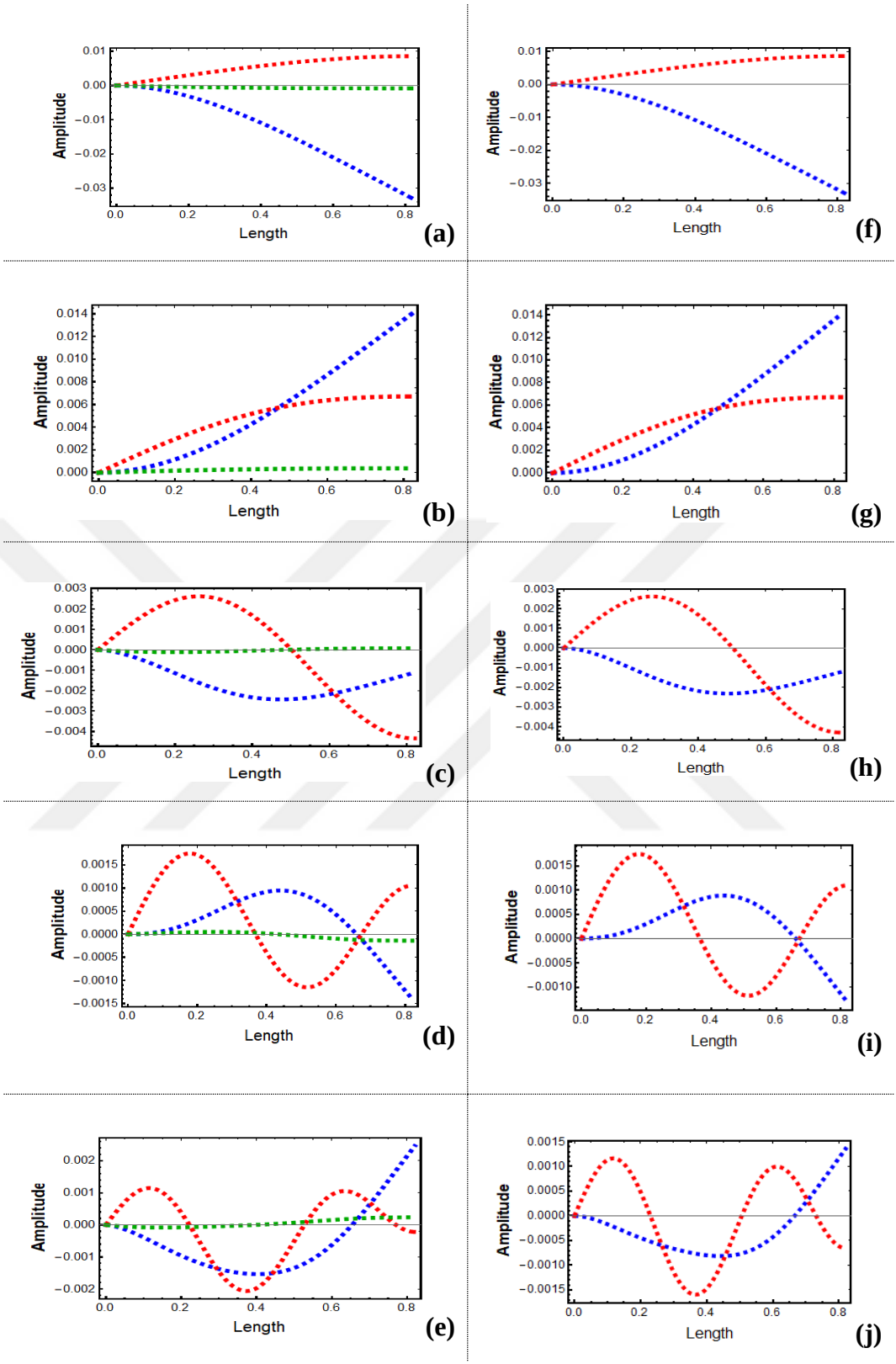

Figure 4.1: First five consecutive vibration mode shapes of thin-walled beam for C-F boundary condition (blue: bending, red: torsion, green: torque), (a)-(e) Timoshenko type model, (f)-(j) Bernoulli-Euler type model.

In the application of Goland aircraft wing example, the first five vibration mode shapes are obtained for C-F boundary condition of both Timoshenko type model and Bernoulli-Euler type model, and then the results are shown in Figure 4.2. The vibration mode shapes obtained for Bernoulli-Euler type model are found to be quite compatible with the vibration mode shapes in reference [63]. Moreover, as in the thin-walled beam example, the mode shapes of Timoshenko type model are found to be very similar to the vibration mode shapes of Bernoulli-Euler type model in terms of both amplitude and form. This shows that the results of Goland wing for Timoshenko type model with the data provided in Table 4.1 are acceptable.

(ii) For a wind turbine blade

For a wind turbine blade application, first of all, the first five consecutive vibration mode shapes of the thin-walled beam are obtained for C-F, C-C, and S-S boundary condition of Timoshenko type model and Bernoulli-Euler type model when the values of the axial load P is $P = +5380\ N$, and then the results obtained are shown in Figure 4.3. As seen in Figure 4.3, the results of Timoshenko type model are quite compatible with the results of reference [63].

Then, the first four consecutive vibration mode shapes of a wind turbine blade are obtained for Timoshenko type model and Bernoulli-Euler type model for different boundary conditions and axial load values of the blade. In this context, first of all, the change of the first four consecutive vibration mode shapes for C-F boundary condition of Bernoulli-Euler type model are obtained for the case of P being $0\ N$ and $190{,}000\ N$, respectively; and then the results were given in Figure 4.4. When the vibration mode shapes in Figure 4.4 were compared with the vibration mode shapes obtained in reference [64], a very good agreement was found between the results. Moreover, Figure 4.4 showed that even if the value of P is increased between $0\ N$ and $190{,}000\ N$, the vibration mode shapes do not change. Subsequently, for the same P values, the vibration mode shapes of Timoshenko type model are obtained for C-F boundary condition and the results were given in Figure 4.5. When Figure 4.4 and Figure 4.5 were compared, it has been seen that the mode shapes of both models are largely similar. This shows that the mode shapes of the wind turbine blade are highly correct for the Timoshenko type model.

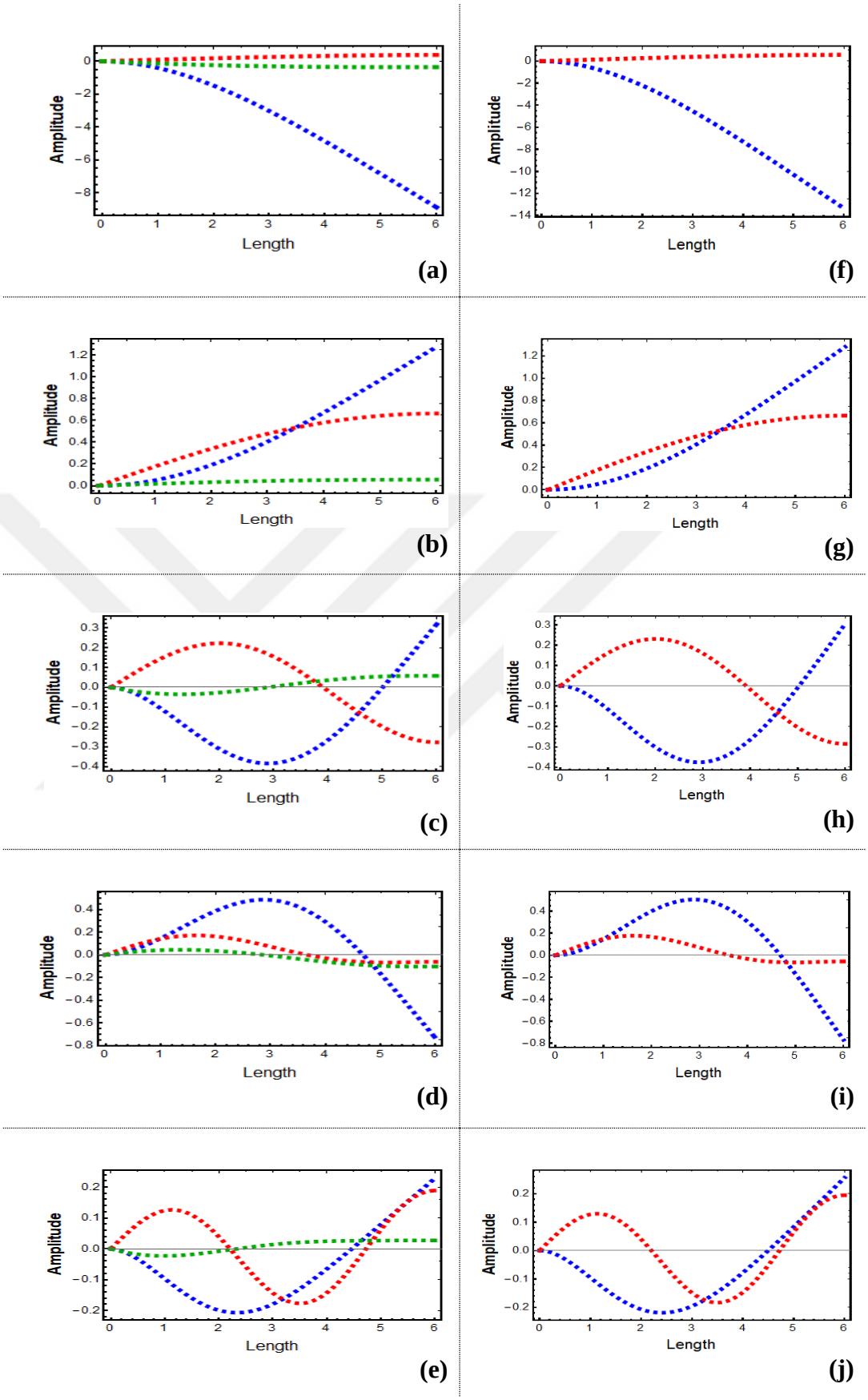

Figure 4.2: First five consecutive vibration mode shapes of Goland wing for C-F boundary condition (blue: bending, red: torsion, green: cross section rotation), (a)-(e) Timoshenko type model, (f)-(j) Bernoulli-Euler type model.

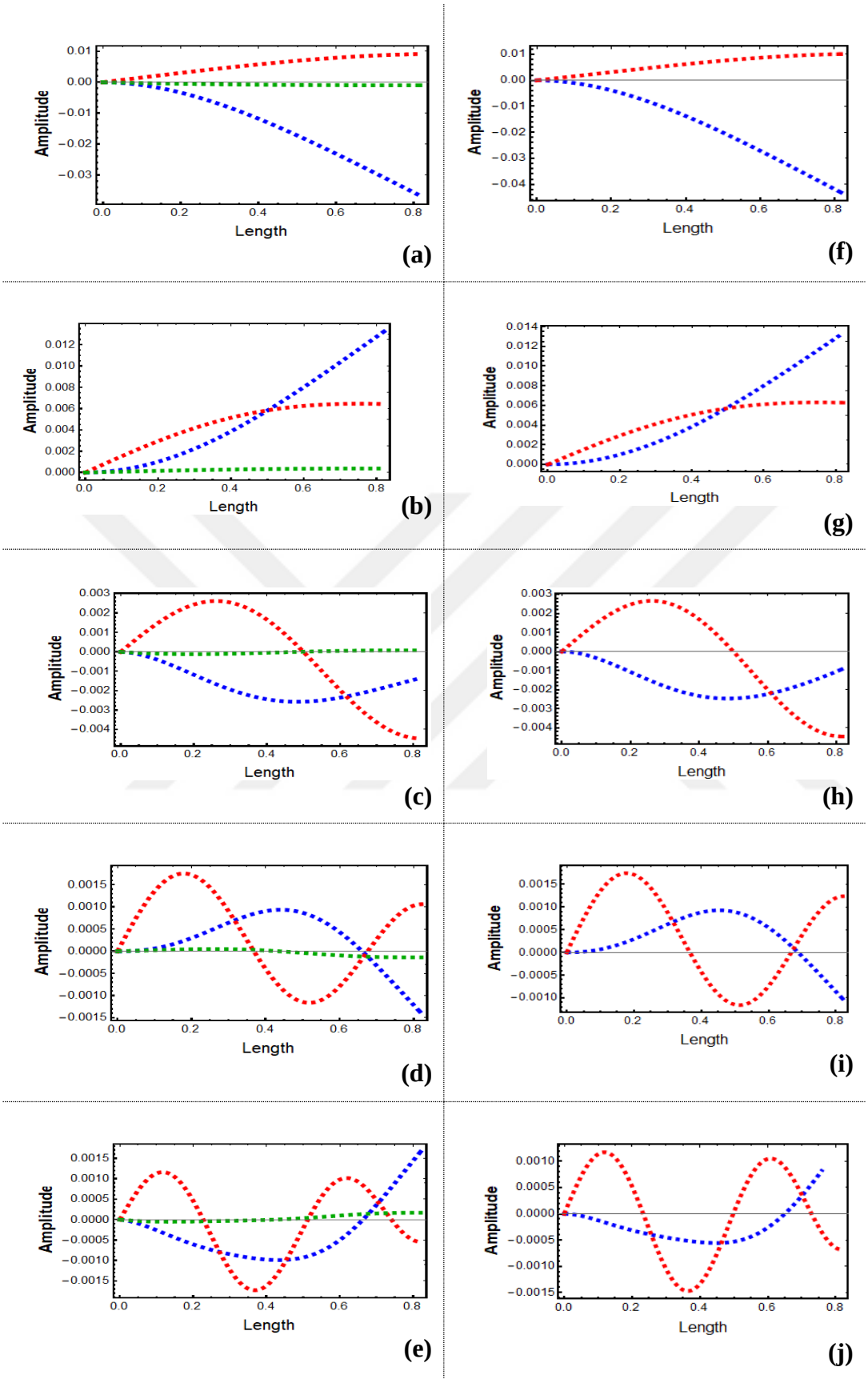

Figure 4.3: First five consecutive vibration mode shapes of axially loaded thin-walled beam for C-F BC (blue: bending, red: torsion, green: cross section rotation) when $P = 5370\ N$, (a)-(e) Timoshenko type model, (f)-(j) Bernoulli-Euler type model.

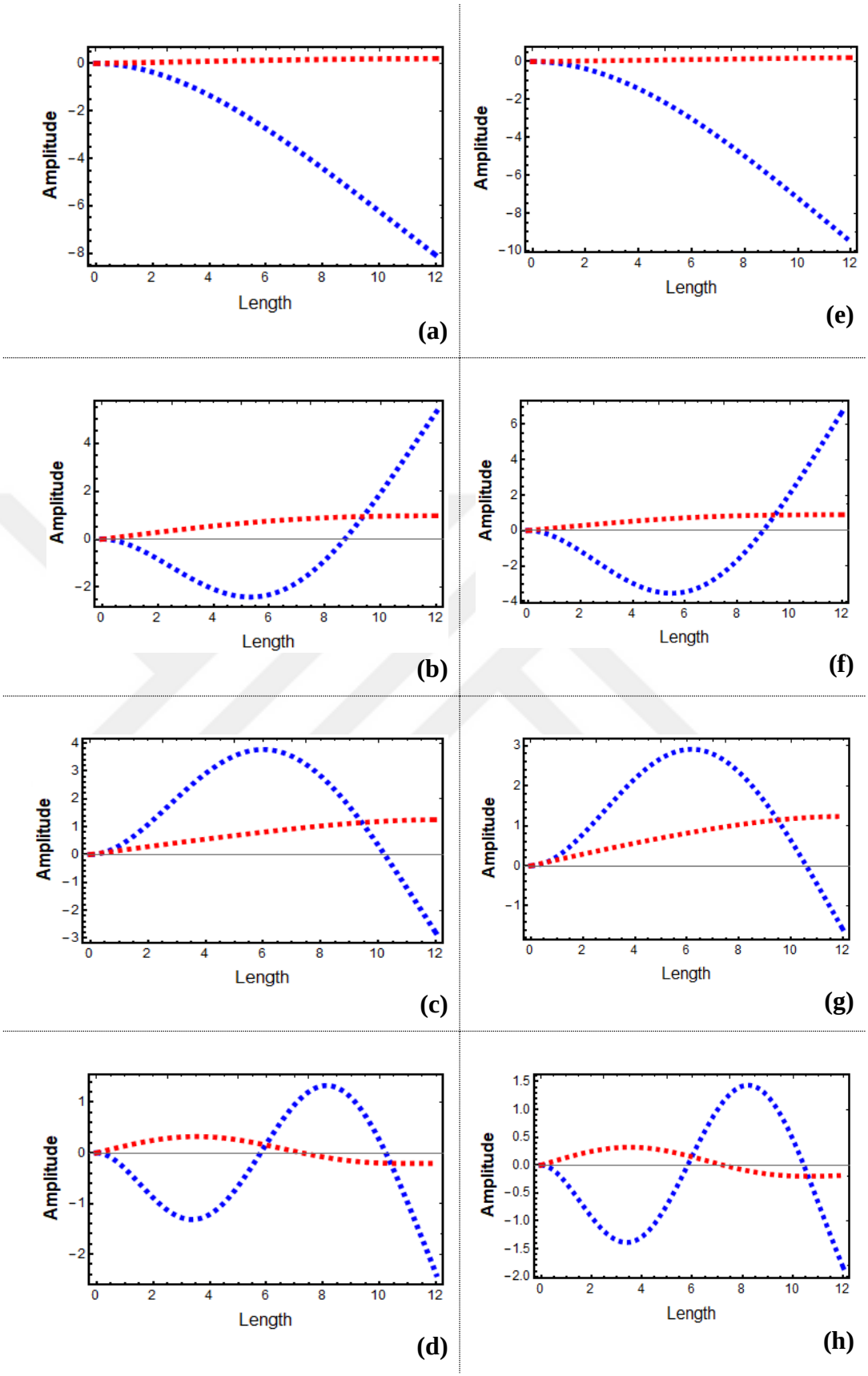

Figure 4.4: First four consecutive vibration mode shapes of a wind turbine blade for Bernoulli-Euler type model with C-F boundary condition (blue: bending, red: torsion), (a)-(d) when $P = 0\ N$, (e)-(h) when $P = 190{,}000\ N$.

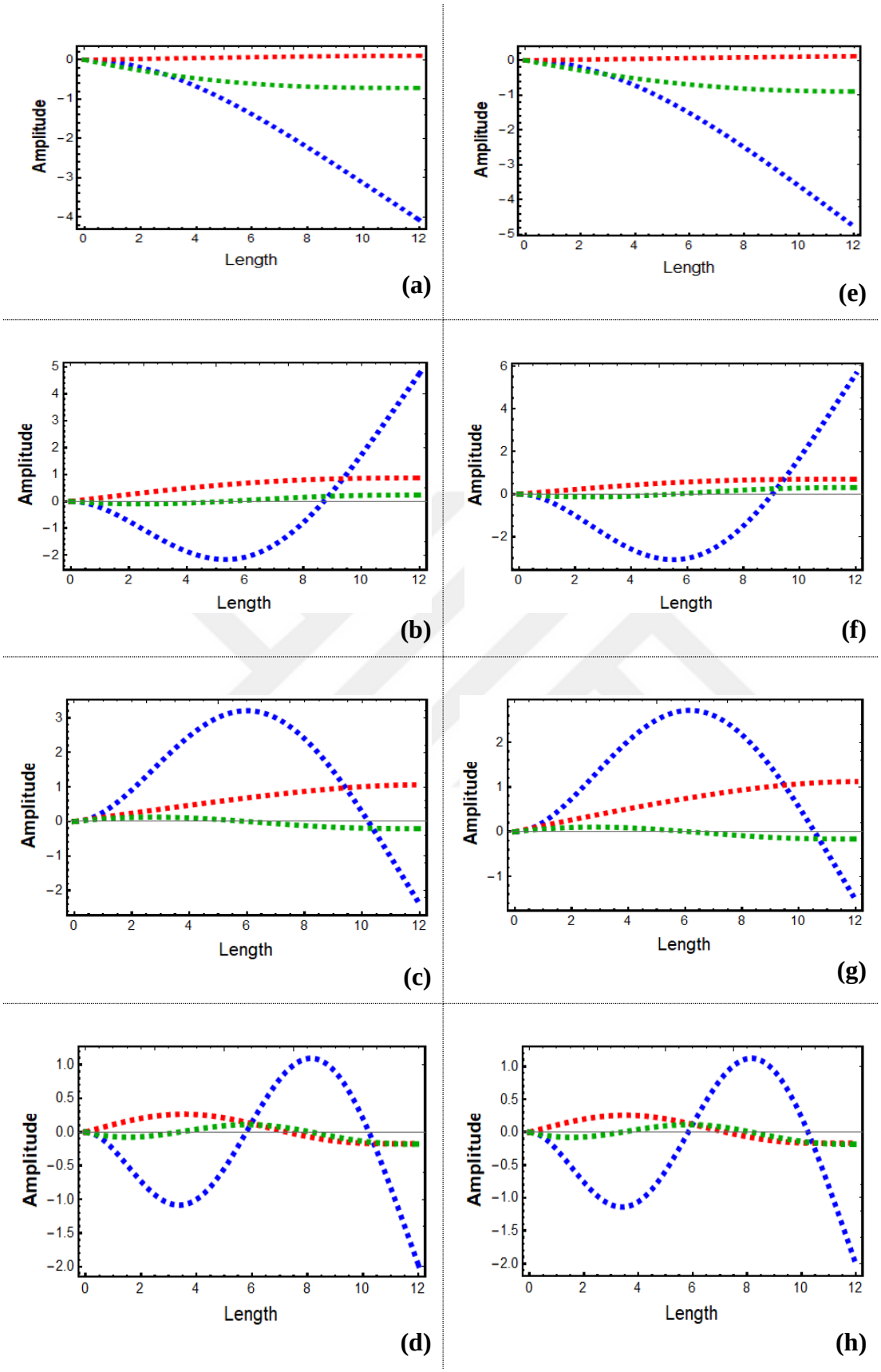

Figure 4.5: First four consecutive vibration mode shapes of a wind turbine blade for Timoshenko type model with C-F boundary condition (blue: bending, red: torsion, green: cross section rotation), (a)-(d) when $P = 0\ N$, (e)-(h) when $P = 190{,}000\ N$.

Then, the vibration mode shapes of the wind turbine blade for C-C and S-S boundary conditions were obtained and then the results were presented for both models as in Figure 4.6- Figure 4.9. As seen in these figures, the results of Bernoulli-Euler type model and Timoshenko type model were quite consistent with each other, as in C-F boundary condition.

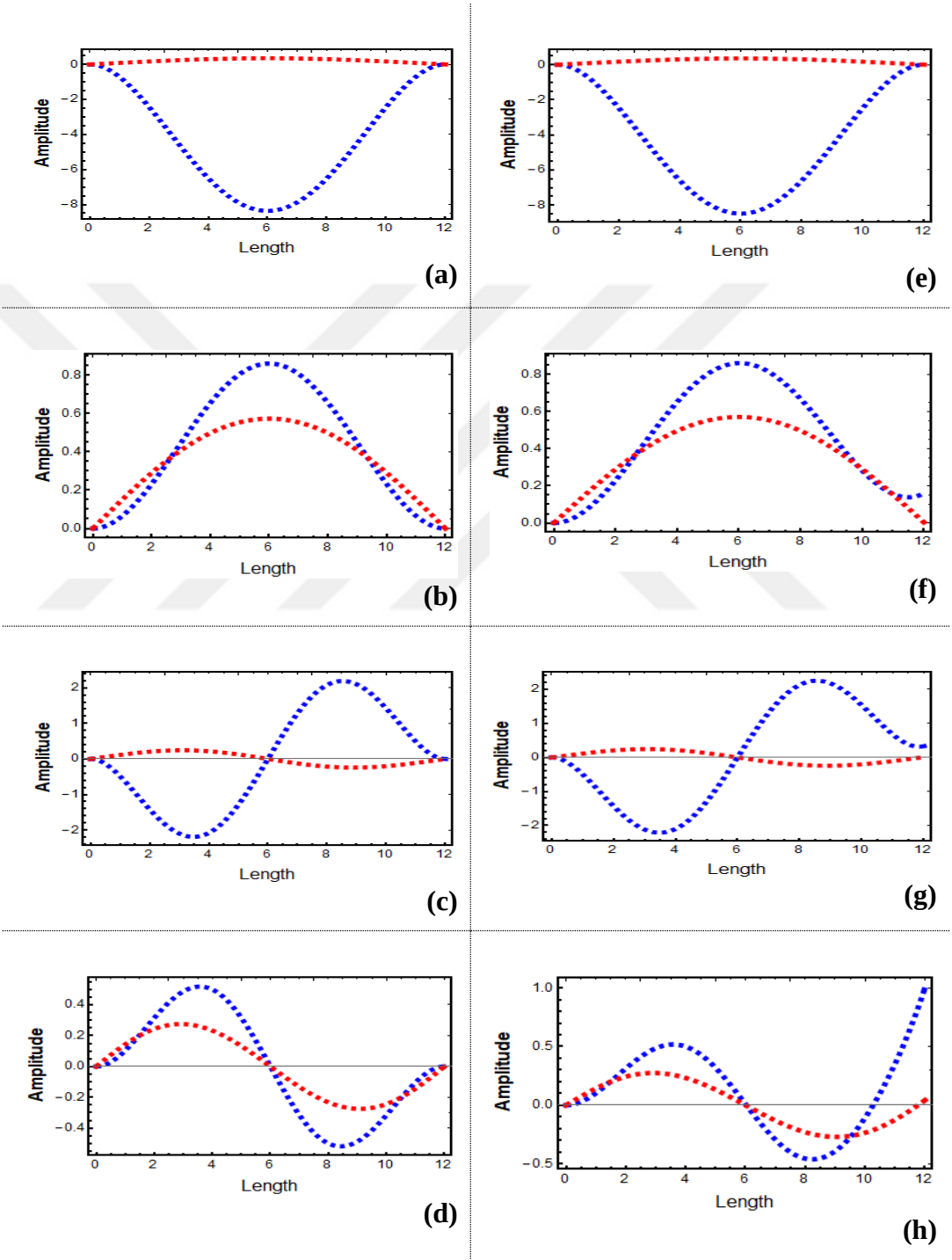

Figure 4.6: First four consecutive vibration mode shapes of a wind turbine blade for Bernoulli-Euler type model with C-C boundary condition (blue: bending, red: torsion), (a)-(d) when $P = 0\ N$, (e)-(h) when $P = 190{,}000\ N$.

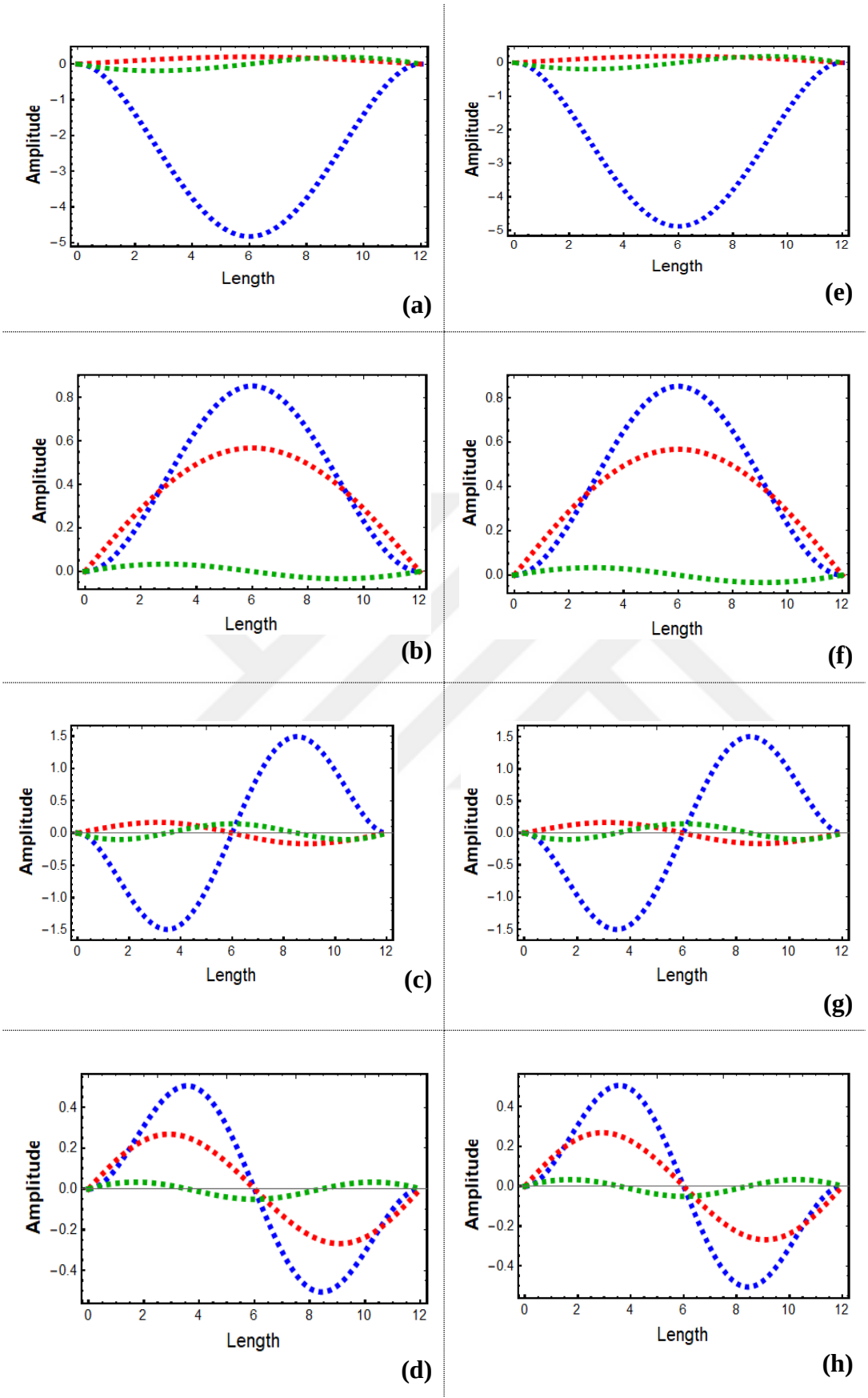

Figure 4.7: First four consecutive vibration mode shapes of a wind turbine blade for Timoshenko type model with C-C boundary condition (blue: bending, red: torsion, green: cross section rotation), (a)-(d) when $P = 0\ N$, (e)-(h) when $P = 190{,}000\ N$.

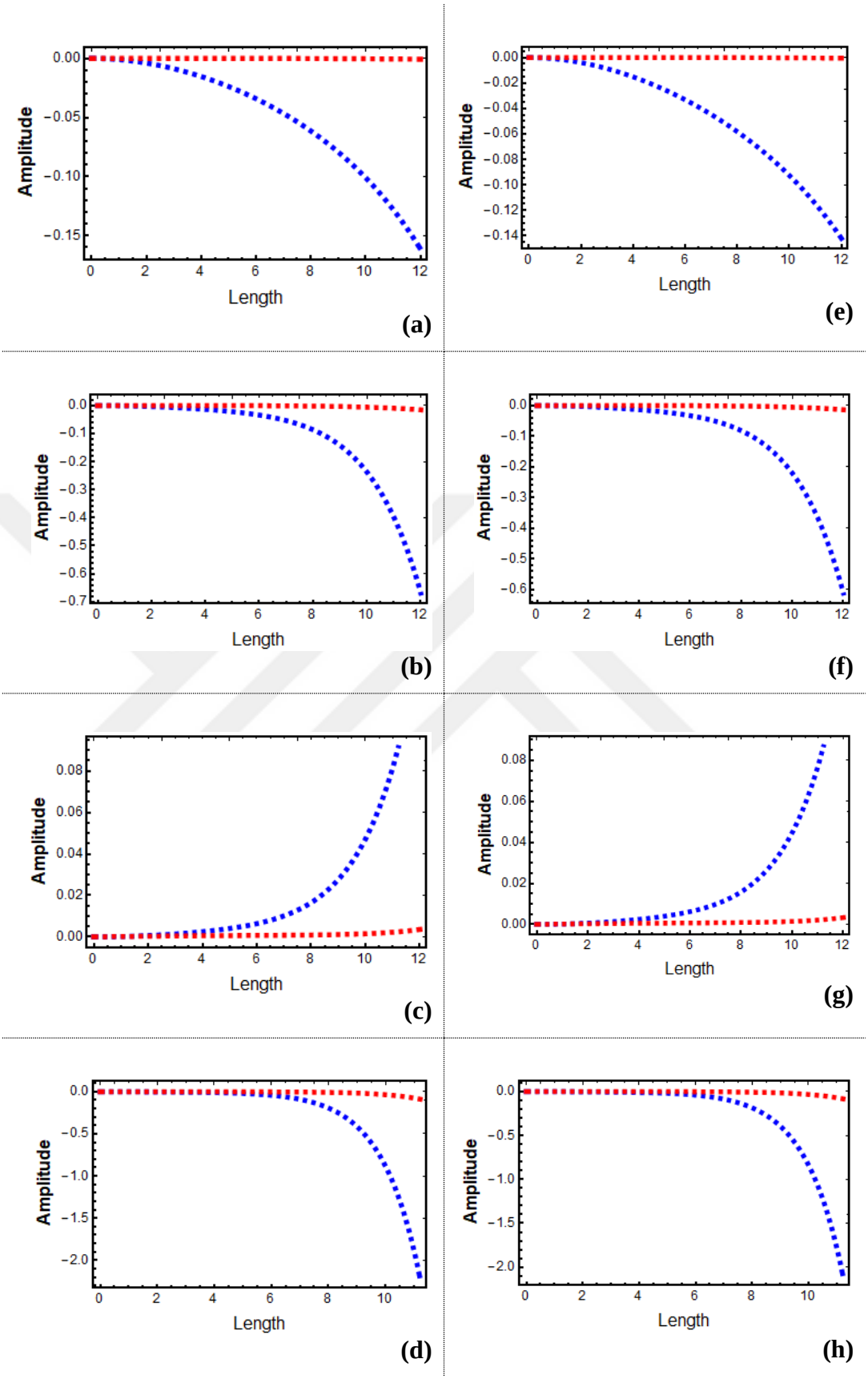

Figure 4.8: First four consecutive vibration mode shapes of a wind turbine blade for Bernoulli-Euler type model with S-S boundary condition (blue: bending, red: torsion), (a)-(d) when $P = 0\ N$, (e)-(h) when $P = 190{,}000\ N$.

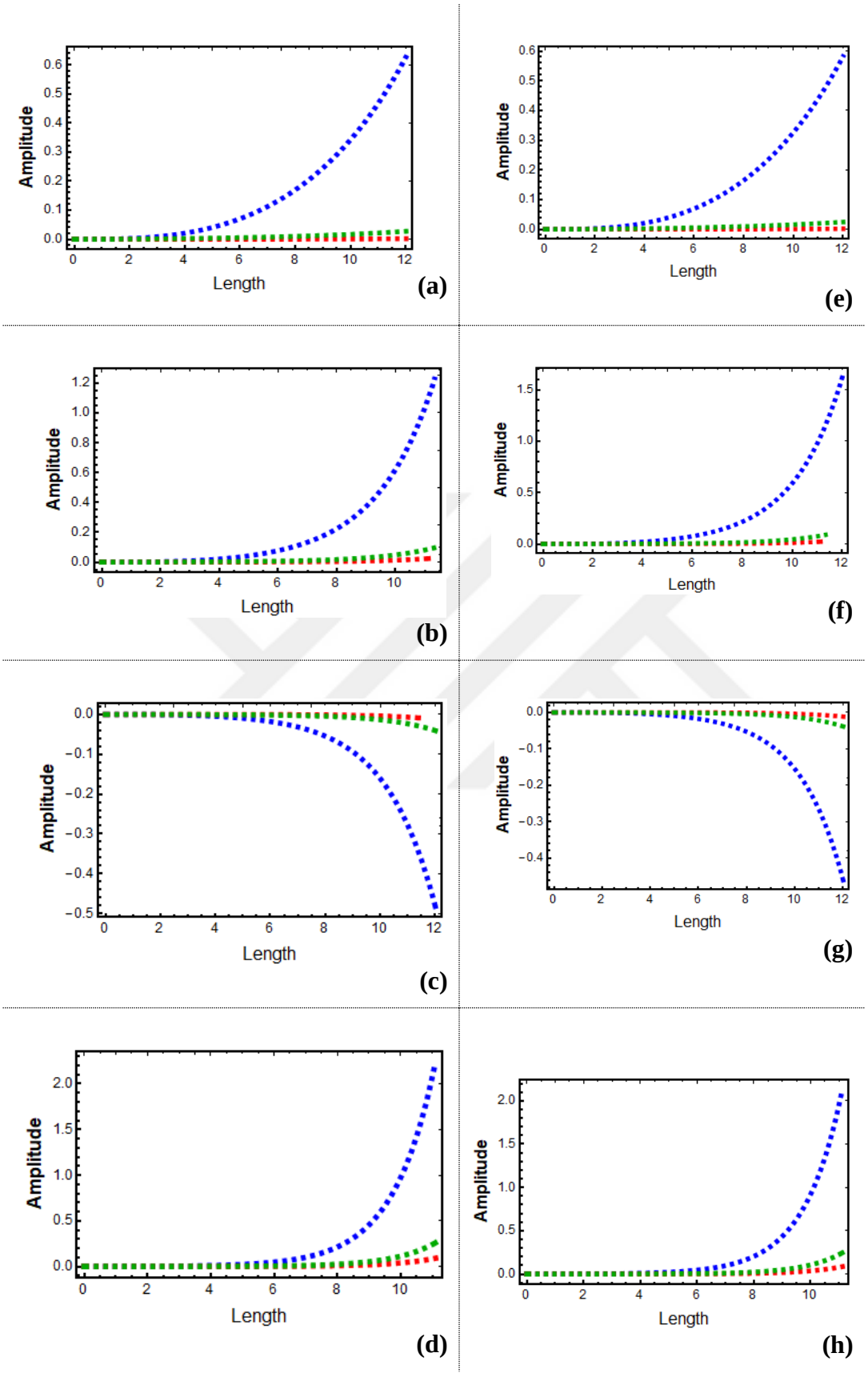

Figure 4.9: First four consecutive vibration mode shapes of a wind turbine blade for Timoshenko type model with S-S boundary condition (blue: bending, red: torsion, green: torque), (a)-(d) when $P = 0\ N$, (e)-(h) when $P = 190{,}000\ N$.

Additionally, according to the safety factor used in the design of aerospace structures, the limit (i.e., ultimate) load that the structure can carry was determined depending on the cross-sectional area of the structure for the aluminum alloy AL2024 T351 (This material is the most used in aviation and aircraft structures and has very strong strength [69]). Then, under this ultimate load, the vibration mode shapes of the structure at different boundary conditions were determined with respect to cross-sectional area of the structure and the direction of the axial crush loading. In general engineering practice, the structures are designed for a factor of security (FOS) times the ultimate load [70]. The FOS is at least 1.5 in aerospace structures [70]. On the other hand, using the data in reference [71], the cross-sectional area A of the wind turbine blade was found to be $0.081\ m^2$. According to mechanical propertis of aerospace aluminium alloy AL 2024-T351 given in [69], the tensile strength $\sigma_{tensile}$ is $428\ MPa$. Thus the ultimate axial load $P_{tensile}$ (i.e., $\left(\frac{\sigma_{tensile}}{FOS}\right) \times A$) at which the wind turbine balde can operate safely was nearly found as $231e+05\ N$. Under this ultimate axial load, the vibration modes of the wind turbine blade were obtained for C-F, C-C, and S-S boundary conditions, and then the results were presented in Figure 4.10- Figure 4.12 for both models. As can be seen from these figures, the vibration mode shapes of the wind turbine blade for the Timoshenko type and the Bernoulli-Euler type model varies considerably under the ultimate axial load compared to its characteristic vibration modes in the absence of axial tensile load. In addition, the vibration mode shapes of the wind turbine blade under the ultimate axial tensile load are significantly affected by the type of the boundary conditions.

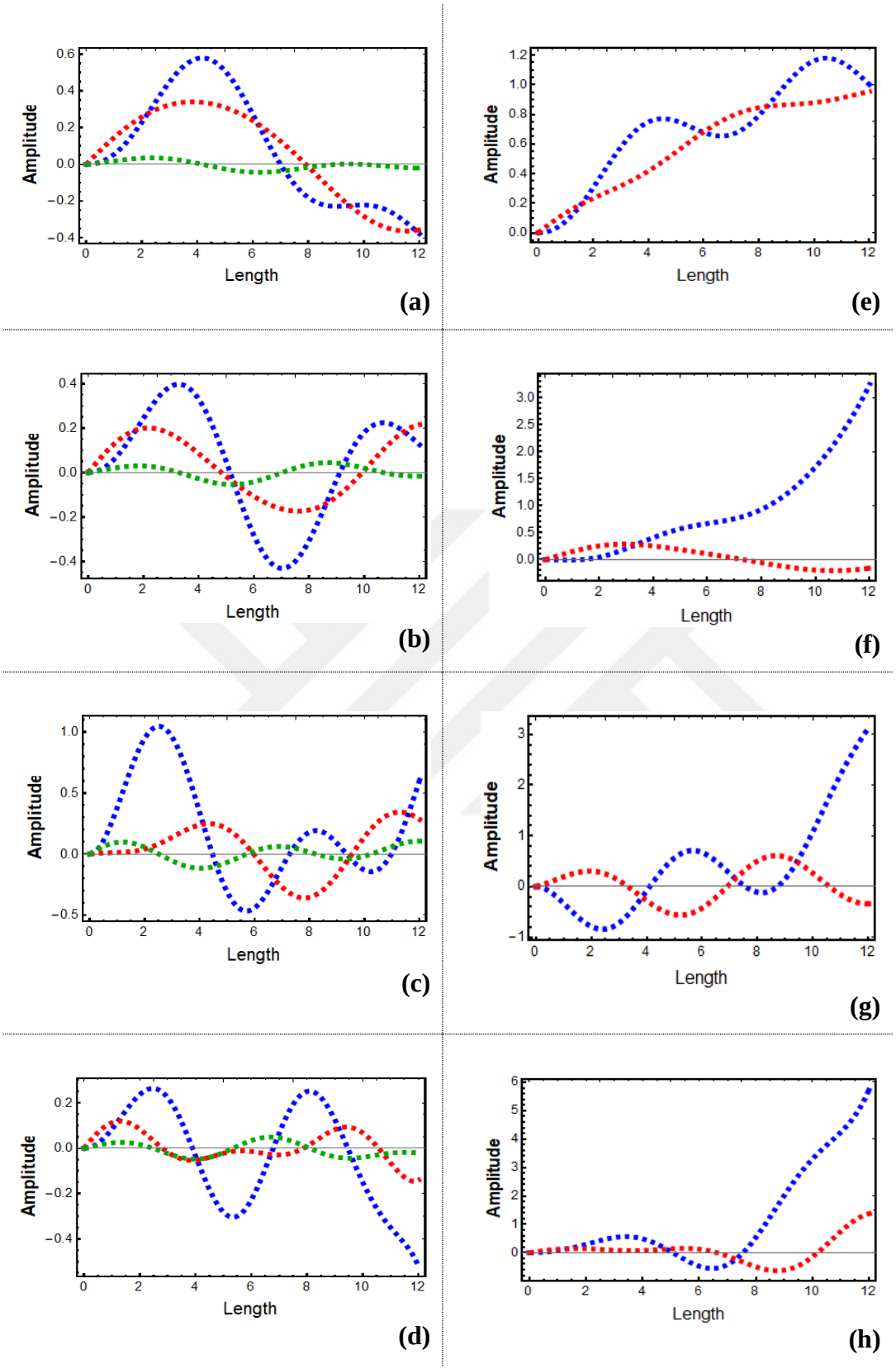

Figure 4.10: First four consecutive vibration mode shapes of a wind turbine blade for C-F boundary condition (blue: bending, red: torsion, green: cross section rotation) when $P = 231e + 05\ N$, (a)-(d) Timoshenko type model, (e)-(h) Bernoulli-Euler type model.

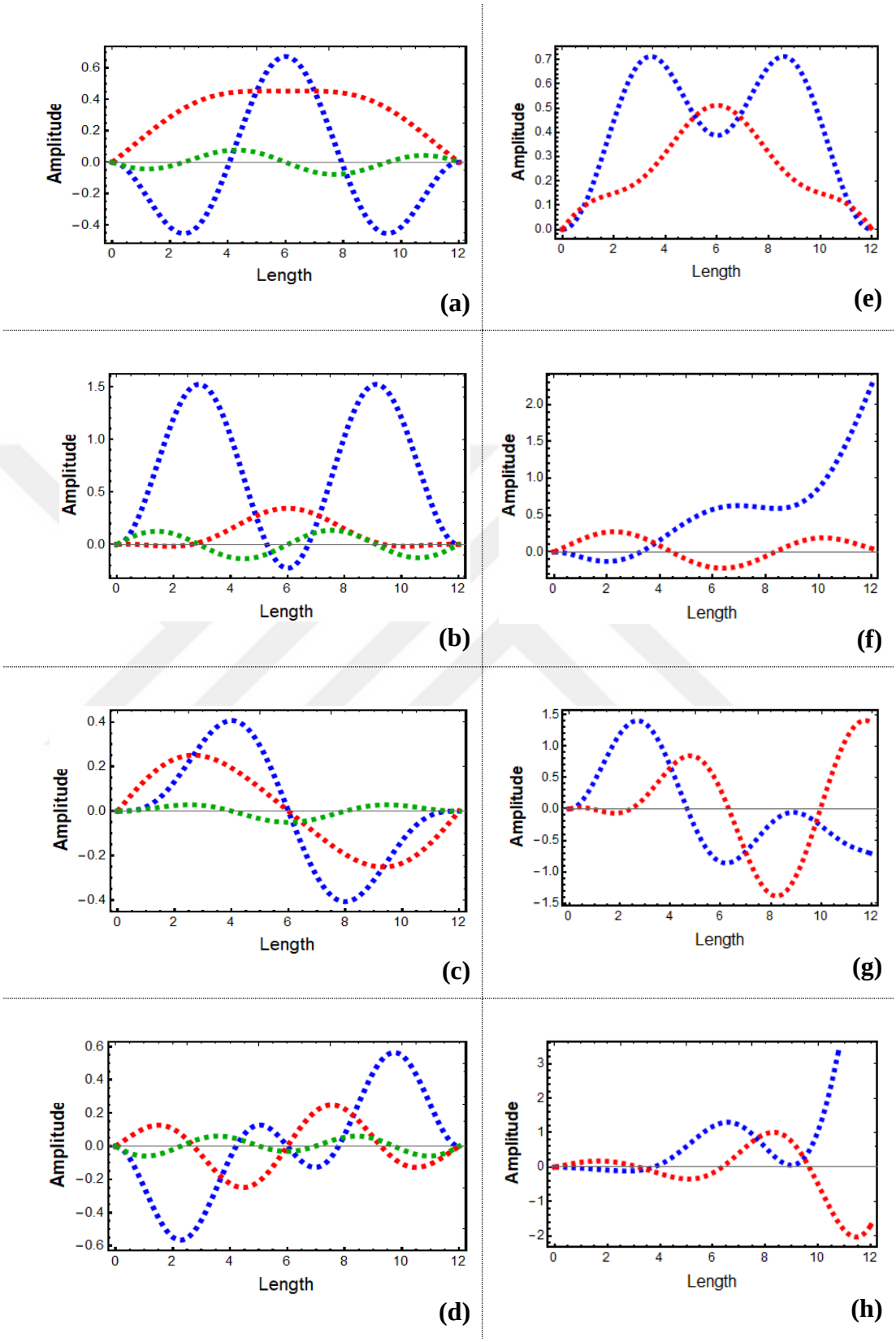

Figure 4. 11: First four consecutive vibration mode shapes of a wind turbine blade for C-C BC (blue: bending, red: torsion, green: cross section rotation) when $P = 171e + 05\ N$, (a)-(d) Timoshenko type model, (e)-(h) Bernoulli-Euler type model.

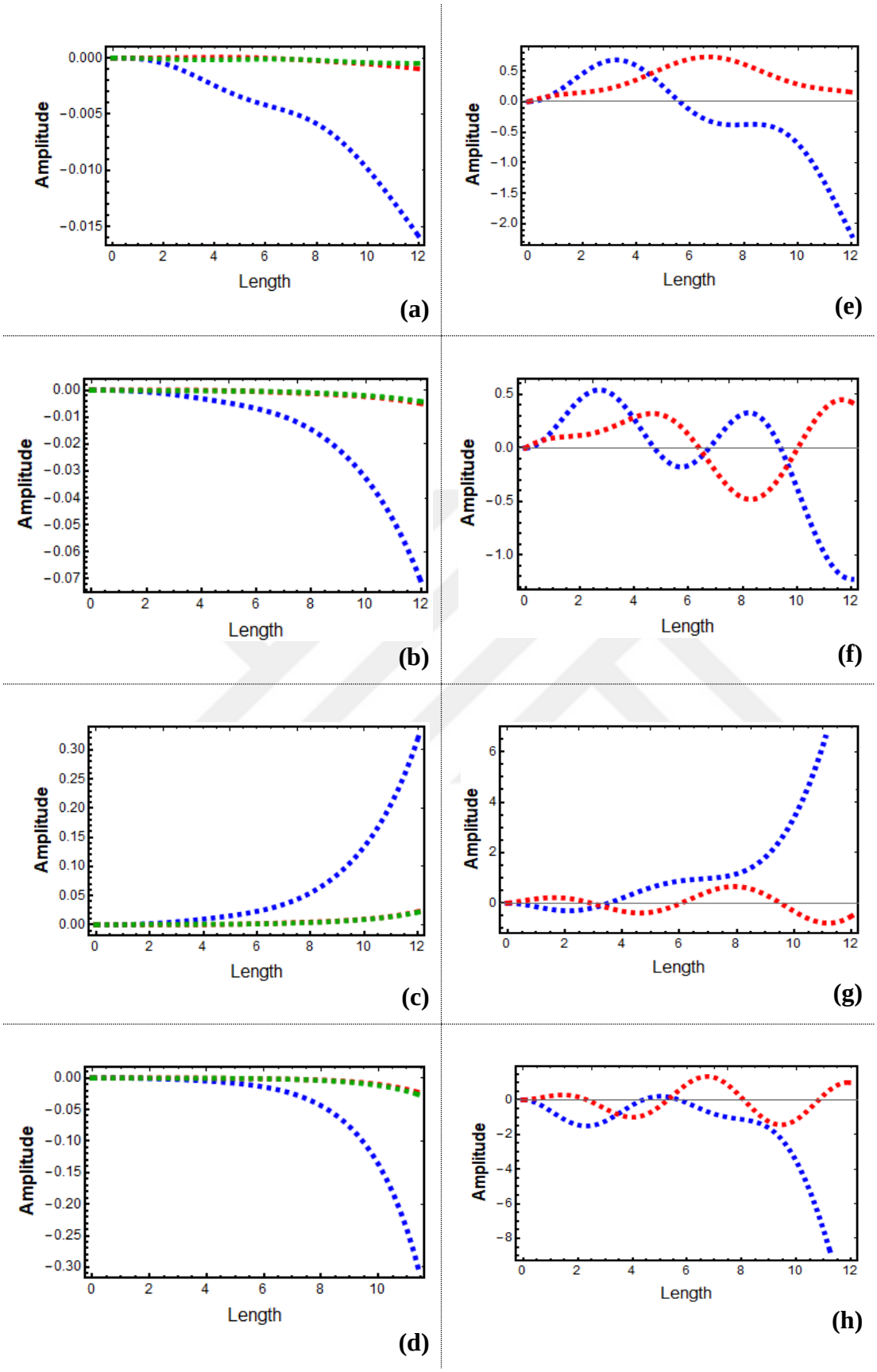

Figure 4.12: First four consecutive vibration mode shapes of a wind turbine blade for S-S BC (blue: bending, red: torsion, green: cross section rotation) when $P = 231e + 05\ N$, (a)-(d) Timoshenko type model, (e)-(h) Bernoulli-Euler type model.

4.2.2 Forced vibration analysis

4.2.2.1 Verification of damage model for an aircraft wing

Martins in the experimental study [14] found that when the pressure impact of lightning including $100\ kA$ lightning current was applied to the center of a pure aluminum panel, the maximal amplitude of the deflection in the lateral direction was found about 3.1 mm approximately at $t = 1\ ms$, which is larger than the duration of mechanical action.

The center of an aircraft wing exposed to lightning is the mid-wing. The mid-wing is in Zone 2A region associated with component B and D waveform of the lightning, as shown in Table 2.4. Due to the nature of lightning, the waveforms of the lightning current affect in a certain order, as shown in Figure 2.3. In the experimental study, Martins considered only D waveform containing $100\ kA$ lightning current in his experimental study. However, in fact, in the mid-wing of an aircraft, both waveform B and waveform D have influence on the wing, respectively, as seen in Table 2.4. The duration of B and D lightning current waveforms were expressed with different approaches in the literature, and one of these approaches is shown in Figure 2.3. Here, waveform B and D act for 5 ms and 500 μs, respectively. On the other hand, Kawakami [13] did not specify a certain duration for B waveform in his study, but he stated that D waveform continues 25 μs. Considering that lightning is a multiple physical event and it is almost impossible to analyze it fully under today's technological conditions, it is exceedingly difficult to say anything about the exact duration of lightning current waveforms. For this reason, in this thesis, considering the sequence and duration of the waveforms of the lightning current suggested in the literature, the effect of waveform B in the first 5 μs and the effect of waveform D in the next first 25 μs are taken into account in the models. In this context, in the case of Bernoulli-Euler type model, the bending deflection at the mid-wing was found to be approximately 0.3 mm for the first 5 μs (under the effect of B waveform) and 3.00 mm for the next 25 μs (under the effect of D waveform), as shown in Figure 4.13 (a,b). Under the same conditions, in the case of Timoshenko type model, the bending deflection is found to be approximately 0.25 mm and 2.5 mm for the first 5 μs and next 25 μs respectively, as shown in Figure 4.13 (e,f). In addition, as shown in Figure 4.13, the deflected shape of the aircraft wing is quite similar in both models. Accordingly, especially for the

bending deflection, even if lightning hits to the mid-wing, the deflections occur in the wing-root and wing-tip due to distributed effect of the pressure model developed.

Compared to these two type models with each other, the amount of the maximum positive deflection at the wing is found around 4.00 mm for Bernoulli-Euler type model and 3.00 mm for Timoshenko type model when lightning hits to mid-wing of the aircraft. Given that the maximum positive deflection was found to be 3.2 mm in the experimental study of Martins [14], it has been seen that Timoshenko type model provides more accurate results. It is expected that the reason for these results is that the values of vibration frequencies obtained from the Timoshenko type model for the same material property are lower and the vibration modes associated with these vibration frequencies have lower amplitudes.

As shown in Table 4.12 and Figure 4.14 – Figure 4.15, the amount of the maximum/minimum deflection at the wing is investigated when lightning strikes to the wing root and wing tip. According to Table 4.12, the maximum amount of deflection occurring at the wing root for both B and D waveforms in terms of bending and torsional deflection is almost the same for both models. However, at the wing tip, Bernoulli-Euler type model has given lower deflection for B waveform, while Timoshenko type model has given lower deflection for D waveform. Furthermore, as seen in Table 4.12, all deflection types decrease as lightning strike point approaches to wing root but increase when they approach to wing tip. This tendency is not the same for all points along the wing [9], but only for selected current impact points.

Table 4.12: Amount of maximum positive deflections at an aircraft wing exposed to pressure loading of lightning.

Amount of maximum deflections at an aircraft wing (mm)							
		2 kA lightning current (Component B)			100 kA lightning current (Component D)		
Lightning strike point (m)	Model type	Bending deflection	Torsional deflection	Rotational deflection	Bending deflection	Torsional deflection	Rotational deflection
Wing-root ($x_0 = 0.4\ m$)	BEM	0.052	0.041	–	0.071	0.015	–
	TM	0.018	0.004	5×10^{-8}	0.053	0.012	0.027
Mid-wing ($x_0 = 3\ m$)	BEM	0.540	0.426	–	4.020	3.422	–
	TM	0.481	0.310	0.05	3.410	3.234	0.223
Wingtip ($x_0 = 5.5\ m$)	BEM	0.583	0.456	–	4.213	3.520	–
	TM	0.460	0.392	0.053	3.564	2.980	0.042

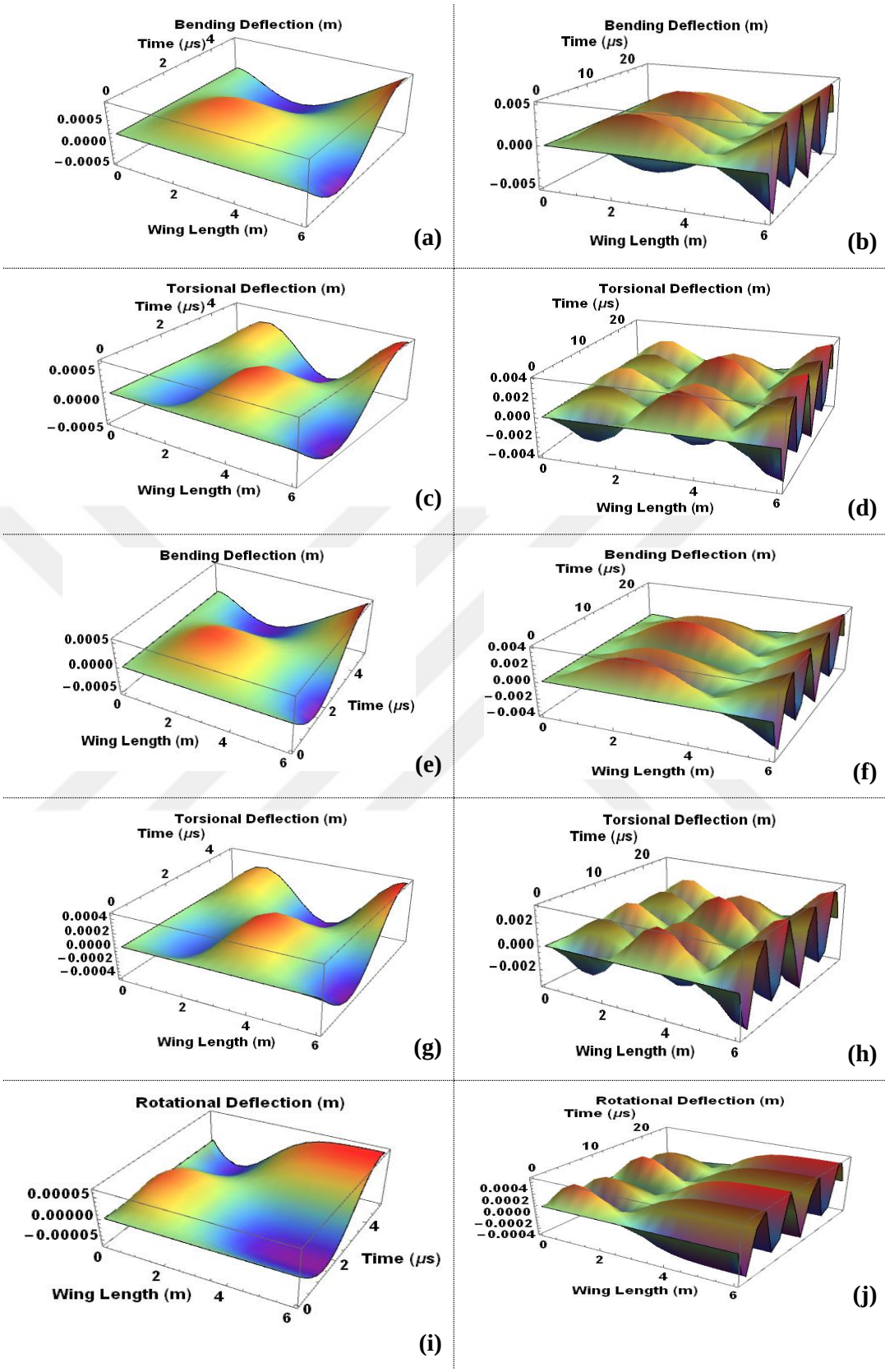

Figure 4.13: Deflected shape of an aircraft wing exposed to lightning strike at mid-wing ($x_0 = 3\ m$), (a-d) bending and torsional deflection by using Bernoulli-Euler type model, (e-j) bending, torsional, and rotational deflection by using Timoshenko type model.

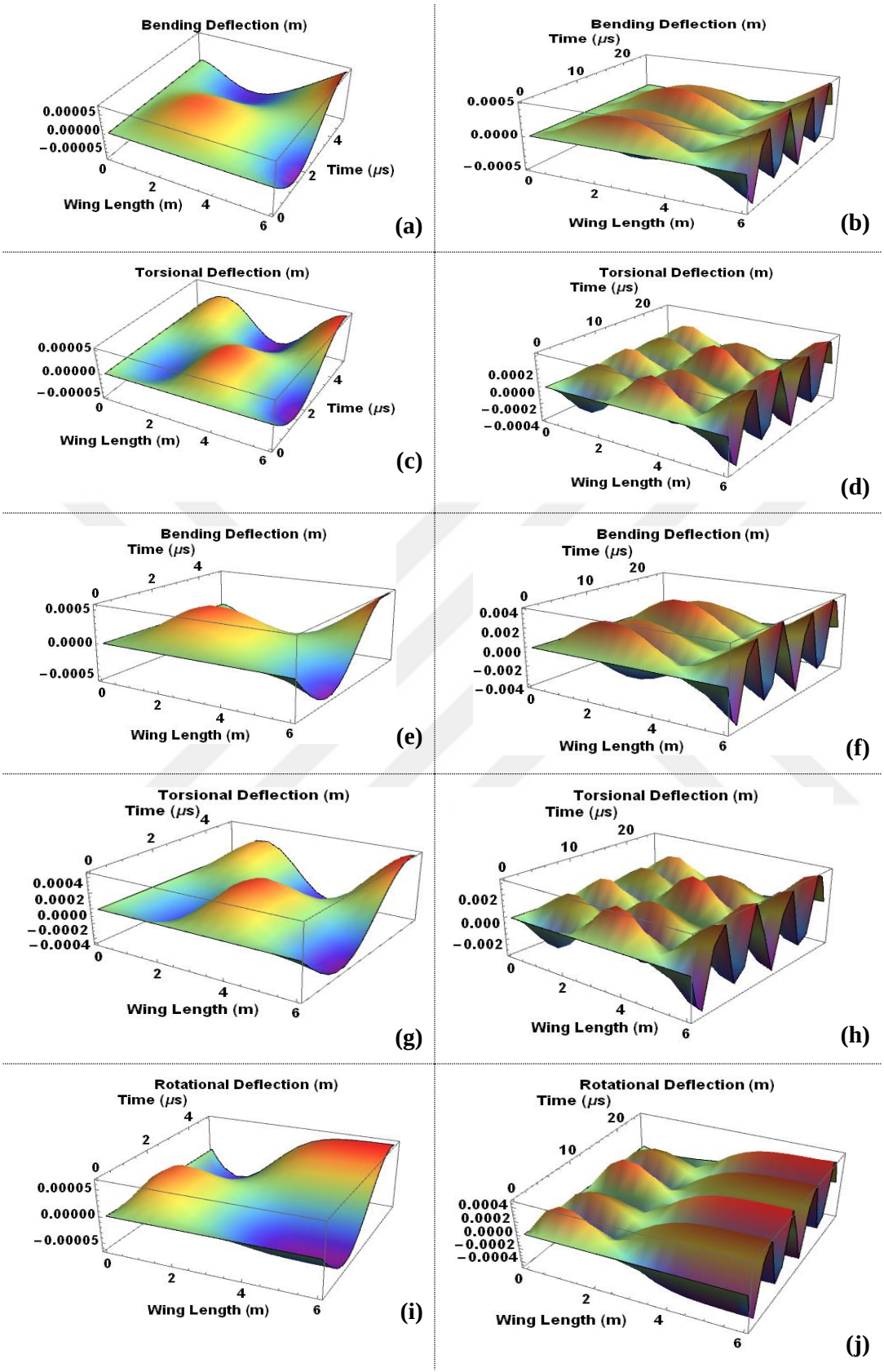

Figure 4.14: Deflected shape of an aircraft wing exposed to lightning strike at wing root $(x_0 = 0.4\,m)$, (a-d) bending and torsional deflection by using Bernoulli-Euler type model, (e-j) bending, torsional, and rotational deflection by using Timoshenko type model.

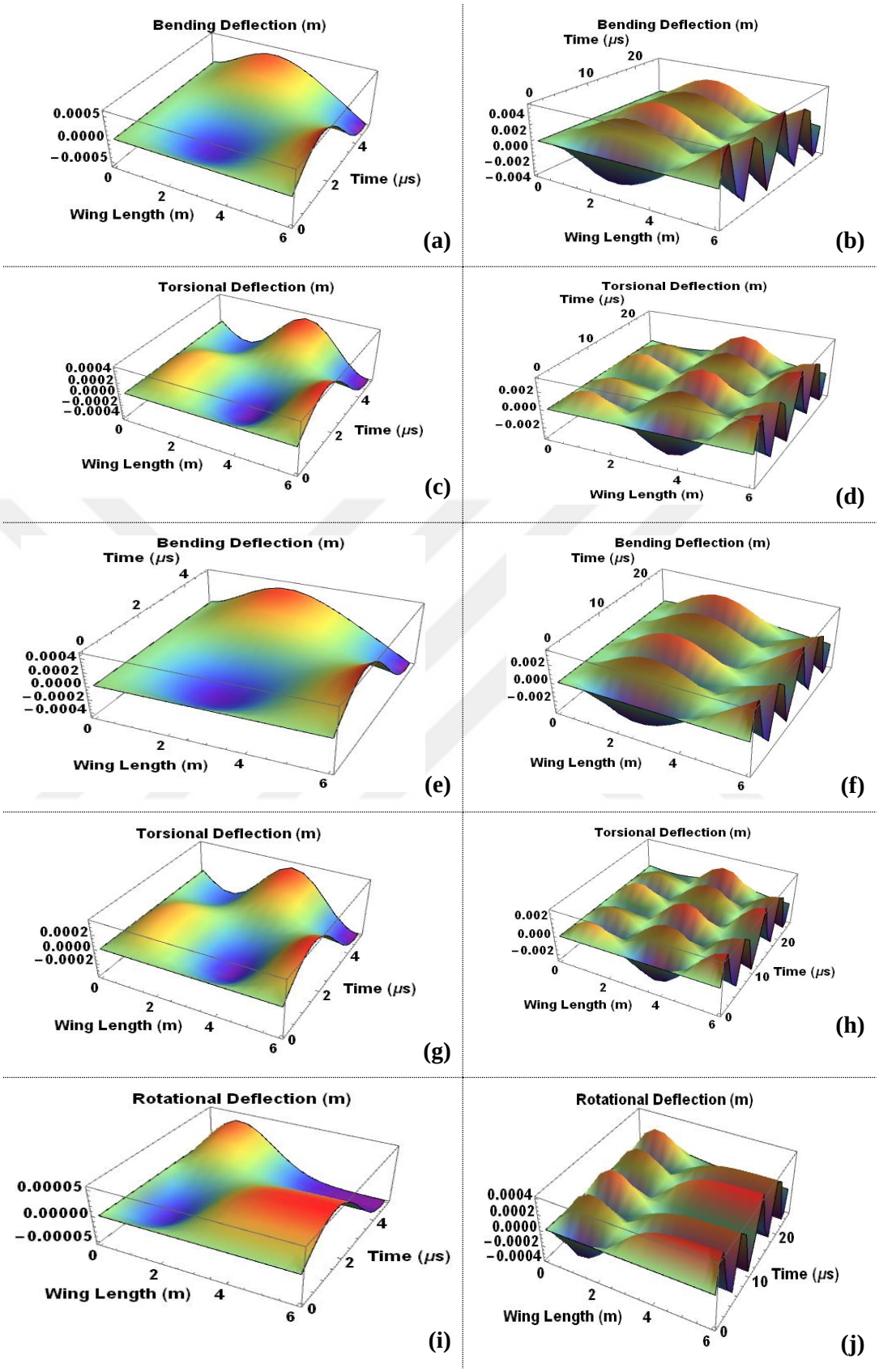

Figure 4.15: Deflected shape of an aircraft wing exposed to lightning strike at wing tip ($x_0 = 5.5\ m$), (a-d) bending and torsional deflection by using Bernoulli-Euler type model, (e-j) bending, torsional, and rotational deflection by using Timoshenko type model.

4.2.2.2 Verification of damage model for a wind turbine blade

Mitchard et al. [31] developed a static numerical model by using COMSOL Multiphysics Software package to predict the amount of the deflection caused by the electromagnetic pressure impact (i.e., electromagnetic force) of lightning strike at the center of a wind turbine blade. Then, they compared the results of the static model for 100 kA lightning current with the results of an experimental study for clamped-clamped boundary condition of the wind turbine blade. In the experimental study, the electromagnetic force was injected to the center of an aluminum plate that is represented a wind turbine blade with clamped-clamped boundary condition in the vertical direction, and then the amount of deflection in the thickness direction of the plate was found as $3.79\ mm$. On the other hand, the authors found that the result of the numerical static model is 8.2 mm.

As an application of the analytical lightning-induced damage model of a wind turbine blade, the model were evaluated for 100 kA lightning current and clamped-clamped boundary condition when the impact of lightning was applied to the middle of the blade. The middle of the blade is in Zone 0A2 region, that is associated with approximately $100\ kA$ lightning current as shown in Table 2.2 and Figure 2.2. In the damage model, since the electromagnetic pressure impact is a flexural loading in the thickness direction of the blade, the result of the bending deflection corresponds to the panel deflection in the thickness direction of the plate. Accordingly, depending on the value of the axial load, Bernoulli-Euler type model and Timoshenko type model were compared with each other in terms of the compatibility with the results of the experimental study. In these models, the amount of the bending deflections at wind turbine blade are 3.98 mm and 2.54 mm for Bernoulli-Euler type model and Timoshenko type model, respectively. Considering the result of the experimental study carrying out by Mitchard et al., the relative errors were found to be nearly 0.05 % and 0.33 % for Bernoulli-Euler type model and Timoshenko type model, respectively. The deflected shapes of the wind turbine blade were given in Figure 4.16 for both types model. Morever, in order to investigate the effects of the boundary conditions on the deflection in the wind turbine blade, the blade deflections were obtained for the C-F and S-S boundary conditions by using both Bernoulli-Euler type model and Timoshenko type model. Firstly, for the C-F boundary condition, the blade deflections were obtained in the absence and existence of the axial force. As stated in free vibration analysis, $P = 231e + 05\ N$ is the ultimate

tensile axial load in which the blade can operate safely. The amount of blade deflections for C-F Boundary condition were obtained and given in Table 4.12. As seen in Table 4.12, The less blade deflections in terms of both bending and torsional deflection were obtained in C-F boundary condition than C-C boundary condition. In addition, when $P = 0\ N$, the Bernoulli-Euler type model provides less deflection in terms of both bending and torsional deflection than the Timoshenko type model. However, when $P = 231e + 05\ N$, the Timoshenko type model provides less deflection in terms of both bending and torsional deflection than the Bernoulli-Euler type model. Furthermore, the amount of the largest deflection is bending, rotational and then torsional deflection, respectively, for C-C and C-F boundary conditions. In the case of the S-S boundary conditions, Bernoulli-Euler type model provides less deflection in bending while Timoshenko type model provides less deflection in torsional deflection. Additionally, rotational deflection is less than the torsional deflection in S-S boundary condition. The deflected shapes of the blade were given in Figure 4.17 - Figure 4.18 for C-F and S-S boundary conditions.

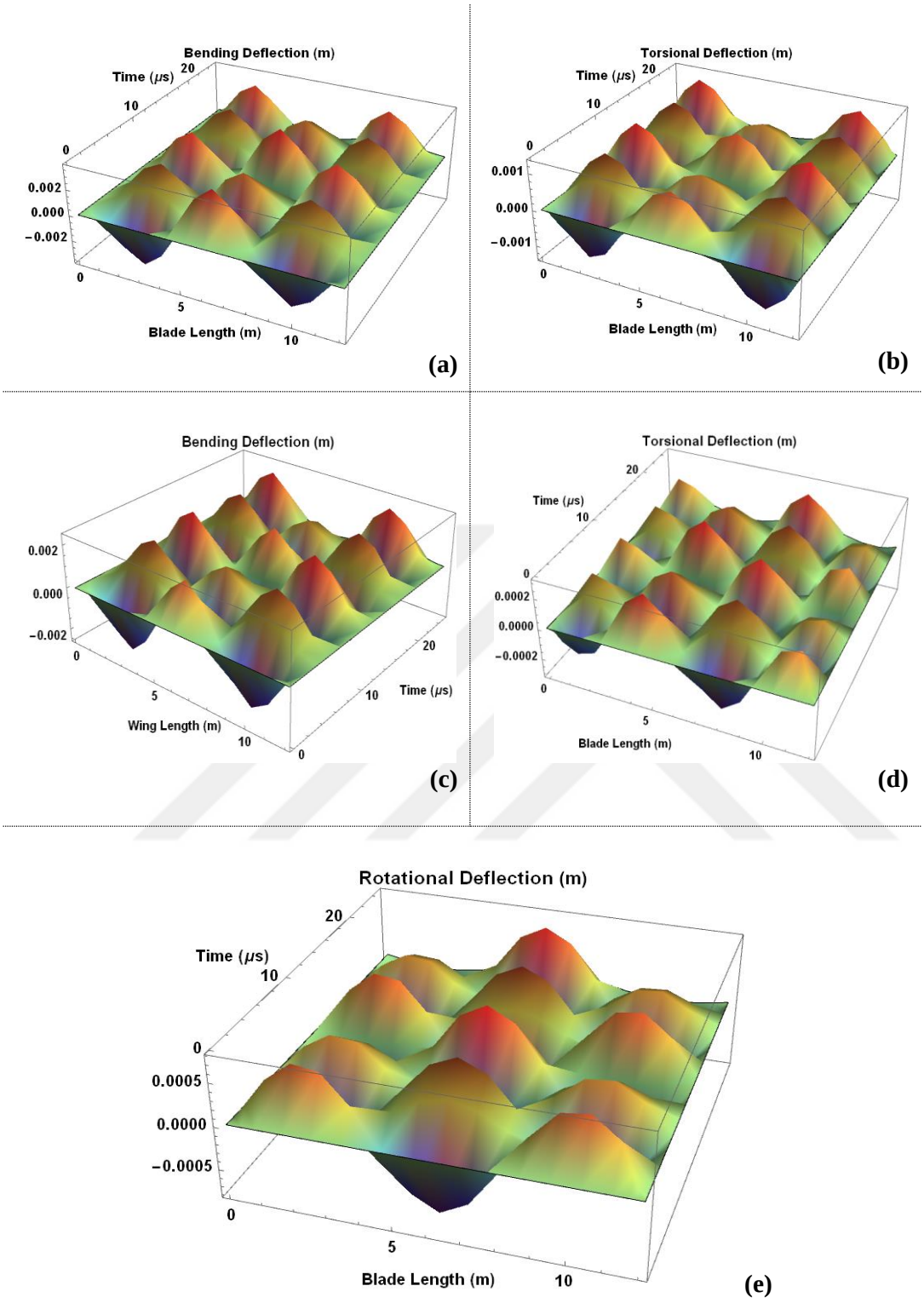

Figure 4.16: Deflected shape of a wind turbine blade exposed to lightning strike at mid-blade in terms of bending, torsional, and rotational deflection for C-C boundary condition by using Bernoulli-Euler type model (a,b) and Timoshenko type model (c,d,e) when $P = 0\ N$.

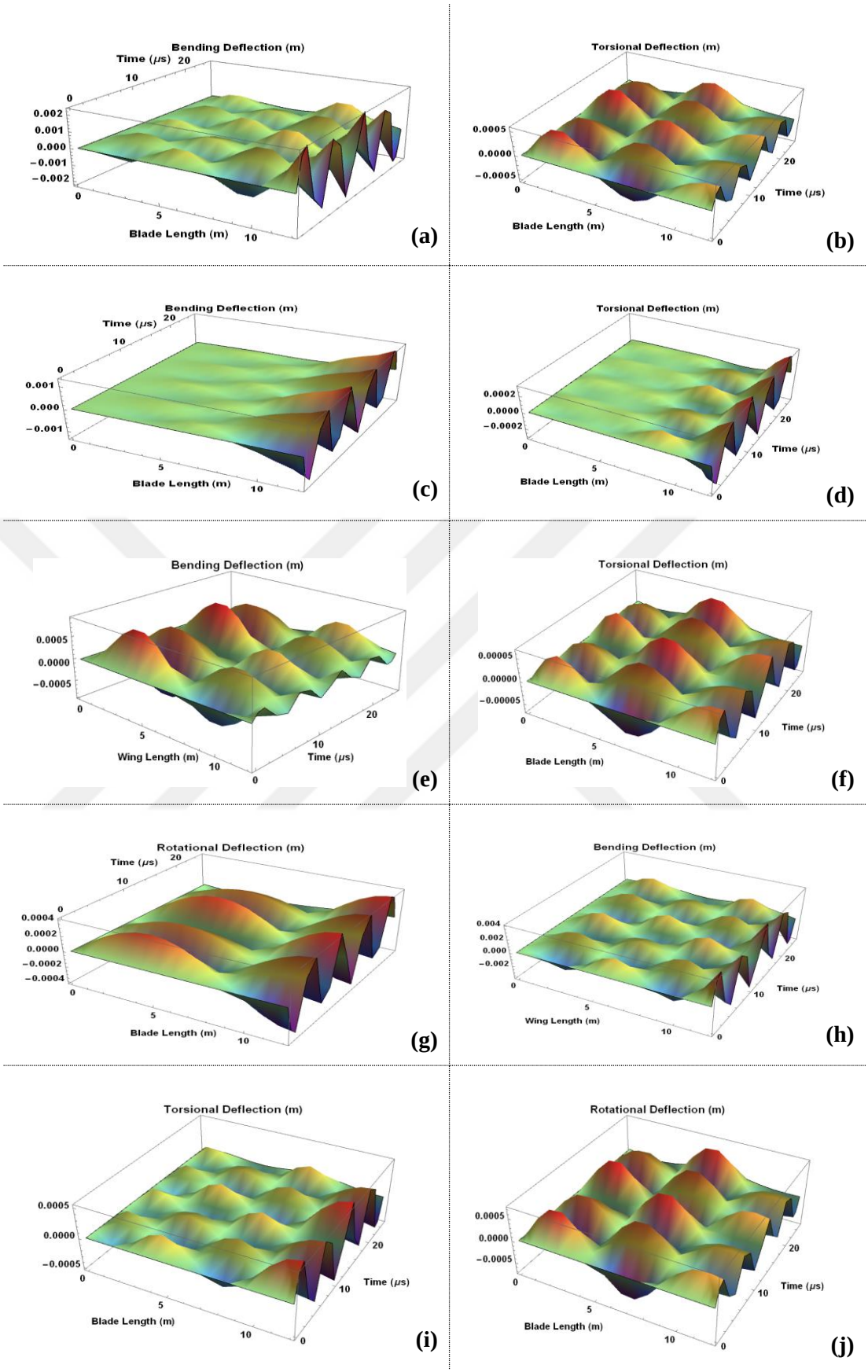

Figure 4.17: Deflected shape of a wind turbine blade exposed to lightning strike at mid-blade for C-F BC by using Bernoulli-Euler type model when $P = 0\ N$ (a, b) and $P = 231e + 05\ \ N$ (c,d) and Timoshenko type model when $P = 0\ N$ (e,f,g) and $P = 231e + 05\ \ N$ (h,i,j).

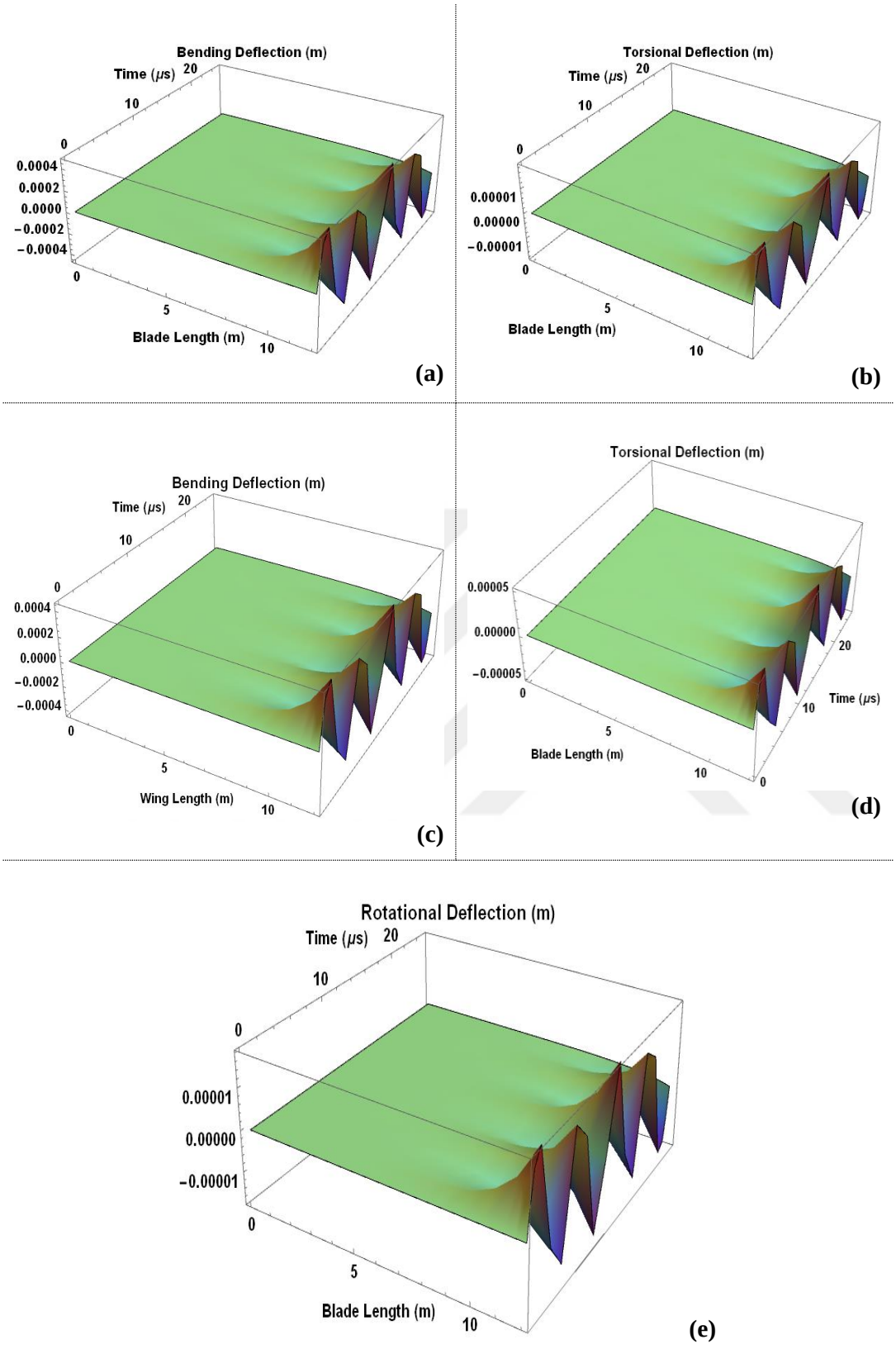

Figure 4.18: Deflected shape of a wind turbine blade exposed to lightning strike at mid-blade in terms of bending, torsional, and rotational deflection for S-S boundary condition by using Bernoulli-Euler type model (a,b) and Timoshenko type model (c,d,e) when $P = 0\ N$.

Table 4.13: Maximum positive lightning-induced deflections (mm) at a wind turbine blade with C-F, C-C, and S-S boundary conditions for both type models.

BC Type	Model Type	Bending deflection	Torsional deflection	Rotational deflection
C-C ($P = 0\ N$)	BEM	3.98	1.47	–
	TM	2.54	0.26	0.75
C-F ($P = 0\ N$)	BEM	2.23	0.51	–
	TM	0.92	0.07	0.38
$C - F$ ($P = 231e + 05\ N$)	BEM	1.52	0.28	–
	TM	3.86	0.46	0.67
S-S ($P = 0\ N$)	BEM	0.47	0.02	–
	TM	0.42	0.05	0.02

5. CONCLUSIONS AND RECOMMENDATIONS

Damages induced by lightning strikes in aircraft structural materials with high thermal and electrical conductivity are mostly caused by the electromagnetic pressure impact, which is the lateral pressure effect of lightning. In the present thesis, lightning-induced damage behavior of an aircraft structural material is investigated analytically. For this purpose, firstly, an analytical-based improved electromagnetic pressure impact model (IEPIM) of lightning was developed, and then two analytical-based damage models were established. The first damage model was for an aircraft wing and the latter damage model was for a wind turbine blade. For each damage model, two different beam theories were considered: Bernoulli- Euler beam theory and Timoshenko beam theory. Then, some applications were carried out to verify the IEPIM and damage models established.

The findings of the thesis concluded that:

1. The results of the IEPIM are quite consistent with the results of two experimental studies for $100\ kA$ lightning current and $200\ kA$ lightning current.
2. In the damage model for an aircraft wing, when the electromagnetic pressure impact including $100\ kA$ lightning current was applied to the middle of the wing, compared to the result of the experimental study that was carried out in the reference, Bernoulli-Euler type model gives 0.26 % relative error while Timoshenko type model gives 0.07 % relative error. Accordingly, Timoshenko type model gives more accurate result than Bernoulli-Euler type model in modeling lightning-induced damage in the middle of the wing. Moreover, in the middle of the wing, the largest deflections are respectively bending, torsional and rotational deflection. On the other hand, when the impact of the lightning including $100\ kA$ lightning current hits to the wing root and wing tip, Bernoulli-Euler type model gives more deflection in terms of bending and torsional deflection; however, for the Timoshenko type model, in the wing root, the rotational deflection is larger than the torsional deflection while it is less in the wing tip.

3. In the damage model of the wind turbine blade, when the impact of the electromagnetic pressure of lightning including $100\ kA$ lightning current hits to the middle of the blade, the Bernoulli-Euler type model and Timoshenko type model give respectively 0.05 % and 0.33% relative error for the bending deflection of the wind turbine blade with C-C boundary condition. Accordingly, the Bernoulli-Euler type model provides more accurate result than the Timoshenko type model to model the lightning-induced damage of a wind turbine blade when the electromagnetic presssure impact of lightning hits to the middle of the blade with clamped-clamped boundary condition. In the investigation of the effects of the boundary condition of the wind turbine blade on the lightning induced blade deflection, in the case of the absence of the axial force, the largest deflections occur respectively, in the C-C, C-F, and S-S boundary conditions. Among these bounday conditions, in the case of the absence of the axial force, the Bernoulli-euler type model gives larger deflection than the Timoshenko type model in terms of bending deflection. In terms of torsional deflection, the Bernoulli-Euler type model gives larger deflection in the C-C and C-F boundary conditions while Timoshenko model gives larger deflection in the S-S boundary condition. Moreover, in the absence of the axial force, the largest deflections are respectively bending, rotational, and torsional deflection. In the case of the existence of the axial force for the C-F boundary conditions, the bending and torsional deflections in the Timoshenko type model are larger than these in the Bernoulli-Euler type model.

Based on the results obtained in this thesis, it has been found that the theoretical results of the thesis are in good agreement with the results of experimental studies in the literature, to the extent that they can be compared with the experimental studies in the literature. However, considering today's laboratory conditions and the current state of advanced computer simulations, it is recommended that the tested results be retested, and the untestable results be tested before the models created in this thesis are put into practice.

REFERENCES

[1] **Plumer, J. A. and Robb, J. D.** (1982). The Direct Effects of Lightning on Aircraft, *IEEE Transactions on Eletromagnetic Compatability*, **2**, 158–172.

[2] **Guerra-Garcia, C., Nguyen, N. C., Peraire, J. and Martinez-Sanchez, M.** (2018). Charge control strategy for aircraft-triggered lightning strike risk reduction, *AIAA Journal*, **56**(5), 1988–2002, doi: 10.2514/1.J056406.

[3] **Curran, E. B., Holle, R. L. and Lo´pez, R. E.** (1999). Lightning Casualties and Damages in the United States from 1959 to 1994, *Journal of Cimate*, **13**, 3448–3464.

[4] **He, Y., Yue, X., Lindbergh, S., Gao, J., Graves, C. and Rakas, J.** (2022). Dissecting lightning strike hazard impact patterns to National Airspace System facilities in the contiguous United States, *Comput Environ Urban Syst*, **91**, doi: 10.1016/j.compenvurbsys.2021.101735.

[4] **He, Y., Yue, X., Lindbergh, S., Gao, J., Graves, C. and Rakas, J.** (2022). Dissecting lightning strike hazard impact patterns to National Airspace System facilities in the contiguous United States, *Comput Environ Urban Syst*, **91**, doi: 10.1016/j.compenvurbsys.2021.101735.

[5] **Zhou, Q., Liu, C., Bian, X., Lo, K. L. and Li, D.** (2018). Numerical analysis of lightning attachment to wind turbine blade, *Renew Energy*, **116**, 584–593, doi: 10.1016/j.renene.2017.09.086.

[6] **Feraboli, P. and Kawakami, H.** (2010). Damage of carbon/epoxy composite plates subjected to mechanical impact and simulated lightning, *J Aircr*, **47**(3), 999–1012, doi: 10.2514/1.46486.

[7] **Sonnadara, U., Kathriarachchi, V., Cooray, V., Montano, R., and Götschl, T.** (2014). Performance of Lightning Locating Systems in Extracting Lightning Flash Characteristics, *J Atmos Sol Terr Phys*, **112**, 31–37.

[8] **Rash, C. E.** (2010). When Lightning Strikes, *AeroSafety World*, **5**, 18–23.

[9] **Soysal, A., Ozkol, I., and Uzal, E.** (2024). An Analytical-Based Lightning-Induced Damage Model for an Aircraft Wing Exposed to Pressure Loading of Lightning, *Math Probl Eng*, **2024**, 1–17, doi: 10.1155/2024/8313135.

[10] **Gohardani, O., Elola, M. C., and Elizetxea, C.** (2014). Potential and prospective implementation of carbon nanotubes on next generation aircraft and space vehicles: A review of current and expected applications in aerospace sciences, *Progress in Aerospace Sciences*, **70**, 42–68, doi: 10.1016/j.paerosci.2014.05.002.

[11] **Bian, X., Wu, Y., Zhou, Q., Jiang, R., Zhang, Y., Chen, L., Qi, Q. and Lyu, W.** (2023). Quantitative characteristics of the striking distance to wind turbine blades based on an improved stochastic lightning model, *IET Generation, Transmission and Distribution*, **17**(10), 2317–2330, doi: 10.1049/gtd2.12808.

[12] **Karch, C., Heidler, F. and Paul, C. (2021).** Protection of Aircraft Radomes against Direct Lightning Strikes-An Overview," doi: 10.3390/atmos.

[13] **Kawakami, H.** (2011). Lightning Strike Induced Damage Mechanisms of Carbon Fiber Composites," University of Washington.

[14] **Sousa Martins, R.** (2016). Experimental and theoretical studies of lightning arcs and their interaction with aeronautical materials, Universite Paris-Saclay, [Online]. Available: https://hal.science/tel-01434026.

[15] **Karch, C., Arteiro, A., and Camanho, P. P**. (2019). Modelling mechanical lightning loads in carbon fibre-reinforced polymers, *Int J Solids Struct*, **162**, 217–243, doi: 10.1016/j.ijsolstr.2018.12.013.

[16] **Muñoz, R., Delgado, S., González, C., López-Romano, B., Wang, D. Y. and Llorca, J.** (2014). Modeling lightning impact thermo-mechanical damage on composite materials, *Applied Composite Materials*, **21**(1), 149–164, doi: 10.1007/s10443-013-9377-9.

[17] **Lee, J., Lacy, T. E. and Pittman, C. U.** (2021). Coupled thermal electrical and mechanical lightning damage predictions to carbon/epoxy composites during arc channel shape expansion, *Compos Struct*, **255**, 2–19, doi: 10.1016/j.compstruct.2020.112912.

[18] **Chemartin, L., Lalande, P., Peyrou, B., Chazottes, A., Elias, P. Q., Delalondre, C., Cheron, B. G. And Lago, F.** (2012). Direct Effects of Lightning on Aircraft Structure: Analysis of the Thermal, Electrical and Mechanical Constraints," *Aerospace Lab*, **5**, 1–15, [Online]. Available: https://hal.science/hal-01184416.

[19] **Lee, J. Y. and Collins, G. J.** (2017). Risk Analysis of Lightning Effects in Aircarft Systems, in *In 2017 IEEE Aerospace Conference*, USA: 2017 IEEE Aerospace Conference, 1–9. doi: 10.1109/AERO.2017.7943671.

[20] **Meirovitch, L. and Tuzcu, I.** (2003). Integrated Approach to the Dynamics and Control of Maneuvering Flexible Aircraft, [Online]. Available: http://www.sti.nasa.gov.

[21] **Alsahlani, A., Rahulan, T. and Abdulhassan, N.** (2017). Composite structural analysis of a high altitude, solar powered unmanned aerial vehicle, *International Journal of Mechanical Engineering and Robotics Research*, **6**(1), 71–76, doi: 10.18178/ijmerr.6.1.71-76.

[22] **Wang, F., Ma, X., Wei, Z., Wu, Y. and Huang, C.** (2023). Lightning damage of composite material driven by multi-physics coupling," *Compos Sci Technol*, **233**, doi: 10.1016/j.compscitech.2022.109886.

[23] **Damghani, M., Saddler, J., Sammon, E., Atkinson, G. A., Matthews, J. and Murphy, A.** (2023). An experimental investigation of the impact response and Post-impact shear buckling behaviour of hybrid composite laminates, *Compos Struct*, **305**, doi: 10.1016/j.compstruct.2022.116506.

[24] **Boushab, D., Gharghabi, P., Lee, J., Lacy Jr, T. E., Pittman Jr, C. U., Mazzola, M. S., and Velicki, A.** (2021). Lightning arc channel effects on surface damage development on a PRSEUS composite panel: An experimental study, *Compos B Eng*, **224**, doi: 10.1016/j.compositesb.2021.109217.

[25] **Guerrero, J. M., Sasikumar, A., Llobet, J. and Costa, J.** (2023). Experimental and virtual testing of a composite-aluminium aircraft wingbox under thermal loading, *Aerosp Sci Technol*, **138**, doi: 10.1016/j.ast.2023.108329.

[26] **Lee, J., Lacy, T. E., Pittman, C. U. and Reddy, J. N.** (2019). Numerical estimations of lightning-induced mechanical damage in carbon/epoxy composites using shock wave overpressure and equivalent air blast overpressure, *Compos Struct*, **224**, doi: 10.1016/j.compstruct.2019.111039.

[27] **Foster, P., Abdelal, G. and Murphy, A.** (2019). Quantifying the Influence of Lightning Strike Pressure Loading on Composite Specimen Damage, *Applied Composite Materials*, **26**(1), 115–137, doi: 10.1007/s10443-018-9685-1.

[28] **Bigand, A., Espinosa, C. and Bauchire, J. M.** (2022). Equivalent mechanical load model methodology to simulate lightning strike impact on protected and painted composite structure, *Compos Struct*, **280**, doi: 10.1016/j.compstruct.2021.114886.

[29] **Qian, Y. F., Ye, Z. F. and Zhang, H. B**. (2019). Impact of modeling simplifications on lightning strike simulation for aeroengine, *Math Probl Eng*, **2019**, 1–11, doi: 10.1155/2019/5176560.

[30] **Harrell, T. M., Thomsen, O. T. and Dulieu-Barton, J. M.** (2023). Predicting the effect of lightning strike damage on the structural response of CFRP wind blade sparcap laminates, *Compos Struct*, **308**, doi: 10.1016/j.compstruct.2023.116707.

[31] **Mitchard, D., Jamoshid, N. S., Stone, C. and Haddad, A.** (2016). Experimental and theoretical evaluation of aluminium deflection due to lightning strikes, in *2016 33rd International Conference on Lightning Protection, ICLP 2016*, Institute of Electrical and Electronics Engineers Inc., doi: 10.1109/ICLP.2016.7791428.

[32] **Lago, F.** (2014). Lightning in aeronautics, *Journal of Physics: Conference Series*, Institute of Physics Publishing, doi: 10.1088/1742-6596/550/1/012001.

[33] **Larsson, A.** (2002). The interaction between a lightning flash and an aircraft in flight, *C. R. Physique*, **3**, 1423–1444.

[34] **Radičević, B. M., Savić, M. S., Madsen, S. F. and Badea, I.** (2012). Impact of wind turbine blade rotation on the lightning strike incidence - A theoretical and experimental study using a reduced-size model, *Energy*, **45**(1), 644–654, doi: 10.1016/j.energy.2012.07.032.

[35] **Garolera, A. C.** (2014). Lightning protection of flap system for wind turbine blades, [Online]. Available: www.elektro.dtu.dk/cee.

[36] **Sweers, G., Bruce, B. and John, G.** (2012). Lightning Strikes: Protection, Inspection, and Repair, *Aero Magazine*, **4**, 19–28, https://www.boeing.com/commercial/aeromagazine/articles/2012_q4/pdfs/AERO_2012q4_article4.pdf

[37] **Gagné, M. and Therriault, D.** (2014). Lightning strike protection of composites, *Progress in Aerospace Sciences*, **64**, 1–16, doi: 10.1016/j.paerosci.2013.07.002.

[38] **Madsen, S. F., Bertelsen, K., Erichsen, H. V., Hansen, A. N. and Lonbaek, K. B.** (2010). Proposal of New Zoning Concept Considering Lightning Protection of Wind Turbine Blades, in *Proposal of new zoning concept considering lightning protection of wing turbine blades*, 1–7.

[39] **Wang Y. and Zhupanska, O. I.** (2015). Lightning strike thermal damage model for glass fiber reinforced polymer matrix composites and its application to wind turbine blades, *Compos Struct*, **132**,1182–1191, doi: 10.1016/j.compstruct.2015.07.027.

[40] **Baker, A. A**. (1984). Repair of Cracked or Defective Metallic Aircraft Components with Advanced Fibre Composites - an Overview of Australian Work, *Compos Struct*, **2**, 153–181.

[41] **Plumer, J. A. and Robb, J. D.** (1982). The Direct Effects of Lightning on Aircraft, *IEEE Trans Electromagn Compat*, **2**, 158–172, doi: 10.1109/TEMC.1982.304010.

[42] **Kawakami, H. and Feraboli, P.** (2011). Lightning strike damage resistance and tolerance of scarf-repaired mesh-protected carbon fiber composites, *Compos Part A Appl Sci Manuf*, **42**(9), 1247–1262, doi: 10.1016/j.compositesa.2011.05.007.

[43] **Radasky, W. and Savage, E.** (2010). Intentional Electromagnetic Interference (IEMI) and Its Impact on the U.S. Power Grid, *Meta*, **1**, 1–3.

[44] **Treyssède, F.** (2010). Vibration analysis of horizontal self-weighted beams and cables with bending stiffness subjected to thermal loads, *J Sound Vib*, **329**(9), 1536–1552.

[45] **Liu, G., Guo, D., Lin, Z., Peng, X., Lin, X., Chen, L., Wang, R. and Lyu, W.** (2023). Exceeding 50% injected lightning energy not sourced: During the analysis of an OGW rupture accident caused by multiple lightning strikes, *Eng Fail Anal*, **143**, doi: 10.1016/j.engfailanal.2022.106779.

[46] **Guo, D., Liu, G., Chen, H., Wang, P. and Lin, X.** (2023). Influence of structural characteristics for overhead ground wire on arc root under lightning strike, *Electrical Engineering*, **105**(5), 3283–3292, doi: 10.1007/s00202-023-01881-9.

[47] **Liu, G., Peng, X., Zhong, M., Wang, R., Wang, P., Guo, D., and Qi, Q.** (2019). A case study of ruptures in overhead ground wire under a large lightning over 400kA, *Eng Fail Anal*, **104**, 1211–1233, doi: 10.1016/j.engfailanal.2019.06.032.

[48] **Cesnik, C. E. S. and Brown, E. L.** (2003). Active warping control of a joined-wing airplane configuration, in *44th AIAA/ASME/ASCE/AHS/ASC Structures, Structural Dynamics, and Materials Conference* , 1715.

[49] **Patil, M. J. and Hodges, D. H.** (2004). On the importance of aerodynamic and structural geometrical nonlinearities in aeroelastic behavior of high-aspect-ratio wings, *J Fluids Struct*, **19**(7), 905–915, doi: 10.1016/j.jfluidstructs.2004.04.012.

[50] **Dwyer, J. R. and Uman, M. A.** (2014). The physics of lightning, *Phys Rep*, **534**(4), 147–241, doi: 10.1016/j.physrep.2013.09.004.

[51] **Chemartin, L., Lalande, P., Montreuil, E., Delalondre, C., Chéron, B. G. and Lago, F.** (2009). Three dimensional simulation of a DC free burning arc. Application to lightning physics, *Atmos Res*, **91**(2–4), 371–380, doi: 10.1016/j.atmosres.2008.07.009.

[52] **Xu, D. A., Shneider, M. N., Lacoste, D. A. and Laux, C. O.** (2014). Thermal and hydrodynamic effects of nanosecond discharges in atmospheric pressure air, *J Phys D Appl Phys*, **47**(23), doi: 10.1088/0022-3727/47/23/235202.

[53] **Fu, K. and Ye, L.** (2019). Modelling of lightning-induced dynamic response and mechanical damage in CFRP composite laminates with protection, *Compos Struct*, **218**, 162–173, doi: 10.1016/j.compstruct.2019.03.024.

[54] **Zhang, L., Mu, J., Ma, H., Dai, G. and Tong, S.** (2023). Research on Fault-Tolerant Control of Combined Airframe Damage of Electric Aircraft," *Aerospace*, **10**(7), doi: 10.3390/aerospace10070611.

[55] **Soysal, A., Özkol, İ. and Uzal, E.** (2023). Investigation of the Behavior of an Aircraft Wing Exposed to Lightning Strike with an Analytical-Based Model, in *10th International Conference on Recent Advances in Air and Space Technologies (RAST)*, 1–5, doi: 10.1109/RAST57548.2023.10197956.

[56] **Kumar, V., Yokozeki, T., Karch, C., Hassen, A. A., Hershey, C. J., Kim, S., Lindahl, J. M.,Barnes, A., Bandari, Y. K., Kunc, V.** (2020). Factors affecting direct lightning strike damage to fiber reinforced composites: A review, *Compos B Eng*, **183**, doi: 10.1016/j.compositesb.2019.107688.

[57] **Kong, K., Dyer, K., Payne, C., Hamerton, I., and Weaver, P. M.** (2023). Progress and Trends in Damage Detection Methods, Maintenance, and Data-driven Monitoring of Wind Turbine Blades – A Review, *Renewable Energy Focus*, **44**, 390–412, doi: 10.1016/j.ref.2022.08.005.

[58] **Eslimy-Isfahany, S. H. R. and Banerjee, J. R.** (1996). Dynamic response of an axially loaded bending-torsion coupled beam, *Journal of Marine Science and Application*, **10**(1), 82–87, doi: 10.1007/s11804-011-1045-6.

[59] **Li, J., Chen, J. and Chen, X.** (2011). Dynamic characteristics analysis of the offshore wind turbine blades, *Journal of Marine Science and Application*, **10**(1), 82–87, doi: 10.1007/s11804-011-1045-6.

[60] **Zhou, J. K.** (1986). *Differential transformation and its applications for electrical circuits*, Wuhan, Huazhong University Press.

[61] **Soysal, A., Özkol, İ., and Uzal, E.** (2022). Flexural-torsional-coupled vibration analysis of Euler-Bernoulli beam by using the differential transform method, *Academic Perspective Procedia*, **5**(3), 26–33, doi: 10.33793/acperpro.05.03.642.

[62] **Li, J., Shen, R., Hua, H. and Jin, X.** (2004). Bending-torsional coupled dynamic response of axially loaded composite Timosenko thin-walled beam with closed cross-section, *Compos Struct*, **64**(1), 23–35, doi: 10.1016/S0263-8223(03)00210-1.

[63] **Eslimy-Isfahany, S. H. R. and Banerjee, J. R.** (2000). Use of generalized mass in the interpretation of dynamic response of bending-torsion coupled beams, *J Sound Vib*, **238**(2), 295–308, doi: 10.1006/jsvi.2000.3160.

[64] **Eslimy-Isfahany, S. H. R. and Banerjee, J. R.** (1995). Response of an axially loaded bending-torsion coupled beam to deterministic and random loads, in *Collection of Technical Papers - AIAA/ASME/ASCE/AHS/ASC Structures, Structural Dynamics and Materials Conference*, AIAA, 2523–2533, doi: 10.2514/6.1995-1448.

[65] **Banerjee, J. R.** (2000). Explicit Modal Analysis of an Axially Loaded Timoshenko Beam With Bending-Torsion Coupling, *J Appl Mech*, **67**, 307–313, [Online]. Available: http://www.asme.org/about-asme/terms-of-use.

[66] **Martins, R. S., Zaepffel, C., Lalande, P., Chemartin, L. and Lago, F.** (2019). Characterization of high-current pulsed arcs ranging from 100-250 kA peak, *J Phys D Appl Phys*, **51**(18), doi: 10.1088/1361-6463/ab0190.

[67] **Jun, L., Rongying, S., Hongxing, H. and Xianding, J.** (2004). Coupled bending and torsional vibration of axially loaded Bernoulli-Euler beams including warping effects, *Applied Acoustics*, **65**(2), 153–170, doi: 10.1016/j.apacoust.2003.07.006.

[68] **Li, J., Shen, R., Hua, H. and Jin, X.** (2004). Coupled bending and torsional vibration of axially loaded thin-walled Timoshenko beams, *Int J Mech Sci*, **46**(2), 299–320, doi: 10.1016/j.ijmecsci.2004.02.009.

[69] **Dursun, T. and Soutis, C.** (2014). Recent developments in advanced aircraft aluminium alloys, *Mater Des*, **56**, 862–871, doi: 10.1016/j.matdes.2013.12.002.

[70] **Larsen, C. E. and Raju, I. S.** (2016). Moving aerospace structural design practice to a load and resistance factor approach, in *57th AIAA/ASCE/AHS/ASC Structures, Structural, Dynamics, and Material Conference*, 230.

[71] **Banerjee, J. R.** (1987). Effects of axial force on the flutter of high aspect ratio aerofoil blades, in *Proceeding of the 13th European Rotorcraft Forum*, 1–10.

CURRICULUM VITAE

Name Surname **:** Aysun SOYSAL

EDUCATION **:**

- **B.Sc.** **:** 2013, Ahi Evran University, Faculty of Science and Letters, Department of Mathematics.
- **M.Sc.** **:** 2017, Yildiz Technical University, Faculty of Chemistry Metallurgy, Department of Mathematical Engineering.

PROFESSIONAL EXPERIENCE AND REWARDS:

- **Reseach and Teaching Assistant**, Bahçeşehir Universrity, Faculty of Engineering and Natural Sciences, Department of Mathematics, 2014- 2023
- **First Award in the Department of Mathematics**, Ahi Evran University, Department of Mathematics (Graduated Ranking 1st), 2009- 2013.

PUBLICATIONS, PRESENTATIONS AND BOOK CHAPTERS ON THE THESIS:

- **Soysal, A., Ozkol, I., Uzal, E.** 2024. Vibration Response Analysis of an Aircraft Structure in terms of Crashworthiness by using Differential Transformation Method, *Gazi University Journal of Science*, 1-18. *(Accepted)(in Press)*
- **Soysal, A., Ozkol, I., Uzal, E.** 2024. An Analytical-Based Lightning Induced Damage Model for an Aircraft Wing Exposed to Pressure Loading of Lightning, *Mathematical Problems in Engineering*, 2024, 1-17, https://doi.org/10.1115/2024/8313135.
- **Soysal, A., Ozkol. I, Uzal, E.** 2024. Analytical Parameter Study for a wind turbine blade. Ege University E.U. Printing and Publishing House. *(Accepted)(in Press)*
- **Soysal, A., Ozkol, I., Uzal, E.** 2023. Investigation of the Behavior of an Aircraft Wing Exposed to Lightning Strike with an Analytical-Based Model, *In 2023 10th International Conference on Recent Advances in Air and Space Technologies (RAST)*, IEEE, 1–5. doi: 10.1109/RAST57548.2023.10197956.
- **Soysal**, **A., Ozkol, I., Uzal, E.** 2022. Flexural-torsional-coupled vibration analysis of Euler-Bernoulli beam by using the differential transform method, *Academic Perspective Procedia*, 5(3), 26–33, doi: 10.33793/acperpro.05.03.642.

- **Soysal**, **A.**, **Ozkol, I., Uzal, E.** 2023. Dynamic Characteristics of an Axially Loaded Coupled Bending Torsion Beam via Differential Transform Method. *In Aviation Technologies and Applications Conference – 2023 (ATAConf'23)*, October 20-21, 2023 İzmir, Türkiye.
- **Soysal, A., Ozkol, I., Uzal, E.** 2023. Investigation of the Behavior of an Aircraft Wing Exposed to Lightning Strike with an Analytical-Based Model, *In 10th International Conference on Recent Advances in Air and Space Technologies (RAST)*, June 7-9, 2023 İstanbul, Türkiye.
- **Soysal, A.**, **Ozkol, I., Uzal, E**. 2022. Flexural-torsional-coupled vibration analysis of Euler-Bernoulli beam by using the differential transform method. *In 2022 10th International Symposium on Innovative Technologies in Engineering and Science (ISITES 2022)*, October 21-23, 2022 Bursa, Türkiye.
- **Soysal, A.** 2022. An analytical approach in modeling mechanical damage behavior of an aircraft wing subjected to lightning strike. *International Conference on Global Practice of Multidisiplinary Scientific Studies*, March 6-8, 2022, Cyprus.
- **Soysal, A.** 2022. An analytical approach in modeling mechanical damage behavior of a helicopter blade subjected to lightning strike. *International Conference on Global Practice of Multidisiplinary Scientific Studies*, March 6-8, 2022, Cyprus.

OTHER PUBLICATIONS, PRESENTATIONS AND PATENTS:

- **Soysal, A.**, **Karakaya, V.** 2016. Measure of Noncompactness and Fractional Differential Equations in Banach Space, *2nd International Conference on Analysis and Its Applications*, July 13-15, 2016 Kırşehir, Türkiye.